1988

Dynamics Of Base-isolated Buildings

Paul Winston Henderson

NOTICE

The quality of this microform is heavily dependent upon the quality of the original thesis submitted for microfilming. Every effort has been made to ensure the highest quality of reproduction possible.

If pages are missing, contact the university which granted the degree.

Some pages may have indistinct print especially if the original pages were typed with a poor typewriter ribbon or if the university sent us an inferior photocopy.

Previously copyrighted materials (journal articles, published tests, etc.) are not filmed.

Reproduction in full or in part of this microform is governed by the Canadian Copyright Act, R.S.C. 1970, c. C-30.

AVIS

La qualité de cette microforme dépend grandement de la qualité de la thèse soumise au microfilmage. Nous avons tout fait pour assurer une qualité supérieure de reproduction.

S'il manque des pages, veuillez communiquer avec l'université qui a conféré le grade.

La qualité d'impression de certaines pages peut laisser à désirer, surtout si les pages originales ont été dactylographiées à l'aide d'un ruban usé ou si l'université nous a fait parvenir une photocopie de qualité inférieure.

Les documents qui font déjà l'objet d'un droit d'auteur (articles de revue, tests publiés, etc.) ne sont pas microfilmés.

La reproduction, même partielle, de cette microforme est soumise à la Loi canadienne sur le droit d'auteur, SRC 1970, c. C-30.

Canada

DYNAMICS OF BASE-ISOLATED BUILDINGS

by

Paul Winston Henderson

Department of Civil Engineering

Submitted in partial fulfillment

of the requirements for the degree of

Doctor of Philosophy

Faculty of Graduate Studies

The University of Western Ontario

London, Ontario

June, 1988

ISBN 0-315-43292-6

ABSTRACT

Base isolation is a novel concept for the protection of buildings up to eight storeys against severe earthquakes. The reduction in seismic forces on the building is achieved by inserting horizontally soft isolation elements between the superstructure and the foundation. As a result, inelastic deformations are limited to the isolators and the fundamental frequency is reduced from 2-3 Hz to typically 0.5 Hz. With the adoption of the base isolation concept, and the research already devoted to it, the questions remain as to the effect of soil-structure interaction, the response to turbulent wind in view of the increased flexibility and approximate methods of analysis for both seismic and wind loading.

In the first part of the study, the complex eigenvalue analysis is used to study the modal properties of three and five storey plane frames. The effect of soil-structure interaction is investigated for footings acting independently and also with dynamic interaction (cross-interaction) included. The effect of introducing vertical flexibility in the isolators (rocking) is examined. The suitability of approximate methods for free vibration analysis, idealizing the buildings as a sliding mass or as a rigid body on springs, is verified.

In the second part of the study, the seismic analysis of a five storey plane frame is performed in the time domain. The effect of base isolation in reducing the accelerations induced in the building is demonstrated. An approximate procedure for the time domain analysis of the

ACKNOWLEDGEMENTS

The author wishes to thank his advisor, Dr. M. Novak for the assistance given throughout this project.

The author would like to thank the staff of the 'Wind Tunnel' for their assistance.

The author gratefully acknowledges the National Research Council of Canada for the financial support of this research project.

Finally, the author would like to dedicate this thesis to his children, Hannah Marie, Sarah Lou and Paul.

TABLE OF CONTENTS

LIST OF PHOTOGRAPHIC PLATES

LIST OF TABLES

LIST OF FIGURES

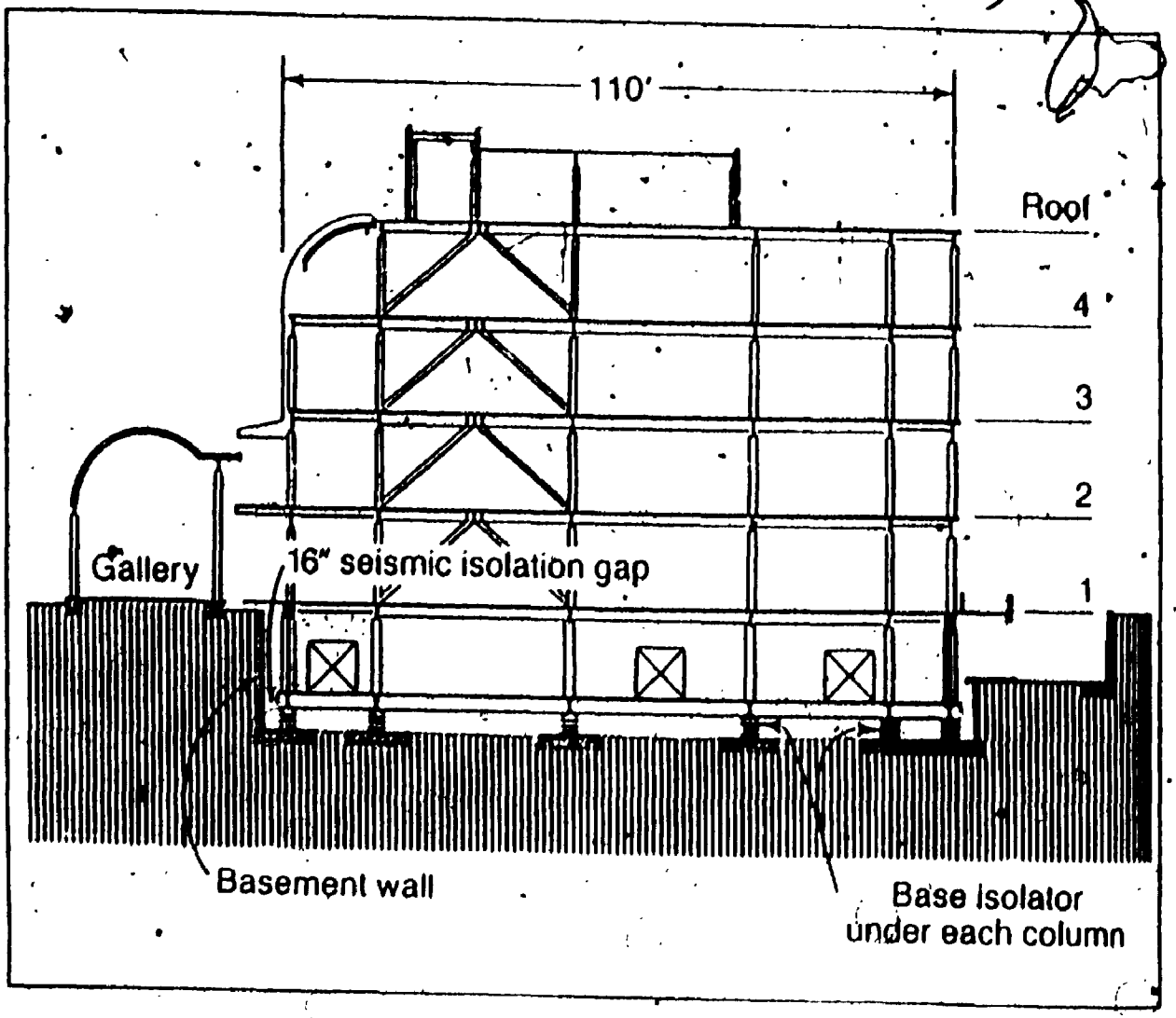

FIGURE 1.3 Foothill Center California, steel frame base-isolated building constructed in 1985 (Tarics and Way, 1984)

CHAPTER 1

INTRODUCTION, OBJECTIVES AND SCOPE

1.1 INTRODUCTION

Earthquakes have devastated cities causing severe damage, fatalities and economic setbacks as witnessed by the 1985 Mexico City earthquake (Popov, 1987). Horizontal ground accelerations are amplified up a conventional building producing inertia forces that are detrimental to the structure and its contents (Figure 1.1). Traditionally, structural engineers have protected structures against severe earthquakes by providing additional strength and ductility. The inelastic deformations lengthen the natural periods and increase the damping of the structure. The increased natural period may reduce the seismic forces by detuning the building from the earthquake excitation. The effect of the damping is to reduce the response of the building. The buildings undergo considerable structural and non-structural damage as well as damage to their contents and this involves even important buildings, such as hospitals, which are required to be functional after earthquakes. Contents, such as telecommunication equipment are rendered ineffective and electrical switchyards lie in ruins when they are most needed. Previous to the 1970s the only solution to this cycle of death, destruction and rebuilding was increasing structural strength and ductility. However, with the application of simple vibration isolation principles, an elegant, alternative solution has been found.

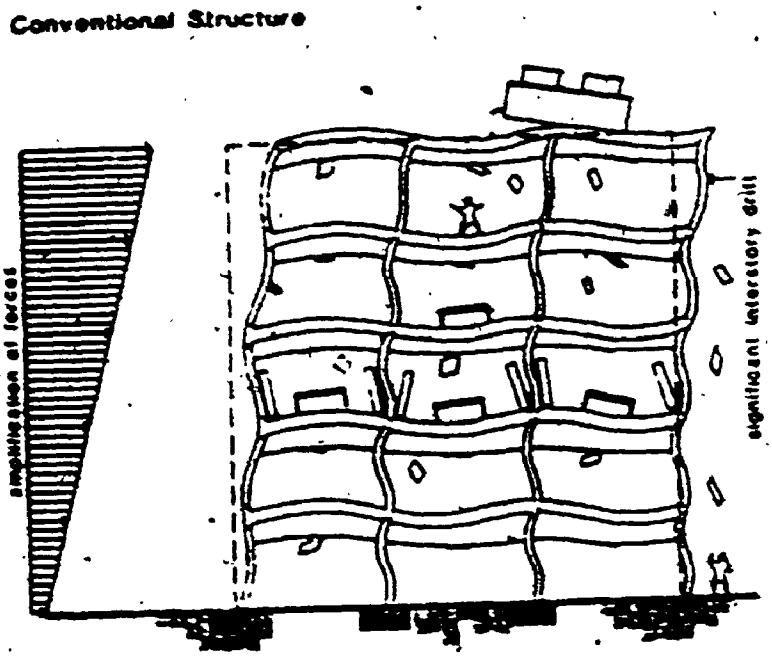

FIGURE 1.1 Buildings having conventional structural systems during earthquakes (Tarics, 1987)

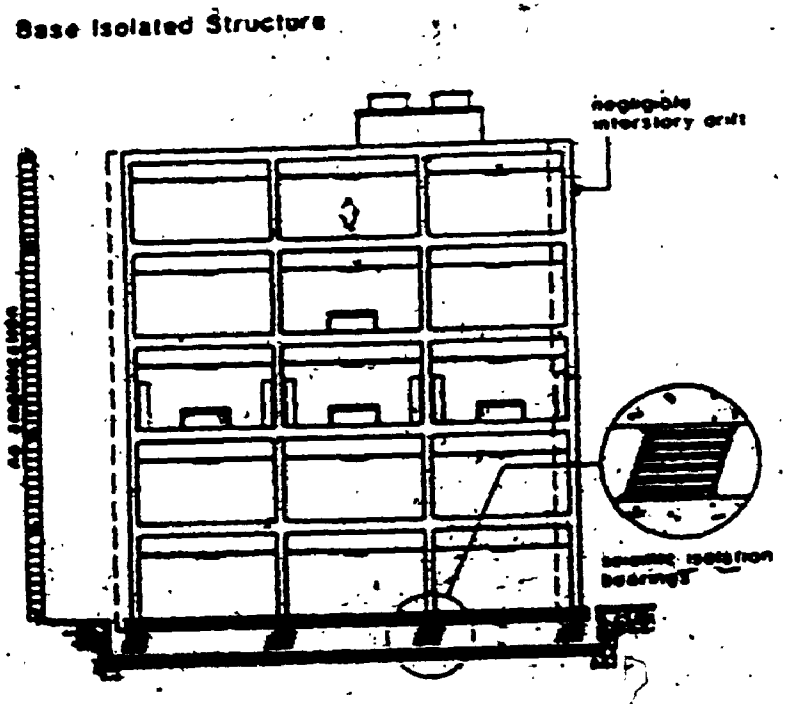

FIGURE 1.2 Buildings on base isolators during earthquakes (Tarics, 1987)

The principle of vibration isolation uses a flexible mounting (helical spring or rubber blocks) to detune an object from its support thereby reducing incoming or outgoing vibrations. Base isolation uses this principle to protect buildings from earthquake excitation. The reduction in seismic loading on the building is achieved by inserting horizontally soft isolation elements between the superstructure and the foundation (Figure 1.2). The inelastic deformations, if any, are limited to the isolating elements and the structure remains elastic. The additional damping provided by the isolators further reduces the resonant component of the response. The building responds very nearly in a rigid body mode with approximately equal displacements at all levels thereby reducing interstorey drifts and possible damage. The accelerations induced in the superstructure are limited to or below the ground acceleration. The isolation effect shifts the natural frequency away from the high energy portion of the earthquake spectrum (typically 2-3 Hz) to a frequency of about 0.5 Hz. This implies that structures whose fundamental frequency is between 2-3 Hz (corresponding to 1-8 storeys) stand to benefit most from base isolation. The vertical load of the structure must be supported as the large relative displacements occur between the superstructure and foundation. For this purpose, various systems, e.g. elastomeric bearings similar to bridge bearings, have been used. A base-isolated building which has been constructed in the U.S.A. is shown in Figure 1.3. The seismic gap between the building and foundation accommodates the relative displacements. Flexible utility connections and sliding accesses are standard details of base-isolated buildings.

Base isolation is particularly suited for retrofitting older

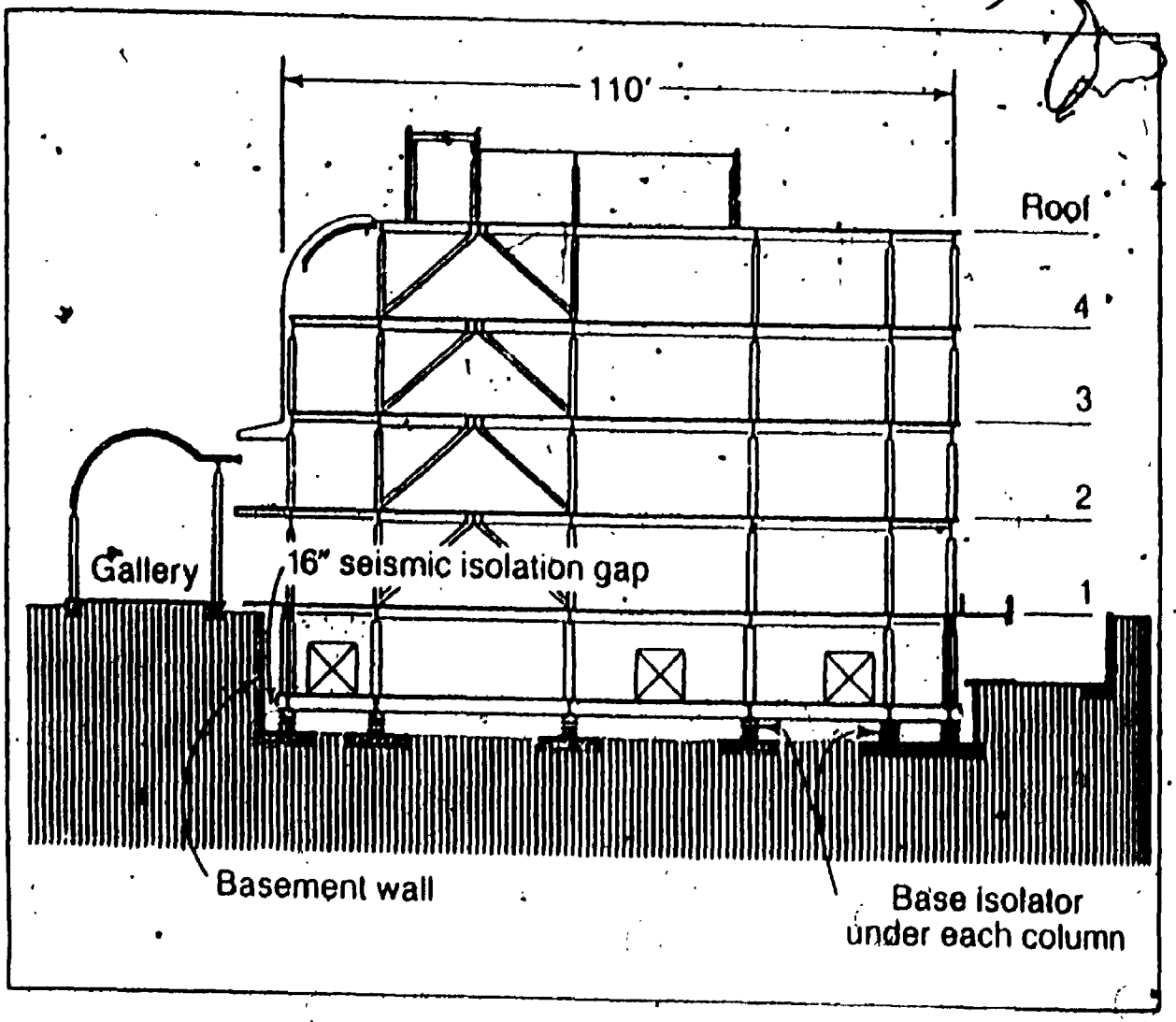

FIGURE 1.3 Foothill Center California, steel frame base-isolated building constructed in 1985 (Tarics and Way, 1984)

buildings, especially those of architectural value, because it reduces the amount of strengthening required for the superstructure. An example of such application is the 92-year-old municipal building in Utah which has been retrofitted by base isolation (Elsesser and Walters, 1987).

Structures founded on soft soils are not suitable for base isolation as the bulk of the energy of the earthquake spectrum would lie at low frequencies (Bucharest 1977 N-S and Mexico City 1985 E-W, SCT).

1.2 OBJECTIVES AND SCOPE

With the adoption of the base isolation concept, questions arise as to the effect of soil-structure interaction, the response to turbulent wind in view of the increased flexibility and approximate methods of analysis for both seismic and wind loading. The objectives of this study are:

- To investigate the effects of soil-structure interaction and rocking resulting from it and from vertical flexibility of the isolators on the modal properties of buildings.
- To investigate the accuracy of approximate methods for computing the modal properties.
- To demonstrate the effectiveness of base isolation for reducing the seismic loading on buildings.
- To establish an appropriate method for the preliminary analysis of base-isolated buildings using time history analysis in conjunction with an approximate idealization of the building.
- To determine the wind parameters in the wind tunnel i.e. mean

wind profile, coherences and longitudinal wind velocity spectrum for the region close to the ground and for open, suburban and urban exposures.

. To determine the wind forces acting on models of low-rise buildings and their drag coefficients.

. Using the experimental results, to formulate a procedure similar to current Codes for the prediction of the response of base-isolated buildings.

. To verify the adequacy of existing Codes for the evaluation of the response of base-isolated buildings to wind.

The scope of the thesis is as follows:

. In this chapter the concept of base isolation is introduced and the objectives of the study are stated.

. Chapter 2 briefly reviews the history of base isolation and describes various base isolation systems.

. In Chapter 3, the properties of base isolators are outlined along with two methods of equivalent linearization.

. The soil impedance functions used in this study are presented in Chapter 4.

. The free vibration analysis of structure-isolator-soil systems are investigated in Chapter 5. Also, approximate methods of free vibration analysis are investigated.

. The seismic analysis of a base-isolated building is investigated in Chapter 6. A simple method of determining the seismic response is demonstrated.

- The wind tunnel experiments are described and the results are presented in Chapter 7.

. In Chapter 8, the alongwind response theory is outlined with appropriate modifications. The response of base-isolated buildings is computed and compared with the response using the Canadian and American Codes. The torsional response is computed and the approximate procedures are presented.

. The conclusions of the study and recommendations for further research are presented in Chapter 9.

CHAPTER 2

BASE ISOLATION REVIEW

2.1 HISTORICAL REVIEW

The first base isolation systems were proposed at the beginning of this century. In 1908, an Italian commission recommended separating a building from its foundation by a layer of sand or rollers while in 1909 a medical doctor proposed the use of a layer of sand (Kelly, 1986). The first use of this concept was in 1921. Frank Lloyd Wright, in designing the Imperial Hotel in Tokyo, isolated this building by supporting the foundation by a series of short piles driven into an 8 foot layer of good soil overlying a layer of soft mud. The soft mud acted as an isolator and the building performed well in the 1923 Tokyo earthquake.

The concept of flexible first storey was introduced by Martel in 1929. He proposed that the lateral stiffness of the columns comprising the first storey be much smaller than the columns of the upper levels. Elastic deformations during an earthquake would occur mainly in the first storey. However, the P-Δ effect associated with such a system could cause the building to collapse. An extension of this concept, known as the soft first-storey, was proposed by Fintel and Khan (1969). The columns were allowed to yield and stability walls with neoprene pads were incorporated. The additional damping was intended to reduce displacements. Nevertheless, there was a large ductility demand and the system would have to yield elastic-perfectly plastic (Chopra, 1973). The Olive View Hospital in California, with architectural features such

More recently, the Friction Pendulum System (FPS) was tested experimentally by the Earthquake Engineering Research Center of the University of California at Berkeley (Mahin, 1987). A cross-section of the FPS correction is shown in Figure 2.4. It operates on the principle of pendulum motion and damping is provided through sliding on a spherical concave surface. For wind and small earthquakes the building responds in a conventional manner. For severe earthquakes, the isolation system is activated thereby increasing the period of vibration and providing friction damping to further reduce the response.

The sleeved-pile concept utilizes a free length of pile to achieve the isolation. The pile is used within a sleeve to limit the lateral displacement. A mild steel tapered plate provides hysteretic damping and acts as a wind restraint. A 12-storey building in New Zealand (Union House) incorporated this system (Boardman et al., 1983).

Roller bearing isolation systems have been proposed (Caspe, 1970, 1984 and Stiemer, 1985). For bi-directional excitation two layers of rollers need to be provided. Also, there is the problem of fusing of the rollers to bearing plates because of high contact stresses. A building in the USSR (Kelly, 1985) used spherical ovoids for isolation and a dry friction element for damping. The building reportedly performed to expectation in a 1977 earthquake.

The spring-dashpot isolation system uses helical springs and viscodampers (Tezcan, 1980; Hüffmann, 1984). The vertical stiffness of the springs is twice the horizontal stiffness and also provides isolation from vertical excitation. This system is more expensive than laminated

2.2 BASE ISOLATION SYSTEMS

The most common type of base isolation systems are laminated bearings (Figure 2.1). These are similar to bridge bearings and comprise layers of rubber bonded to thin steel plates to provide high vertical stiffness and low horizontal shear stiffness. The bearings are typically 300-500 mm square or in diameter with 3 mm thick steel plates and 16 mm thick rubber layers. The thickness of the rubber layers and steel plates may vary with the overall thickness being between 250-400 mm. The high vertical stiffness, resulting from Poisson's ratio = 0.5, supports the weight of the building while the low horizontal stiffness provides isolation in this direction. The rubber may be natural rubber but recently rubber compounds (rubber containing filler) have been used.

Additional damping is obtained in one of several ways. In the construction of the William Clayton Building a lead core was inserted (Figure 2.1) to provide hysteretic damping by pure shear deformation (Robinson and Tucker, 1977). The damping is increased from 3% for the rubber to 10-15% with the lead plug. However, the lead tends to fracture or work into the rubber. High viscosity rubber without the lead core was used in the Foothill Communities Law and Justice Center in California to provide 10-20% damping for high and low strains respectively (Celebi and Kelly, 1985). The high initial stiffness is reduced by a factor of four or five as the strain approaches 50%. As the strains exceed 100%, the stiffness again increases providing a fail-safe action. Hysteretic damping may be provided by steel members yielding in torsion or flexure (Figure 2.2). In Japan the dampers used in a building

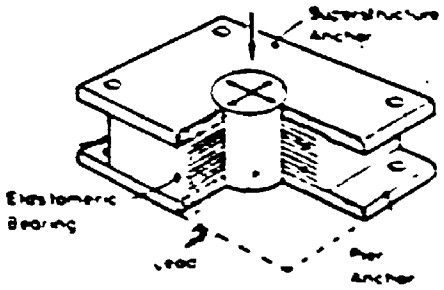

FIGURE 2.1 Laminated bearing with lead core

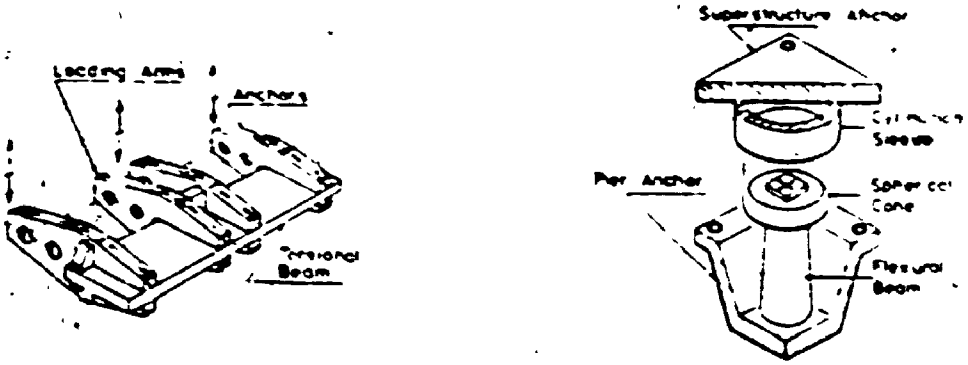

(a) (b)

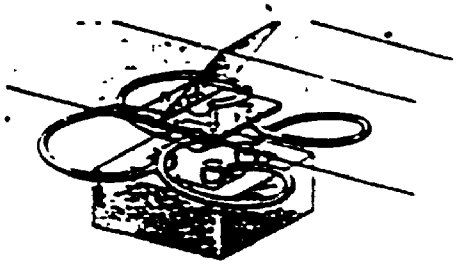

(c)

FIGURE 2.2 Steel hysteretic dampers (a) torsional beam (b) flexural beam (c) coils (Okumura Corp.)

constructed by the Okumura Corporation, consist of steel coils 50 mm in diameter (Figure 2.2c).

The E.D.F. system (Electricité de France) is used for the seismic protection of nuclear power plants (Plichon, 1978 and Wolf, 1983). The reactor and its ancillary buildings are collected on a raft forming a nuclear island. The upper raft rests on a lower raft and are separated by an isolation system which consists of laminated neoprene bearings with lead bronze-stainless steel slip plates on top of each bearing (Figure 2.3). The bearings isolate small earthquakes while sliding occurs on the slip plates for large earthquakes. The plates have a friction coefficient of 0.2 which allows a standard power plant design for a seismic loading of 0.2g. A nuclear power plant incorporating this system has been constructed in South Africa. This system is reportedly costly and therefore is not suited for ordinary construction.

In the sliding system, the isolation is obtained by purely sliding friction. It was observed in China that masonry buildings in which the reinforcement did not extend into the foundation, performed better during the 1976 Tang Shan earthquake. In one building a horizontal crack occurred and there was a residual displacement of 6 cm. From these observations a system for low-cost low-rise houses emerged (Li, 1987). It consists of placing a layer of screened sand between two smooth plates separating the building and its foundation and forming the isolation system. A one-storey building, built of poor material and incorporating this system, was tested by an explosively generated ground motion. The building survived by sliding.

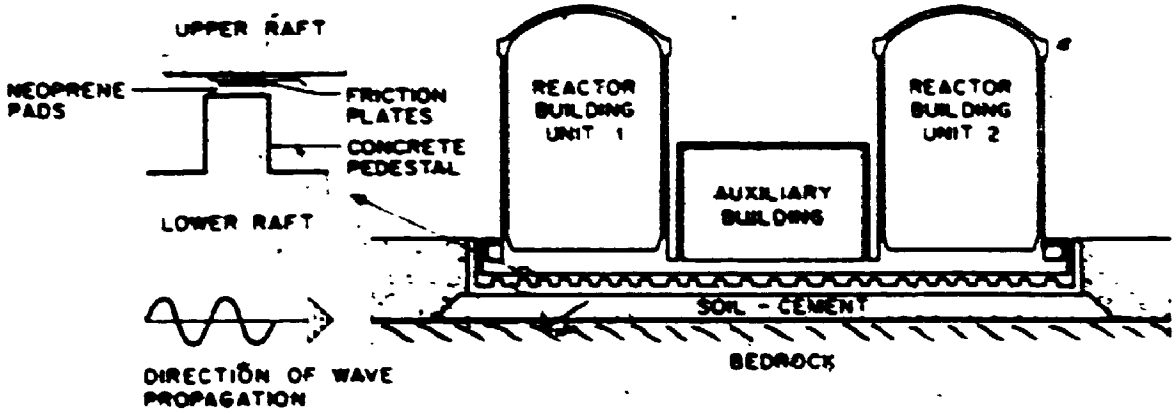

FIGURE 2.3 Nuclear island on aseismic bearings (Wolf, 1983)

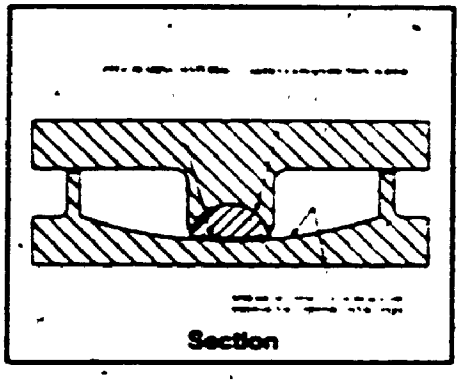

FIGURE 2.4 Section view of the FPS connection (Mahin, 1987)

More recently, the Friction Pendulum System (FPS) was tested experimentally by the Earthquake Engineering Research Center of the University of California at Berkeley (Mahin, 1987). A cross-section of the FPS correction is shown in Figure 2.4. It operates on the principle of pendulum motion and damping is provided through sliding on a spherical concave surface. For wind and small earthquakes the building responds in a conventional manner. For severe earthquakes, the isolation system is activated thereby increasing the period of vibration and providing friction damping to further reduce the response.

The sleeved-pile concept utilizes a free length of pile to achieve the isolation. The pile is used within a sleeve to limit the lateral displacement. A mild steel tapered plate provides hysteretic damping and acts as a wind restraint. A 12-storey building in New Zealand (Union House) incorporated this system (Boardman et al., 1983).

Roller bearing isolation systems have been proposed (Caspe, 1970, 1984 and Stiemer, 1985). For bi-directional excitation two layers of rollers need to be provided. Also, there is the problem of fusing of the rollers to bearing plates because of high contact stresses. A building in the USSR (Kelly, 1985) used spherical ovoids for isolation and a dry friction element for damping. The building reportedly performed to expectation in a 1977 earthquake.

The spring-dashpot isolation system uses helical springs and visco-dampers (Tezcan, 1980; Hüffmann, 1984). The vertical stiffness of the springs is twice the horizontal stiffness and also provides isolation from vertical excitation. This system is more expensive than laminated

bearings and the rocking motions may induce high accelerations at corners. For conventional buildings vertical isolation is not necessary. However, as will be shown in a later chapter, large damping ratio may be obtained from this system.

CHAPTER 3

PROPERTIES OF BASE ISOLATORS

3.1 PROPERTIES OF LAMINATED BEARINGS

Laminated bearings have evolved as a practical means of base isolating buildings, as discussed in Chapter 2. Three devices, steel, lead or high viscosity rubber are used to provide hysteretic damping. These devices have different characteristics but their load deflection relationship can be approximated by a bilinear hysteretic loop.

Steel devices exhibit different characteristics depending on the mode of straining. Testing of a single taper cantilever, Figure 3.1, indicated that the elastic and post-yielding stiffnesses are (Blakeley et al., 1979)

$$\frac{k_1}{Qd} = 85\ m^{-1} \quad \text{and} \quad \frac{k_2}{Qd} = 5\ m^{-1}$$

where k_1 is the elastic stiffness, k_2 is the post-yield stiffness and Qd is the force in the dissipator at zero displacement. The stiffnesses for the torsional beam device are 20% greater.

The load displacement relationship for a lead/rubber bearing is shown in Figure 3.2. The laminated bearing without the lead plug (rubber in Figure 3.2) describes a very small hysteretic loop and therefore behaves approximately elastic. The stiffnesses of the lead/rubber bearing are

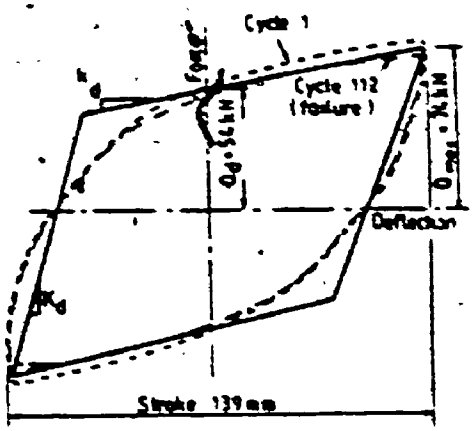

FIGURE 3.1 Force-deflection hysteretic loop for steel taper device (Tyler, 1977)

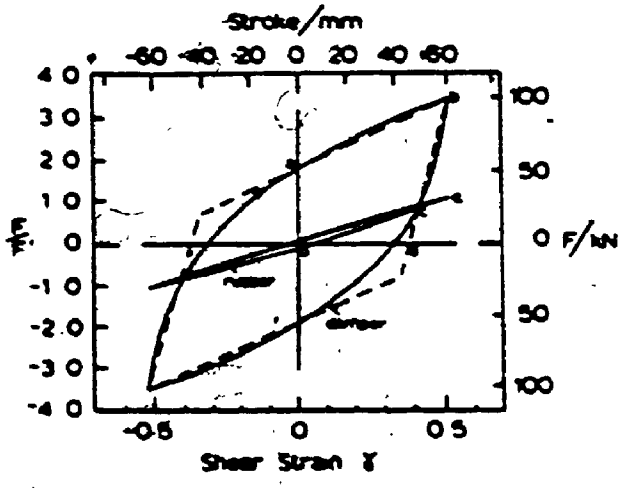

FIGURE 3.2 Force-deflection hysteretic loop for lead/rubber device (Robinson, 1977)

$$\frac{k_1}{Qd} = 113\ m^{-1} \quad \text{and} \quad \frac{k_2}{Qd} = 14\ m^{-1}$$

The area of the lead cylinder controls the ratio of the post-yield stiffness of the lead/rubber bearing to the stiffness of the elastomeric bearing alone.

More recently, high viscosity rubber bearings became available. They have a shear modulus at low strains (less than 5%) which is four to five times greater than the value at 50% strain (Celebi and Kelly, 1985). Figure 3.3 shows the hysteretic curve for a high viscosity rubber bearing used in the Foothill Communities Law and Justice Center. Damping ratios of 10 to 20% were estimated, using the area of the hysteresis loop and the maximum elastic stored energy. The larger value is for lower strains while the smaller value is for higher strains. These bearings exhibit strain hardening for strains in excess of 100% (Kelly, 1986).

3.2 EQUIVALENT LINEARIZATION OF BASE ISOLATORS

Linearization is used to simplify computations and consequently to reduce computational cost. The non-linear soil-isolator-structure system, described with appropriate linear parameters, can be analyzed using the complex eigenvalue approach. The equivalent linear system depends on the properties of the non-linear system and the magnitude of displacement. Consequently, equivalent linearization has been derived for harmonic, random and earthquake excitations. In this study, harmonic and earthquake equivalent linearization are discussed and used.

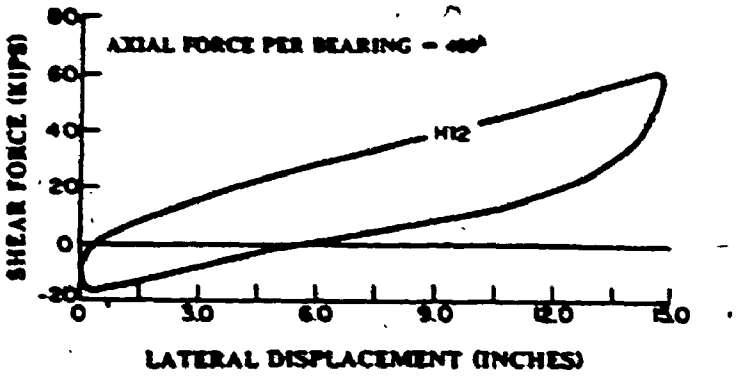

FIGURE 3.3 Hysteretic curve for high viscosity rubber bearing (Celebi, 1985)

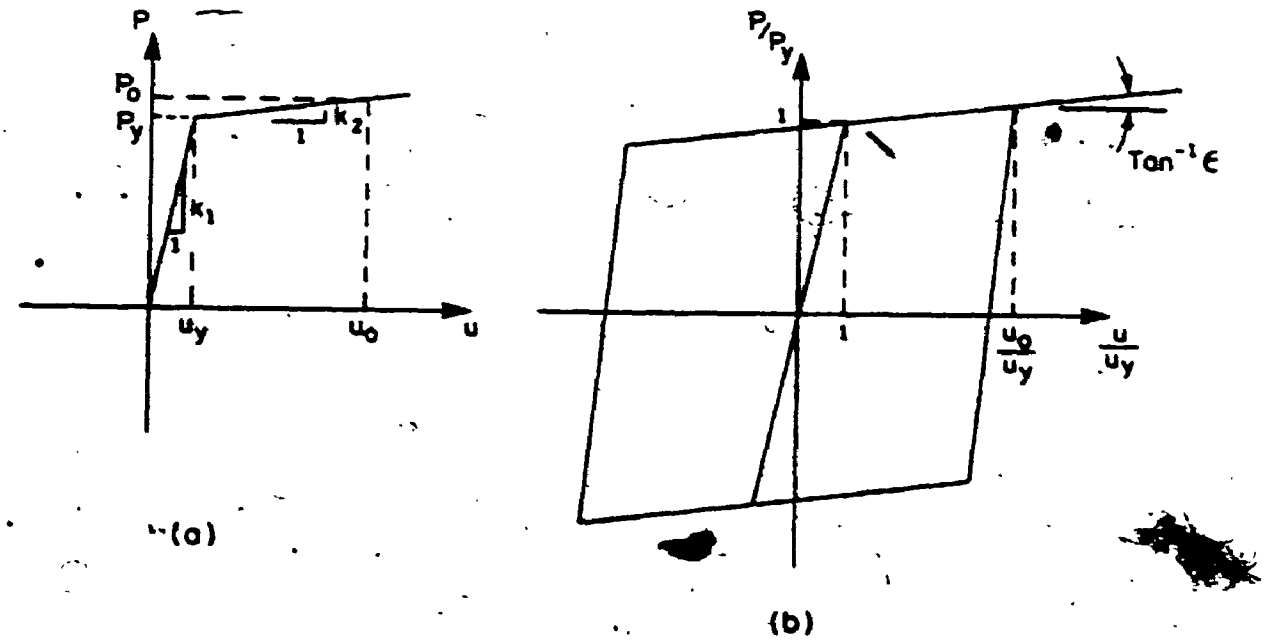

FIGURE 3.4 Bilinear hysteretic loops
(a) Force-displacement relationship of base isolators
(b) Normalized bilinear hysteresis loop

3.2.1 Equivalent Linearization for Harmonic Excitation

Equivalent linearization for harmonic excitation is suitable for free vibration analysis and also for earthquake excitation for which an 'effective amplitude' is used. There are many methods of equivalent linearization for harmonic excitation (Jennings, 1968 and Hadjian, 1982). The basic principle is to assume one of the parameters (stiffness or damping) of the equivalent linear system and to compute the other. Of the models proposed, the Geometric Stiffness is the simplest and yet adequate and is also quite acceptable on the grounds of physical representation of the stiffness and damping of the system (Hadjian, 1982). This model was proposed by Rosenblueth and Herrara (1964) and will be given further consideration herein.

The bilinear hysteresis loop is shown in Figure 3.4. For the Geometric Stiffness model, the stiffness of the equivalent system, k_e, is equal to the secant stiffness

$$k_e = \frac{P_o}{u_o} \tag{3-1}$$

where P_o is the force on the isolator at u_o, its maximum displacement. The characteristic strain energy of the loop, W_s, is taken as the area under the secant modulus in positive displacement. The equivalent viscous damping ratio, ζ_e, is given by

$$\zeta_e = \frac{\Delta W}{4\pi W_s} \tag{3-2}$$

where ΔW is the energy dissipated per cycle or the area bounded by the hysteresis loop. Then, the equivalent viscous damping ratio is expressed as

(Watanabe and Tochigi, 1985)

$$\zeta_e = \frac{2}{\pi} \frac{1-\alpha}{1+\alpha(y_o-1)} \frac{(y_o-1)}{y_o} \qquad (3\text{-}3)$$

where α is the ratio of the post-yielding stiffness, k_2, to the elastic (initial) stiffness, k_1, and y_o is the ratio of the displacement, u_o, to the yield displacement, u_y, i.e. $y_o = u_o/u_y$.

3.2.2 Equivalent Linearization for Earthquake Excitation

Several models have been proposed for earthquake excitation (Hadjian, 1982). Of these, the Iwan model (Iwan, 1980) is selected for use. Iwan analyzed six non-linear systems subjected to an ensemble of twelve earthquakes and computed the inelastic response spectra. From these spectra, he proposed effective linear period and damping parameters as a function of the ductility ratio. The empirical relationships for the period and damping are

$$\frac{T_e}{T_o} = 1 + 0.121(y_o-1)^{0.939} \qquad (3\text{-}4)$$

and

$$\zeta_e = \zeta_o + 0.0587(y_o-1)^{0.371} \qquad (3\text{-}5)$$

where T_e is the equivalent linear period, T_o is the initial period (associated with the elastic stiffness), ζ_e is the equivalent damping, ζ_o is the viscous damping at small amplitudes ($y_o \simeq 1$) and $y_o = u_o/u_y$ is the ductility ratio.

CHAPTER 4

FOUNDATION IMPEDANCE FUNCTIONS

4.1 IMPEDANCE FUNCTIONS FOR RECTANGULAR FOOTINGS

In order to study the dynamic interaction between structures and the supporting soil (soil-structure interaction), it is necessary to determine the impedance functions of the soil. In its basic form, the approach typically consists of evaluating the steady-state force-displacement relationship of a massless foundation resting on a viscoelastic halfspace.

Wong and Luco (1976) presented a method that was applicable to flat rigid foundations of arbitrary shape placed on the surface of an elastic medium. The contact area, between the foundation and soil, was divided into sub-regions (squares). The contact stresses (of unknown magnitude) were assumed to be uniform within each sub-region. The displacements were cast in terms of these uniform stresses with the displacement boundary conditions taken into account. After evaluating the contact stresses, the forces on the massless foundation were computed and the force-displacement relation was determined. The authors found good agreement between their results and Luco and Westman's (1971) solution for a circular foundation. This technique became widely used. In a subsequent report (1978), the authors compiled an extensive list of impedance functions for rectangular foundations of different aspect ratios and varying soil parameters. The method described above (Wong and Luco, 1976) was used in their evaluation.

Pais and Kausel (1985) used regression analysis to fit polynomial

expressions to selected numerical results. The impedance function for rectangular surface foundations can be expressed in general as

$$K^d = (K_1 + iK_2) = K_s(\bar{k} + ia_o\bar{c}) \qquad (4\text{-}1)$$

where K^d is the impedance function (dynamic stiffness), K_1 is the real (in-phase) stiffness, K_2 is the imaginary (out-of-phase) component related to the damping in the medium, K_s is the static stiffness of the foundation, and $\bar{k}$ and $\bar{c}$ are dimensionless stiffness and damping coefficients respectively. The dimensionless frequency, a_o, is defined as

$$a_o = \frac{\omega B}{V_s} \qquad (4\text{-}2)$$

in which V_s is the shear wave velocity of the medium, B is the half-width of the foundation and ω is the circular frequency. The equivalent viscous damping is given by

$$c = \frac{K_2}{\omega} = \frac{K_s a_o \bar{c}}{\omega} = \frac{K_s B \bar{c}}{V_s} \qquad (4\text{-}3)$$

The 'real' stiffness is given by

$$K = K_s \bar{k} \qquad (4\text{-}4)$$

Using the above equations, the polynomial expressions proposed by Pais and Kausel are restated as follows:

Vertical vibration

$$K_v = K_{sv}\,\bar{k}$$

$$K_{sv} = \frac{GB}{(1-\nu)}\,[3.1(L/B)^{0.75} + 1.6]$$

$$\bar{k} = 1.0\,\frac{d\,a_o^2}{b+a_o^2} \qquad (4\text{-}5)$$

$$d = 0.4 + \frac{0.2}{L/B}$$

$$b = \frac{1.0}{1+3\left(\frac{L}{B} - 1\right)}$$

$$c_v = \frac{GB^2}{V_s}\left(3.4 + \frac{L}{B}\right)$$

Horizontal vibration

$$K_u = K_{su}\bar{k}$$

$$K_{su} = \frac{GB}{(2-\nu)}\left[6.8\left(\frac{L}{B}\right)^{0.65} + 2.4\right] \qquad (4\text{-}6)$$

$$\bar{k} = 1.0$$

$$c_u = \frac{GB^2}{V_s}\left(\frac{4L}{B}\right)$$

Rocking vibration

$$K_\psi = K_{s\psi}\bar{k}$$

$$K_{s\psi} = \frac{GB^3}{(1-\nu)}\left[3.73\left(\frac{L}{B}\right)^{2.4} + 0.27\right] \qquad (4\text{-}7)$$

$$\bar{k} = 1.0 - \frac{0.55a_o^2}{b+a_o^2}$$

$$b = 0.6 + \frac{1.4}{(L/B)^3}$$

$$c_\psi = \frac{GB^4}{V_s}\left[\frac{4a}{3}\left(\frac{L}{B}\right)^3 \frac{a_o^2}{f+a_o^2}\right]$$

$$f = \frac{1.8}{1.0 + 1.75(\frac{L}{B} - 1)}$$

In the above formulae L is the half-length, the coefficient, a, is

$$a = \sqrt{2(1-\nu)/(1-2\nu)} \quad , \quad a \geq 2.45 \qquad (4\text{-}8)$$

where ν = Poisson's ratio of soil and subscripts v, u and θ refer to vertical translation, horizontal translation and rocking respectively (Figure 4.1). In this study, square foundations are assumed (L/B = 1). Pais and Kausel compared the impedance functions of a square foundation with the results of Wong and Luco. The graphs are reproduced in Figure 4.2.

For the buildings considered (Chapter 5), the dimensionless frequency is less than 0.6. The approximate and numerical formulae compared well over this range except for the imaginary component of the vertical impedance function (Figure 4.2).

Material damping in the medium may be incorporated approximately by the correspondence principle in lieu of using the complex shear modulus. The complex stiffnesses described in the above equations are multiplied by $(1+i2\beta)$. The material damping ratio, β, is related to the loss angle, δ, by

$$\beta = \frac{1}{2} \tan\delta = \frac{1}{2} \frac{G'}{G} \qquad (4\text{-}9)$$

in which G' and G are the imaginary and real components of the complex shear modulus respectively. Performing the multiplication and separating the real and imaginary parts gives once more the true stiffness, K', and

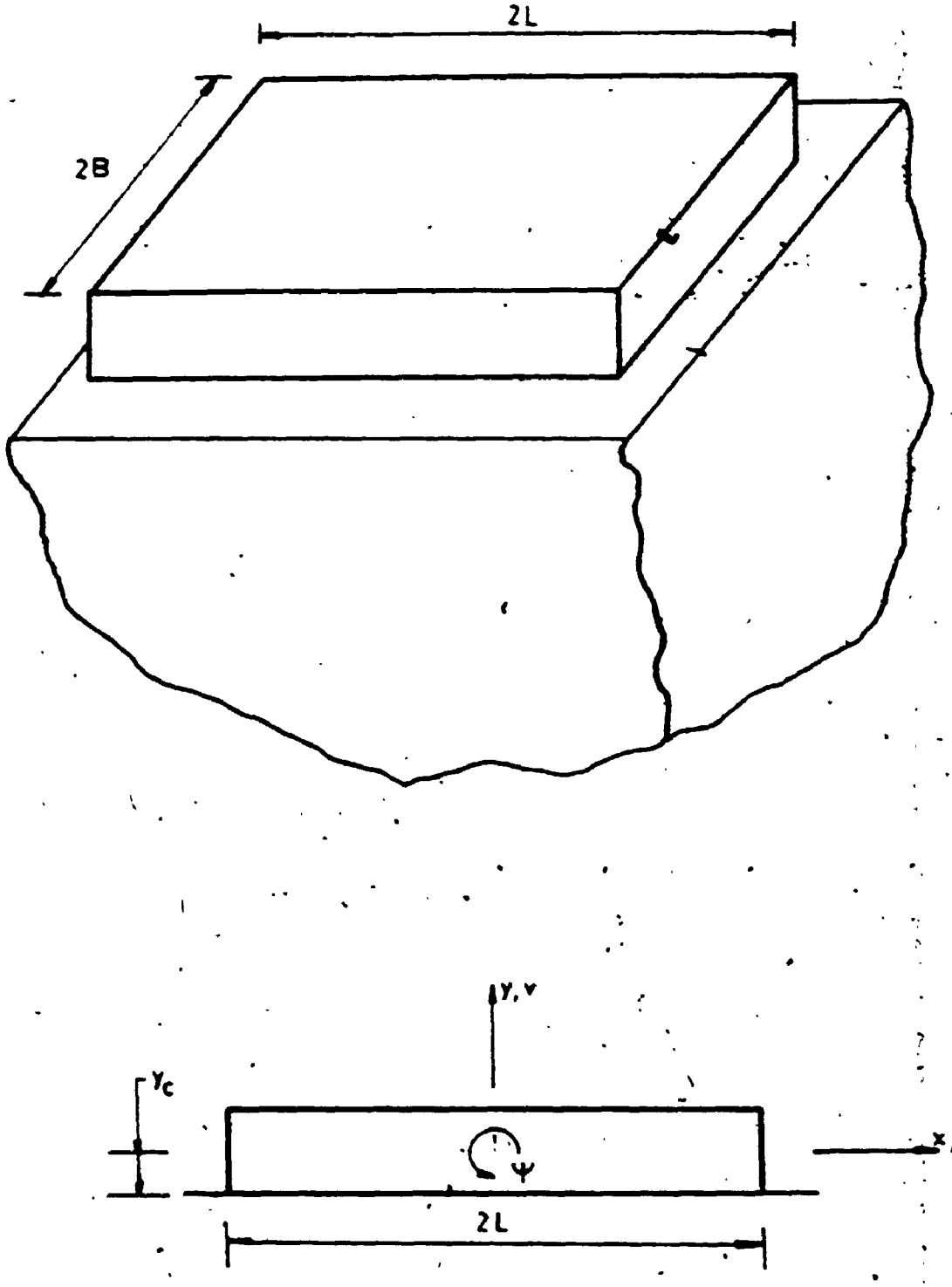

FIGURE 4.1 Rectangular surface foundation

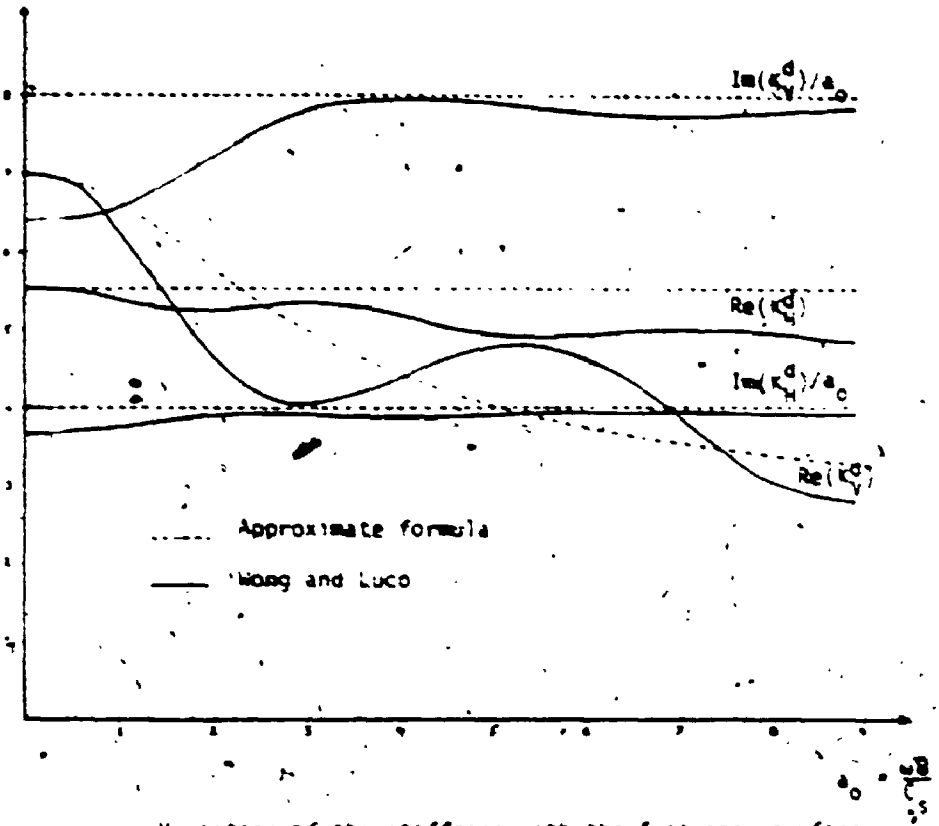

Variation of the stiffness with the frequency-surface foundation L/B = 1. (vertical and horizontal modes)

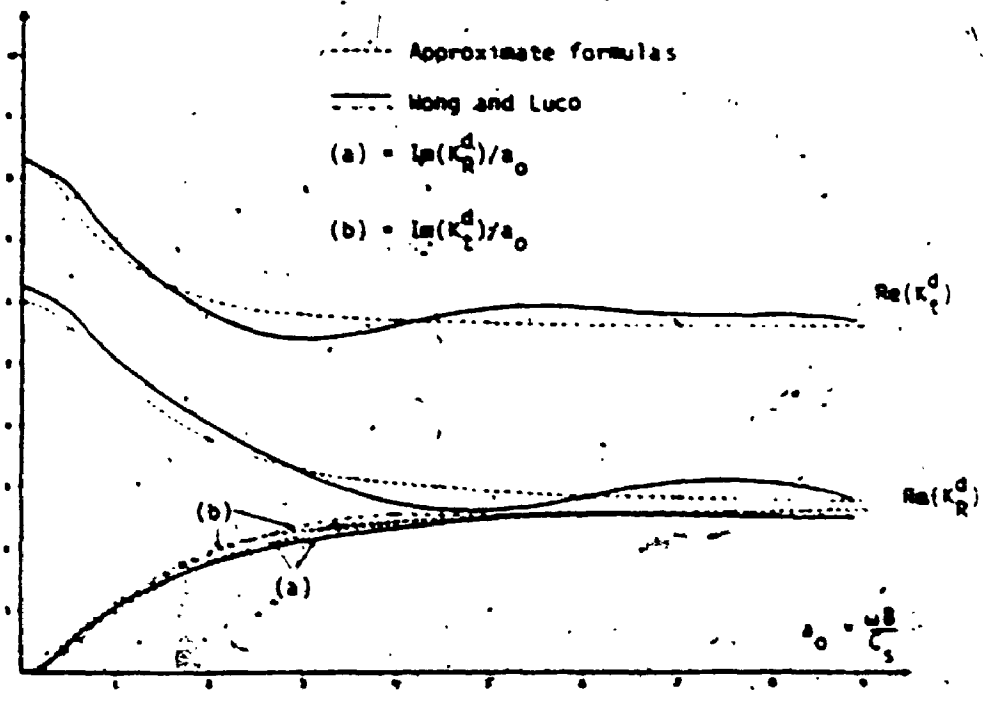

Variation of the stiffness with the frequency-surface foundation L/B = 1 (rocking and torsion)

FIGURE 4.2 Impedance functions for a square foundation (Pais and Kausel, 1985)

the equivalent viscous damping constant, c'. The adjustment to the above equations is

$$K' = K - 2\beta c\omega$$
$$c' = c + \frac{2\beta K}{\omega} \qquad (4\text{-}10)$$

For this study the frequency, ω, was taken as the fundamental natural frequency, ω_1. Equations 4.10 are adequate for low dimensionless frequencies. For higher frequencies, the complex shear modulus has to be included in a_0 also.

The equations described so far were derived with reference to the centre of the base of the foundation (foundation-soil interface). For computational purposes, it is desirable to use the centre of mass of the foundation as the reference point. The stiffness and damping matrices are transformed to this reference point by the following expressions

$$[K] = [T]^T[K'][T]$$
and $$(4\text{-}11)$$
$$[c] = [T]^T[c'][T]$$

where the transformation matrix [T] is given by

$$[T] = \begin{bmatrix} 1. & \bar{y}_c & 0 \\ 0 & 1. & 0 \\ 0 & 0 & 1. \end{bmatrix} \qquad (4\text{-}12)$$

with the displacements taken in order as u, ψ and v at the centre of mass, distant y_c from the surface of the medium.

Many other data on impedance functions are also available. For large foundations, a layered halfspace should be assumed instead of the homogeneous one.

4.2 SOIL-STRUCTURE INTERACTION WITH DYNAMIC INTERACTION OF FOOTINGS

The buildings considered in this study rest on individual footings (Chapter 5; Figures 5.1 and 5.2). In computing the foundation impedance functions, the cross-interaction of the footings is first neglected resulting in a tridiagonal impedance matrix. Dynamic interaction (dynamic cross-interaction) depends on the frequency of vibration, the inertia, size and separation of the footings, and the flexibility of the footings and its effect in altering the displacement field. The cross impedances are oscillatory, with sign reversals, depending on the frequency of vibration (i.e., the wavelength of the waves generated in the medium) and the separation of the adjacent footings. Therefore, cross-interaction may increase or decrease the stiffness and damping coming from the soil.

When computing the flexibility matrix for footing-soil-footing interaction analysis, footing inertia as well as the influence of the adjacent footings on the displacement field are neglected. The displacement under the rigid base is computed at a representative location of the displacement field due to a flexible footing and the displacements (flexibilities) of the other footings and established at the centre of each of them. An elastic halfspace is assumed.

4.2.1 Displacement Field at the Halfspace Surface

Consider a halfspace loaded over a rectangular surface element by a vertical dynamic pressure (Figure 4.3)

$$\sigma_{yy}(x,y=0,z,t) = \begin{cases} -\bar{p}\exp(i\omega t) & \left|\frac{x}{a}\right|, \left|\frac{z}{b}\right| \leq 1, \\ 0 & \left|\frac{x}{a}\right|, \left|\frac{z}{b}\right| > 1 \end{cases} \qquad (4\text{-}13)$$

in which the amplitude of the complex dynamic pressure

$$\bar{p} = \frac{\bar{F}}{ab} \qquad (4\text{-}14)$$

$\bar{F}$ is the amplitude of the harmonic load and a and b are the half-widths of the loaded area. The dynamic vertical displacement field at the half-space surface is written as

$$v(x,o,z,t) = v(x,z)\exp(i\omega t) \qquad (4\text{-}15)$$

in which the amplitude of the displacement is

$$v(x,z) = \frac{\bar{F}}{aG}\left[f(x,z) + ig(x,z)\right] \qquad (4\text{-}16)$$

G is the soil shear modulus and f and g are the real and imaginary parts, respectively, of the complex compliance. Gaul (1977) presented the following solution for the vertical displacement in which material damping of the soil is incorporated by complex Lamé moduli:

$$v(x,o,z,t) = v(x,z)\exp(i\omega t)$$

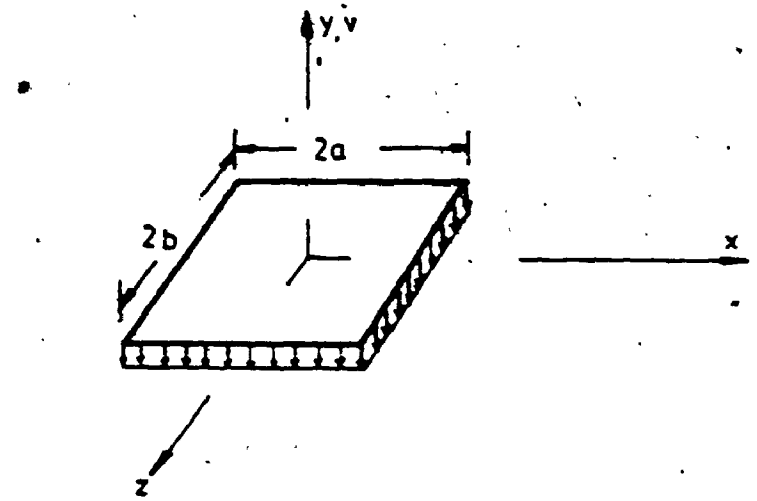

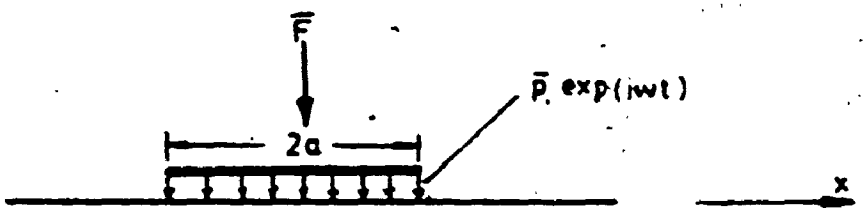

FIGURE 4.3 A rectangular loaded element resting on a viscoelastic halfspace

$$\frac{v(x,z)aG}{F} = f(x,z)+ig(x,z) = \frac{2}{(2\pi)^2}\int_{K_v=0}^{\infty} A_0 K_v \overset{*}{H}(K_v)$$

$$\left[\int_{\theta=0}^{\pi/2} T(A_0K_v,\theta)d\theta\right]dK_v$$

$$\overset{*}{H}(K_v) = \frac{\bar{v}G\overset{*}{K}_v}{\bar{\sigma}} = \frac{U_D\left[-(1-n^2(\omega))\cos\frac{\phi_D}{2} - 2n(\omega)\sin\frac{\phi_D}{2} + \right.}{(1+n^2(\omega))[2K_v^2-1)^2-n^2(\omega)-4K_v^2U_SU_D\cos(\frac{\phi_S+\phi_D}{2}) +}$$

$$\left.\frac{i<-(1-n^2(\omega))\sin\frac{\phi_D}{2} + 2n(\omega)\cos\frac{\phi_D}{2}>]}{i<2n(\omega)(2K_v^2-1)-4K_v^2U_SU_D\sin(\frac{\phi_S+\phi_D}{2})>]}\right.$$

$$a_o = \frac{\omega a}{V_s} \quad U_D = [(K_v^2-n^2)^2+(n^2n(\omega))^2]^{1/4} \quad \phi_D = \arctan\frac{n^2\eta(\omega)}{K_v^2-n^2}, \quad 0\leq\phi_D<\pi$$

$$A_o = \frac{a_o}{[1+n^2(\omega)]^{1/2}} \quad U_S = [(K_v^2-1)^2+n^2(\omega)]^{1/4} \quad \phi_S = \arctan\frac{n(\omega)}{K_v^2-1}, \quad 0\leq\phi_S<\pi$$

$$T(A_0K_v,\theta) = \sum_{i,k=1}^{2}(-1)^{i+k}\frac{\sin(a_iA_0K_v\cos\theta)\sin(b_kb_oA_oK_v\sin\theta)}{(A_0K_v\cos\theta)(b_oA_oK_v\sin\theta)} \quad n^2 = \frac{1-2\nu}{2(1-\nu)}$$

$$b_o = b/a \quad a_{1,2} = (x/a \pm 1) \quad b_{1,2} = (z/b \pm 1) \qquad (4\text{-}17)$$

In the above expressions, a_o is the dimensionless frequency, ω is the angular frequency, V_s is the soil shear wave velocity, ν is Poisson's ratio and $\eta(\omega)$ is the material damping parameter. For the constant hysteretic model, $\eta(\omega) = \eta$, and the complex shear modulus is $G^* = G(1+i\eta)$. The damping ratio, $\beta = \eta/2$, and η is, therefore, the tangent of the loss angle. Analogous expressions can be written for the vertical and rocking compliances.

4.2.2 Foundation Compliance and Impedance Matrices

Suen (1987) compared Gaul's (1977) compliance functions for a square rigid base with compliance functions of a flexible base at a representative location, (2a/3, 2b/3), and by averaging over nine points. The three solutions agree well for low dimensionless frequency, $a_o \leq 0.5$. Therefore, the compliance of the loaded rigid footing is computed from the complex displacement at this representative location while the compliance of adjacent footings is computed from the complex displacement at their centres.

For a set of n footings, supporting a plane frame, the foundation compliance matrix is complex, symmetric and of dimension 3n x 3n, i.e.

$$[F_f] = \begin{vmatrix} [f]_{11} & \cdots & [f]_{1i} & \cdots & [f]_{1n} \\ \vdots & & \vdots & & \vdots \\ [f]_{i1} & \cdots & [f]_{ii} & \cdots & [f]_{in} \\ \vdots & & \vdots & & \vdots \\ [f]_{n1} & \cdots & [f]_{ni} & \cdots & [f]_{nn} \end{vmatrix} \qquad (4\text{-}18)$$

The 3 x 3 diagonal submatrices, $[f]_{ii}$, are the compliances of the individual footings for vertical translation, v, horizontal translation, u, and rocking, ψ, at the footing-soil interface. The off-diagonal submatrices, $[f]_{ij}$, are the cross-compliances of the adjacent footings. When a footing is subjected to a load in any one degree-of-freedom, the adjacent footings undergo displacements in all three degrees-of-freedom. Inverting the complex compliance matrix $[F_f]$ gives the complex impedance matrix $[K_f]$. The stiffness of the foundation, $[k_f]$, is the real part of $[K_f]$ and the foundation damping matrix is

$$[c_f] = Im[K_f]/\omega_j \qquad (4\text{-}19)$$

where ω_j is the natural frequency of the jth vibration mode.

CHAPTER 5

FREE VIBRATION ANALYSIS OF STRUCTURE-ISOLATOR-SOIL SYSTEMS

5.1 INTRODUCTION

Modal superposition is a common technique for the dynamic analysis of structures. The first step is the free vibration analysis. There are two types of free vibration analysis; analysis of undamped modes and analysis of damped modes. The first one yields the normal modes and natural frequencies. It is usual to perform the undamped analysis, classical analysis, and to assign the damping to each vibration mode more or less arbitrarily. The mode shapes, eigenvectors, feature stationary nodes with every point attaining its maximum displacement simultaneously. The damped modal analysis may assume proportional, Rayleigh, damping ($[c] = \alpha[m] + \beta[k]$) in which case the mode shapes are the same as the undamped modes but the natural frequencies are reduced. This reduction is small for the damping usually encountered in structures.

Non-classical analysis incorporates non-proportional damping. The vibration modes thereby obtained are complex and no longer feature stationary nodal points. Also, the maximum displacements are not attained simultaneously but feature phase shifts. The damping due to soil is non-proportional. A non-classical free vibration analysis reveals the damping acquired by each mode in a mathematically accurate way.

Regardless of the type of dynamic analysis chosen, a free vibration analysis is usually carried out. It reveals the vibration characteristics

of the structure and enables the modification of mass, stiffness, and in some instances damping, before a dynamic analysis of response to loads is carried out. The first few modes of vibration can be used in a modal analysis as a check for subsequent analyses.

5.2 EQUATIONS OF MOTION AND THEIR SOLUTION

5.2.1 Equations of Motion

The equations of motion of an n degree-of-freedom system may be written in matrix form as

$$[m]\{\ddot{x}\} + [c]\{\dot{x}\} + [k]\{x\} = \{p(t)\} \qquad (5\text{-}1)$$

where [m], [c] and [k] are nxn mass, damping and stiffness matrices respectively, $\{p(t)\}$ is the nxl vector of excitation, and $\{x\}$, $\{\dot{x}\}$ and $\{\ddot{x}\}$ refer to the nxl vectors of displacement, velocity and acceleration respectively. The damped free vibration equations are obtained by setting the excitation vector to zero, giving

$$[m]\{\ddot{x}\} + [c]\{\dot{x}\} + [k]\{x\} = \{0\} \qquad (5\text{-}2)$$

For the undamped free vibration analysis, the damping matrix and the velocity vector are dropped from Equation (5-2).

When lumped masses are used the mass matrix [m] is diagonal with the diagonal elements associated with the rotational degrees of freedom being zero if rotary inertia is neglected. For the consistent mass approach, the matrix [m] contains off diagonal terms. In soil-structure interaction, rotary inertia of the foundation is included. The stiffness

matrix is generally sparse or banded.

In general, there are six degrees-of-freedom at each joint (node), three translations and three rotations. In this study, a plane frame system with three degrees-of-freedom (one horizontal translation, one vertical translation and one rotation) at each joint is considered. If the degrees of freedom are numbered sequentially from the top of the structure down to the base, the following forms of the matrices occur:

$$[m] = \begin{matrix} m_s & \\ & [m_f] \end{matrix} \quad ; [c] = \begin{matrix} c_s & \\ & [c_f] \end{matrix} \quad ; [k] = \begin{matrix} k_s & \\ & [k_f] \end{matrix} \qquad (5\text{-}3)$$

where the subscripts f refer to the foundation and s refers to the superstructure. Mass, stiffness and damping terms of the superstructure occupy the entire matrices while the terms associated with the foundation are assembled (added) in their corresponding degrees-of-freedom. The foundation stiffness and damping matrices are frequency dependent. Therefore, the assembled stiffness and damping matrices with soil-structure interaction are frequency dependent. To avoid solving the non-linear eigenvalue problem, the foundation impedances are assumed to be frequency independent and the eigenvalue solution is obtained iteratively.

The number of equations obtained are large, requiring much computer time for the solution of the eigenvalue problem. Usually, one is interested in only the first few vibration modes. It is therefore appropriate to reduce the number of equations required to be solved. This can be done by assembling all the degrees-of-freedom and condensing the matrices before the solution of the eigenvalue problem is performed.

5.2.2 Reduction of Mass, Stiffness and Damping Matrices

Static condensation has been used in structural analysis to reduce the number of equations to be solved (Gnaedinger and Neville, 1978 and Wilson, 1974). The degrees-of-freedom to be retained are called masters while those eliminated are called slaves. The equilibrium equations, $F = [k] x$, can be partitioned such that

$$\begin{Bmatrix} F_m \\ F_s \end{Bmatrix} = \begin{bmatrix} k_m & k_{ms} \\ k_{sm} & k_s \end{bmatrix} \begin{Bmatrix} x_m \\ x_s \end{Bmatrix} \qquad (5\text{-}4)$$

By symmetry $[k_{sm}]$ is the transpose of $[k_{ms}]$ where m refers to masters and s to slaves. The forces, F_s, are zero. The slaves, x_s, can be eliminated from Equation (5-4) to give

$$\{F_m\} = ([k_m] - [k_{ms}][k_s]^{-1} [k_{sm}]) \{x_m\} \qquad (5\text{-}5)$$

Thus, the condensed stiffness matrix is

$$[k_c] = [k_m] - [k_{ms}] [k_s]^{-1} [k_{sm}] \qquad (5\text{-}6)$$

Equation (5-5) is equivalent to a coordinate transformation

$$\{x\}_{nx1} = [T]_{nxm} \{x_m\}_{mx1} \qquad (5\text{-}7)$$

where the transformation matrix [T] is given by

$$[T] = \begin{bmatrix} [I] \\ -[k_s]^{-1} [k_{sm}] \end{bmatrix} \qquad (5\text{-}8)$$

where I is the unit matrix of dimensions mxm.

The triple products in this equation reduce to real constants which are greater than or equal to zero for forces opposing the motion. Defining these products as

$$\{\phi_j^*\}^T [m]\{\phi_j\} = M_j$$

$$\{\phi_j^*\}^T [k]\{\phi_j\} = K_j$$

$$\{\phi_j^*\}^T [c]\{\phi_j\} = C_j \qquad (5\text{-}19)$$

the roots (complex conjugate eigenvalue pairs) of Equation (5-18) for mode j can be expressed as

$$\mu_{1,2} = -\frac{C_j}{2M_j} \pm i \frac{\sqrt{(4M_jK_j - C_j^2)}}{2M_j} \qquad (5\text{-}20)$$

Rewriting this equation as

$$\mu_{1,2} = -\zeta_j \bar{\omega}_j \pm i \bar{\omega}_j \sqrt{(1-\zeta_j^2)} \qquad (5\text{-}21a)$$

or

$$\mu_{1,2} = -\zeta_j \bar{\omega}_j \pm i \omega_j' \qquad (5\text{-}21b)$$

where,

$$\bar{\omega}_j = \sqrt{K_j/M_j} = |\mu_j| \qquad (5\text{-}22)$$

the damping ratio in the jth mode is

$$\zeta_j = \frac{C_j}{2\bar{\omega}_j M_j} = -\frac{\text{Re } \mu_j}{|\mu_j|} \qquad (5\text{-}23)$$

and the damped circular natural frequency in the jth mode is

$$[c_r] = [c_m] - [c_{ms}][k_s]^{-1}[k_{sm}] - [[k_s]^{-1}[k_{sm}]]^T$$

$$\times [[c_{sm}]^T - [c_s][k_s]^{-1}[k_{sm}]] \qquad (5\text{-}9c)$$

Equations (5-9a) and (5-9c) reduce to Equation (5-9b) ~~if k is~~ substituted for m and c respectively. Once the reduced mass, stiffness and damping matrices are evaluated the solution of the eigenvalue problem can be obtained.

5.2.3 Modal Damping Using the Complex Eigenvalue Analysis

The solution of the damped (nonconservative) free vibration equations is called a complex eigenvalue analysis. The eigenvalues and eigenvectors obtained are complex and the eigenvalues can be used to establish the damping in each mode.

The, n, second order differential equations (Equation 5-1) can be transformed into a 2n first order system (Pipes, 1969; Fraser, 1946; Veletsos, 1986; Novak, 1983; Foss, 1958)

$$[A]\{\dot{z}\} + [B]\{z\} = \{F(t)\} \qquad (5\text{-}10)$$

where

$$\{z\} = \begin{Bmatrix} \{\dot{x}\} \\ \{x\} \end{Bmatrix}, \quad \{F(t)\} = \begin{Bmatrix} \{0\} \\ \{p(t)\} \end{Bmatrix}$$

and

$$[A] \begin{bmatrix} [0] & [m] \\ [m] & [c] \end{bmatrix}, \quad [B] = \begin{bmatrix} -[m] & [0] \\ [0] & [k] \end{bmatrix}$$

displacements of the joints. The isolators are assumed massless. The footings are treated as rigid bodies and thus possess both mass and mass moments of inertia.

5.4.2 The Structure

The stiffness of the beams and columns is computed from the usual stiffness matrix for elastic plane frame members (Weaver, 1980), matrix [K].

Hysteretic behaviour of the members is modelled by a complex elastic modulus

$$E^* = E + iE' \qquad (5\text{-}27)$$

where the real (in-phase) elastic modulus, E, is complemented by an imaginary (out-of-phase) component E'. The dimensionless ratio E' E is expressed in terms of the loss angle, δ, as

$$\tan\delta = \frac{E'}{E} \qquad (5\text{-}28)$$

or in terms of the material damping ratio assumed to be frequency independent and defined as

$$\beta = \frac{E'}{2E} = \frac{\Delta W}{4\pi W_s} \qquad (5\text{-}29)$$

in which ΔW is the area bounded by the hysteretic loop and W_s is the strain energy. Then, the complex elastic modulus is

$$E^* = E(1 + i2\beta) \qquad (5\text{-}30)$$

where μ is a parameter (eigenvalue) and $\{C\}$ a 2n column vector. Substituting (5-14) in (5-13) and dropping the exponential term we have the complex eigenvalue problem

$$([D] - \mu[I])\{C\} = \{0\} \tag{5-15}$$

which can be solved by a suitable subroutine e.g. EISPACK's RGG. The non-trivial solution of Equation (5-15) requires that

$$\det([D] - \mu[I]) = \{0\} \tag{5-16}$$

Equation (5-16) is of 2nth degree in μ. The 2n roots of the equation are complex eigenvalues which occur as complex conjugate pairs if the coefficients are real numbers with corresponding complex conjugate eigenvectors. Each eigenvalue has a negative or zero real part. For high values of damping the imaginary part of the eigenvalue becomes zero.

The lower n elements of the eigenvector $\{C\}$ represent the modal displacements $\{\phi\}$, while the upper n elements are the modal velocities, $\{\dot{\phi}\}$. The displacements of the system in mode j are given by

$$\{x_j\} = \{\phi_j\} e^{\mu_j t} \tag{5-17}$$

Substituting in the free vibration equation (5-2) and premultiplying by $\{\phi_j^*\}^T$, the transpose of the jth conjugate mode gives

$$(\{\phi_j^*\}^T[m]\{\phi_j\})\mu^2 + (\{\phi_j^*\}^T[c]\{\phi_j\})\mu + (\{\phi_j^*\}^T[k]\{\phi_j\}) = \{0\} \tag{5-18}$$

The triple products in this equation reduce to real constants which are greater than or equal to zero for forces opposing the motion. Defining these products as

$$\{\phi_j^*\}^T [m]\{\phi_j\} = M_j$$

$$\{\phi_j^*\}^T [k]\{\phi_j\} = K_j$$

$$\{\phi_j^*\}^T [c]\{\phi_j\} = C_j \qquad (5\text{-}19)$$

the roots (complex conjugate eigenvalue pairs) of Equation (5-18) for mode j can be expressed as

$$\mu_{1,2} = -\frac{C_j}{2M_j} \pm i \frac{\sqrt{(4M_jK_j - C_j^2)}}{2M_j} \qquad (5\text{-}20)$$

Rewriting this equation as

$$\mu_{1,2} = -\zeta_j \bar{\omega}_j \pm i \bar{\omega}_j \sqrt{(1-\zeta_j^2)} \qquad (5\text{-}21a)$$

or

$$\mu_{1,2} = -\zeta_j \bar{\omega}_j \pm i \omega_j' \qquad (5\text{-}21b)$$

where,

$$\bar{\omega}_j = \sqrt{K_j/M_j} = |\mu_j| \qquad (5\text{-}22)$$

the damping ratio in the jth mode is

$$\zeta_j = \frac{C_j}{2\bar{\omega}_j M_j} = -\frac{\text{Re } \mu_j}{|\mu_j|} \qquad (5\text{-}23)$$

and the damped circular natural frequency in the jth mode is

$$\omega_j = \bar{\omega}_j \sqrt{1-\zeta_j^2} = \text{Im } \mu_j \qquad (5\text{-}24)$$

The complex eigenvector, $\phi = \phi_1 + i\phi_2$, has a phase shift

$$\theta = \arctan \frac{\phi_2}{\phi_1} \qquad (5\text{-}25)$$

For non-classical damping, the imaginary components are non-zero and the phase shift changes from station to station. There are no stationary nodal points and the maximum or minimum displacements do not occur at all points at the same instant.

Damping satisfying the identity (Caughey and O'Kelly, 1965)

$$[c][m]^{-1}[k] = [k][m]^{-1}[c] \qquad (5\text{-}26)$$

is termed classical Rayleigh damping. $[c] = \alpha[m] + \beta[k]$, is a particular case of Equation (5-26). For classical damping, the eigenvectors are real ($\phi_2 = 0$) and are identical to the undamped modes. Then the modulus of the eigenvalue, $\bar{\omega}_j$, is equal to the undamped circular natural frequency.

5.3 BUILDINGS ANALYZED

Figures 5.1 and 5.2 show the plane frames that are analyzed. The buildings are reinforced concrete of monolithic construction. The columns are of constant square cross-section throughout the height of the buildings. The beams on the first and second floors are deeper to reflect the greater loads stipulated in building codes for these floors. The effective slab width acting as a T-beam is taken as one quarter the

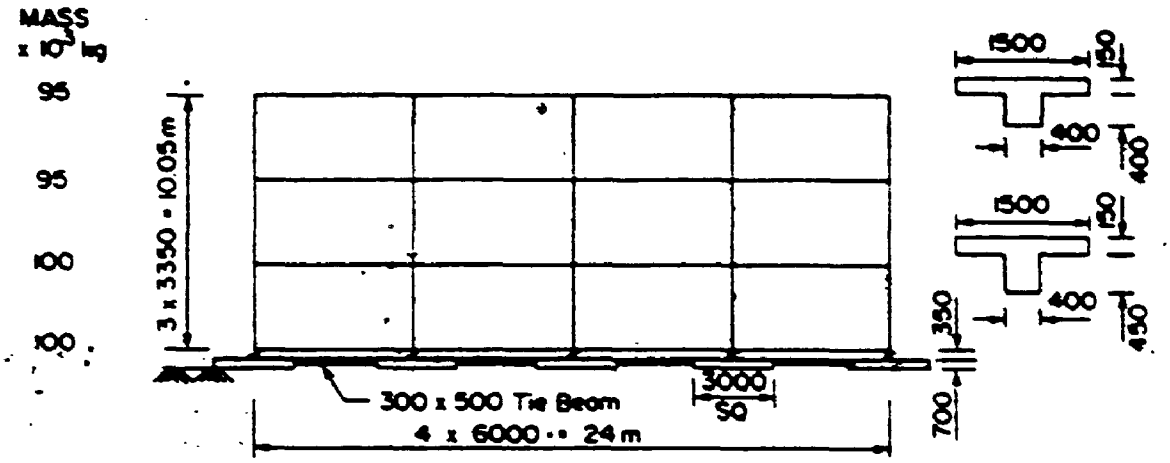

FIGURE 5.1 Three-storey base-isolated building

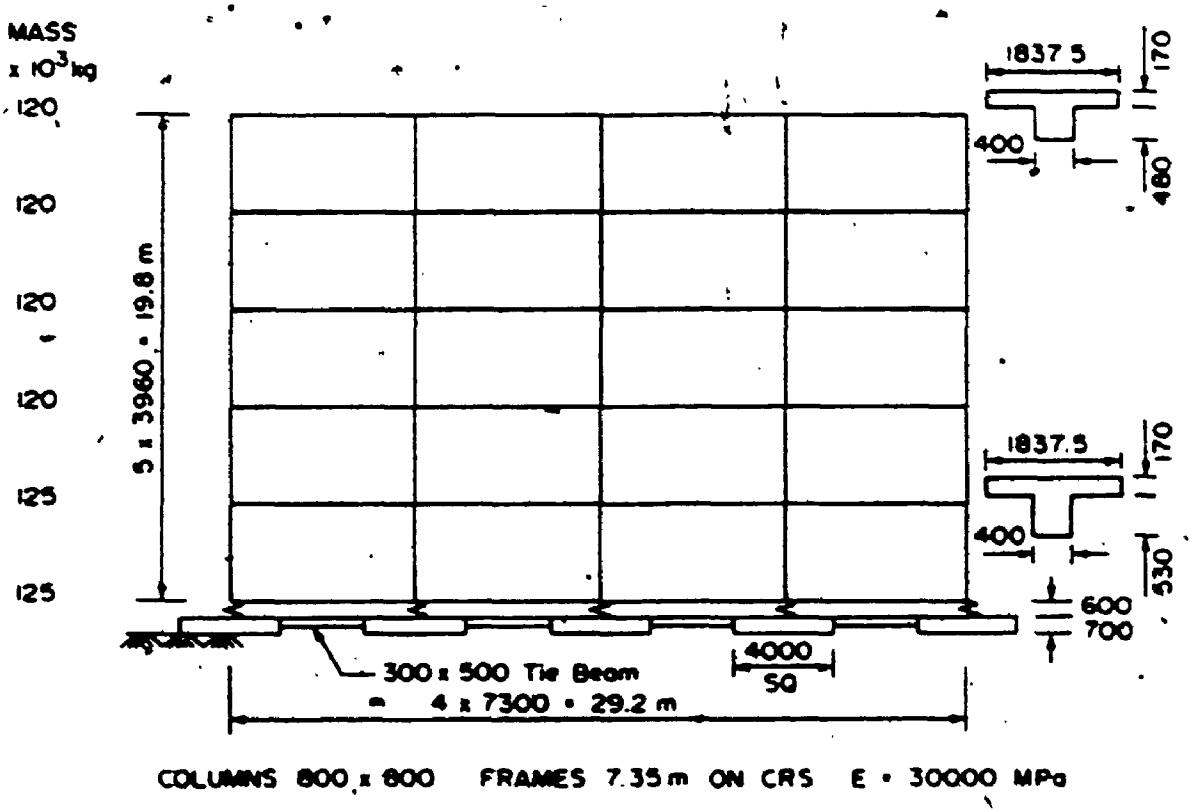

FIGURE 5.2 Five-storey base-isolated building

centre-to-centre distance of frames. The gross cross-sections are used in computing the moment of inertia and cross-sectional area. No reductions are applied to these values as the superstructure of base-isolated buildings are expected to remain elastic during an earthquake.

The base isolators are capable of displacing in the horizontal and vertical directions and also in rotation. The rotational stiffness is initially assumed to be zero as it was found that its inclusion did not influence the results. The ratio of the vertical to the horizontal stiffness is varied to reflect the type of isolator being used. The horizontal stiffness is selected to provide effective isolation of the building.

The footings are square and are connected by tie beams. The soil is a viscoelastic halfspace with shear wave velocity, V_s, of 150 m/s and a bearing capacity between 100-120 KPa. For the unisolated building, the shear wave velocity is varied between 100 and 350 m/s.

The floors of the building are taken as rigid diaphragms. Consequently, all joints on each floor have the same horizontal translation. The same constraint is applied to the footings which are connected by tie beams. A relaxation of the footing constraint proved this assumption to be well justified.

5.4. MASS, STIFFNESS AND DAMPING MATRICES

5.4.1 The Masses

The mass of the floors and columns is lumped at the nodes on each floor. The floor rotational inertia is accounted for through vertical

displacements of the joints. The isolators are assumed massless. The footings are treated as rigid bodies and thus possess both mass and mass moments of inertia.

5.4.2 The Structure

The stiffness of the beams and columns is computed from the usual stiffness matrix for elastic plane frame members (Weaver, 1980), matrix $[K_1]$.

Hysteretic behaviour of the members is modelled by a complex elastic modulus

$$E^* = E + iE' \tag{5-27}$$

where the real (in-phase) elastic modulus, E, is complemented by an imaginary (out-of-phase) component E'. The dimensionless ratio E'/E is expressed in terms of the loss angle, δ, as

$$\tan\delta = \frac{E'}{E} \tag{5-28}$$

or in terms of the material damping ratio assumed to be frequency independent and defined as

$$\beta = \frac{E'}{2E} = \frac{\Delta W}{4\pi W_s} \tag{5-29}$$

in which ΔW is the area bounded by the hysteretic loop and W_s is the strain energy. Then, the complex elastic modulus is

$$E^* = E(1 + i2\beta) \tag{5-30}$$

To account for structural damping, the complex stiffness matrix is formulated using the complex elastic modulus as

$$[K] = [K_1] + i[K_2] \tag{5-31}$$

in which the imaginary component is

$$[K_2] = 2\beta[K_1] \tag{5-32}$$

The matrix of equivalent viscous damping of structural members is defined as

$$[c_m] = \frac{[K_2]}{\omega_1} = \frac{2\beta}{\omega_1}[K_1] \tag{5-33}$$

where ω_1 is the first modal frequency. For the reinforced concrete members, the material damping ratio, β, is taken as 1%.

5.4.3 The Isolators

The force-displacement relationship of the base isolators is assumed to be governed by a bilinear hysteretic loop (Figure 3.4). The post yielding stiffness, k_2, is taken as 1.0 Wt per metre with Wt being the weight of the building. This stiffness represents the summation of the horizontal stiffnesses of the isolators. The initial stiffness, k_1, is 5 k_2 and the yield force, P_y, is 0.05 Wt.

Two levels of the displacement u_0 are considered and termed small strain and large strain. For the first level of displacement, small strain, the isolators remain in the elastic range and their horizontal stiffness is equal to the initial stiffness, k_1. This state is for

displacements $\leq$10 mm expected under wind loading or small earthquakes. For the second level of displacement (large strain), expected under design earthquake loading, the isolators undergo large displacements for which a nominal value of 300 mm is adopted.

The vertical stiffness of isolators is typically 100 to 400 times the horizontal stiffness. A vertical stiffness of 200 times the horizontal stiffness is chosen for the isolated or no rocking case. In addition, the buildings are analyzed with a much smaller vertical stiffness of the isolators equal to twice the horizontal stiffness. This case involves the building rocking as well as sliding.

The area of the hysteretic loop is a measure of the energy dissipated in the isolators. The hysteretic loop indicated in Figure 3.4 implies nonlinearity. However, the complex eigenvalue approach presumes linearity and viscous damping. For large strains, an equivalent linear stiffness of 1.13 Wt per metre and an equivalent viscous damping ratio of 7.2% is computed using the geometric stiffness method outlined in Chapter 3. For small strain, the damping ratio is taken as 1%. The damping matrix is established from Equation (5-33).

5.4.4 The Foundations

The impedance functions are computed using the approximate equations of Pais and Kausel (1985), given in Chapter 4. The fundamental frequency of the building, ω_1, is used in computing the impedance functions. The footing damping and stiffness matrices thereby obtained are transformed to the centre of mass of the foundation (Equation 4-11).

Interaction between individual footings is first neglected and then examined separately.

5.5 SOLUTION PROCEDURE

Since the soil impedances and the damping of the reinforced concrete members are frequency dependent, an initial estimate of the building's fundamental frequency is made using the expression $\omega = 2\pi \times 10/N$, where N is the number of storeys. The mass, stiffness and damping matrices are assembled in global coordinates using standard algorithms (Weaver, 1980). The horizontal translations at each floor and the foundation level are taken as the master degrees-of-freedom and the others are condensed. For a building with N storeys, the number of masters is N, N+1 and N+2 for the case of a fixed base, base isolation and base isolation with soil-structure interaction respectively.

The complex eigenvalues and eigenvectors are computed using the EISPACK's RGG subroutine. The natural frequencies and modal damping ratios are computed from Equations (5-23) and (5-24). The new value of the fundamental frequency is used to compute impedance matrices and the structural damping matrix. The solution procedure is repeated until successive values of the fundamental frequency differ slightly (0.1 radian). Since the damping matrices are established using the fundamental natural frequency, the damping in the higher modes is adjusted by the factor ω_1/ω_j giving

$$\zeta_j = \zeta'_j \frac{\omega_1}{\omega_j} \qquad (5\text{-}34)$$

where ξ_j is the modal damping based on the frequency ω_j.

5.6 RESULTS

The frames shown in Figures 5.1 and 5.2 as well as two other frames, half the width (i.e. with two bays), were analyzed for the following base conditions: a) fixed base, b) frames on base isolators with no rocking (isolated), c) frames on isolators with rocking, and d) frames on isolators with no rocking and soil-structure interaction included (isolated + soil). Also, the unisolated four bay frames were analyzed with soil-structure interaction.

The variation in the damped natural frequencies and damping due to soil (soil damping) with shear wave velocity are shown in Figures 5.3 and 5.4, for the unisolated four bay frames. The variation in total damping is listed in Table 5.1. The damped natural frequencies decrease while the damping derived from the soil increases with decreasing shear wave velocity. The structural damping decreases for the softer soil which is attributed to a reduction in curvature of the superstructure caused by sliding and rocking of the foundation.

The damped natural frequencies and modal damping ratios for the fixed base and base-isolated conditions are listed in Tables 5.2 and 5.3. The following observations emerge:

Base isolation shifts the fundamental frequency of the building away from the high-energy portion of the earthquake spectrum (2 1/2-3 Hz) with the exception of deep, soft deposits where isolation is not

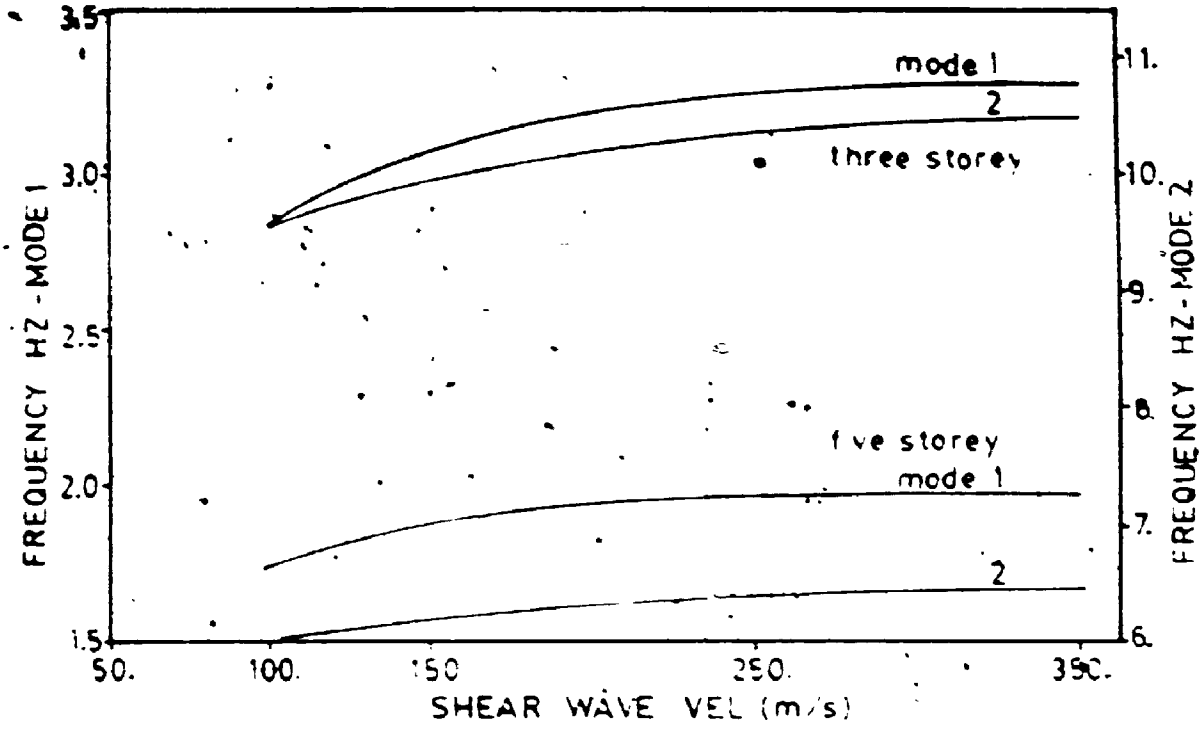

FIGURE 5.3 Variation in damped natural frequency with soil shear wave velocity - unisolated

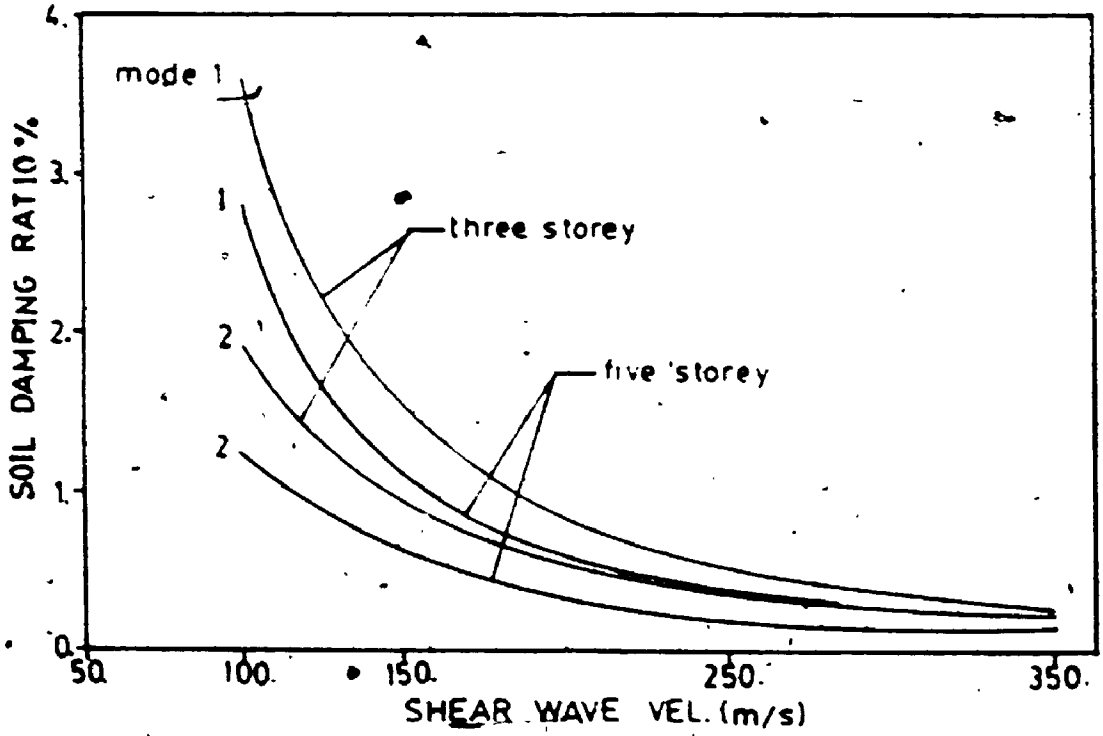

FIGURE 5.4 Variation in soil damping with soil shear wave velocity - unisolated

TABLE 5.1 Variation in total damping with soil shear wave velocity - Unisolated

	THREE STOREY - FOUR BAYS		FIVE STOREY - FOUR BAYS	
	Damping Ratio			
Shear Wave Velocity (m/s)	Mode 1	Mode 2	Mode 1	Mode 2
100	4.37	2.85	3.6	2.1
150	2.39	1.82	2.0	1.5
250	1.42	1.31	1.3	1.2
350	1.22	1.18	1.2	1.1

TABLE 5.2 Damped natural frequencies (Hz) and damping ratios (%) of base isolated three storey buildings (Isolation: k_h=5 W/m, β = 1% for small strain or k_h=1.13 W/m, β = 7.2% for large strain; k_v=200 k_h for isolated and k_v=2k_h for rocking; footing area 9 m^2; soil: V_s=150 m/s, β=5%, ν=0.25, ρ=1800 kg/m^3)

		Mode	1		2		3		4		5	
		Base	Hz	%	Hz	%	Hz	%	Hz	%	Hz	%
Two Bays		Fixed	3.50	1.0	11.36	1.0	20.7	1.0	-	-	-	-
	Small Strain	Isolated	1.07	1.0	5.28	1.0	10.1	1.0	20.1	1.0	-	-
		Iso&Soil	1.06	1.1	4.97	1.6	10.0	1.0	19.8	1.0	20.8	>100
		Rocking	0.74	1.0	1.77	1.0	10.9	1.0	17.5	1.0	-	-
	Large Strain	Isolated	0.52	7.1	4.03	2.9	10.8	1.1	18.0	1.1	-	-
		Iso&Soil	0.52	7.1	3.98	3.3	10.8	1.1	18.1	1.1	20.9	>100
		Rocking	0.36	7.1	0.82	7.2	10.3	1.1	16.5	1.0	-	-
Four Bays		Fixed	3.08	1.0	10.73	1.0	19.1	1.0	-	-	-	-
	Small Strain	Isolated	1.07	1.0	5.26	1.0	10.6	1.0	18.7	1.0	-	-
		Iso&Soil	1.06	1.1	5.11	1.3	10.6	1.0	18.6	1.0	24.3	>100
		Rocking	0.94	1.0	1.84	1.0	10.4	1.0	16.2	1.0	-	-
	Large Strain	Isolated	0.52	7.1	4.03	2.9	10.2	1.1	17.4	1.1	-	-
		Iso&Soil	0.52	7.1	4.01	3.1	10.2	1.0	17.2	1.1	22.7	>100
		Rocking	0.44	7.1	1.81	7.2	10.2	1.0	15.1	1.0	-	-

TABLE 5.3 Damped natural frequencies (Hz) and damping ratios (%) of base isolated five storey buildings (Isolation: k_h=5 W/m, β=1% for small strain or k_h=1.13 W/m, β=7.2% for large strain; k_v=200 k_h for isolated and k_v=2 k_h for rocking; footing area 16 m^2; soil: V_s=150 m/s, β=5%, ν=0.25, ρ=1800 kg/m^3)

		Mode	1		2		3		4		5	
		Base	Hz	%	Hz	%	Hz	%	Hz	%	Hz	%
Two Bays		Fixed	2.06	1.0	6.81	1.0	13.16	1.0	21.00	1.0	-	-
	Small Strain	Isolated	0.99	1.0	3.55	1.0	7.78	1.0	13.19	1.0	-	-
		Iso&Soil	0.97	1.3	3.36	1.7	7.77	1.0	12.91	1.1	20.87	>100
		Rocking	0.55	1.0	1.96	1.0	7.69	1.0	10.58	1.0	-	-
	Large Strain	Isolated	0.51	6.9	2.88	2.9	7.60	1.1	12.27	1.2	-	-
		Iso&Soil	0.51	6.9	2.72	3.3	7.60	1.1	12.04	1.2	20.79	>100
		Rocking	0.27	7.1	0.86	7.3	7.32	1.1	9.7	1.1	-	-
Four Bays		Fixed	2.02	1.0	6.56	1.0	12.42	1.0	19.47	1.0	-	-
	Small Strain	Isolated	0.98	1.0	3.56	1.0	7.55	1.0	12.61	1.0	-	-
		Iso&Soil	0.97	1.2	3.47	1.4	7.55	1.0	12.46	1.1	20.92	>100
		Rocking	0.74	1.0	1.89	1.0	7.49	1.0	9.64	1.0	-	-
	Large Strain	Isolated	0.51	6.9	3.10	2.0	7.38	1.1	11.98	1.1	-	-
		Iso&Soil	0.51	6.9	3.00	2.3	7.38	1.1	11.81	1.1	20.82	>100
		Rocking	0.37	6.9	0.85	7.1	7.27	1.1	8.98	1.0	-	-

effective; this coupled with the beneficial increase in damping can substantially reduce the seismic loading on the building. However, the reduction in the fundamental frequency brings the building toward the high energy portion of the wind spectrum (1 60 Hz).

The rocking isolators are more effective in reducing the fixed base frequencies in the first two modes and provide more damping in these modes, particularly for large strains and the second mode.

The three-storey frames benefit more from the rocking isolators in the second mode for large strains than the five storey frames. In the third mode, there are only small differences for the various base conditions.

Soil-structure interaction is negligible for the conditions assumed.

The mode shapes of the three storey building are shown for four bays in Figure 5.5, and for two bays in Figure 5.6. The first and second vibration modes of the five storey building (four bays) are shown in Figure 5.7. For no rocking, the buildings slide on the isolators in the first mode with the mode shape being almost unity throughout. This mode shape has been confirmed by vibration tests on a base-isolated building constructed by the Okumura Corporation in Japan. For rocking, the buildings rock as well as slide on the isolators.

The damping in the first mode is equal to the damping assigned to the isolator. This also applies in the second mode for the rocking isolators. The second mode is influenced quite significantly by rocking. The second mode displays a linear variation of displacements for rocking.

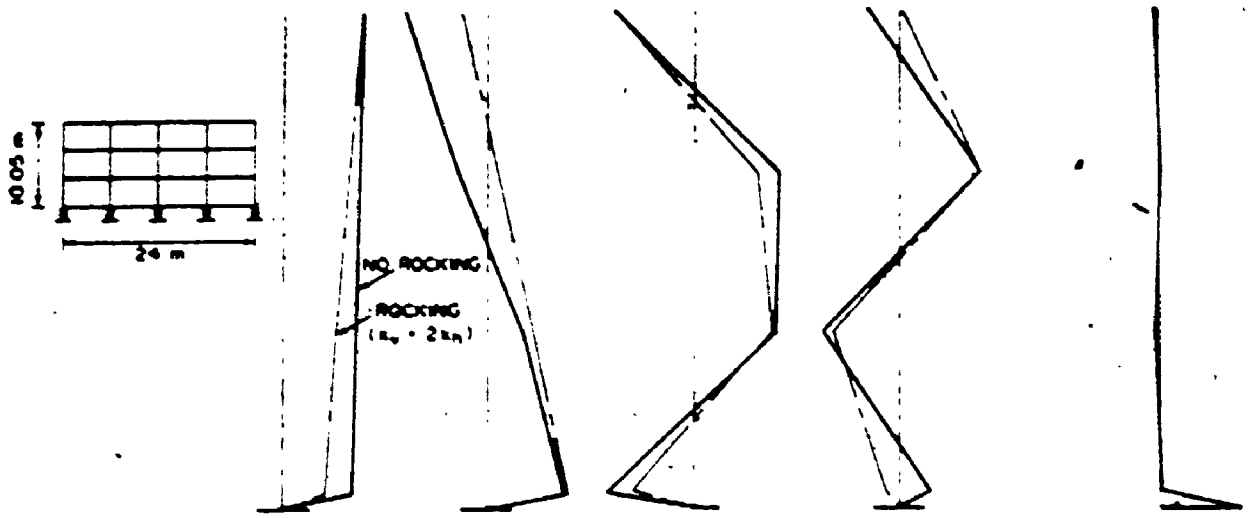

MODE	1	2	3	4	5
FIXED	3.38	10.73	19.11	—	—
NO ROCKING	1.07	5.26	11.58	18.70	—
SOIL + BI	1.06	5.11	11.57	18.58	24.02
ROCKING	0.91	1.84	11.44	16.18	—

FIGURE 5.5 Mode shapes and damped natural frequencies of base-isolated three storey-four bay building

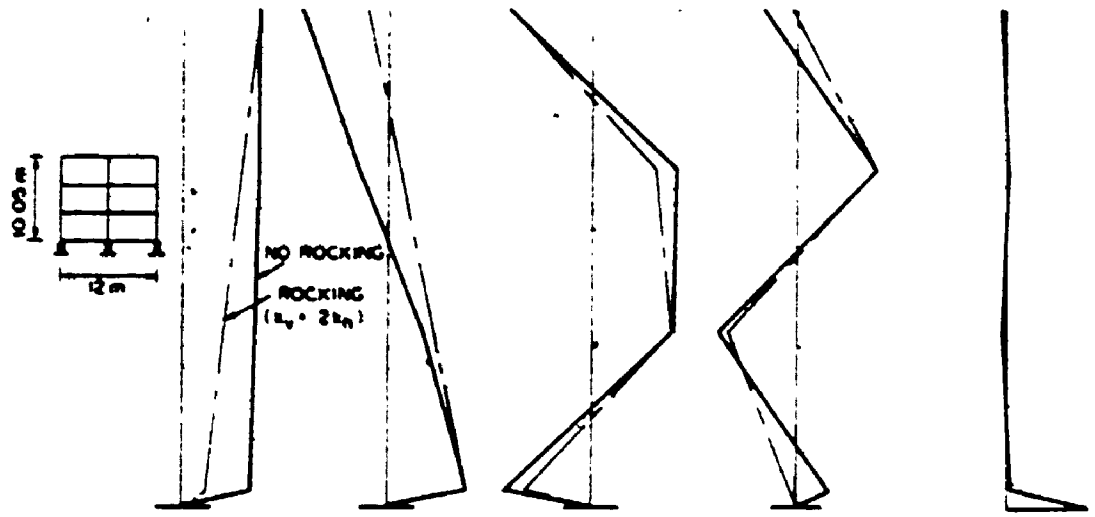

MODE	1	2	3	4	5
FIXED	3.50	11.36	20.73	—	—
NO ROCKING	1.07	5.28	12.12	20.06	—
SOIL + BI	1.06	4.97	12.11	19.83	23.82
ROCKING	0.74	1.77	11.93	17.46	—

FIGURE 5.6 Mode shapes and damped natural frequencies of base isolated three-storey two-bay building

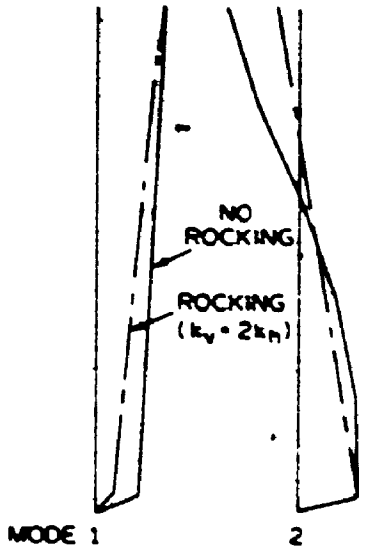

FIGURE 5.7 First and second mode shapes of base-isolated, five storey-four bay building

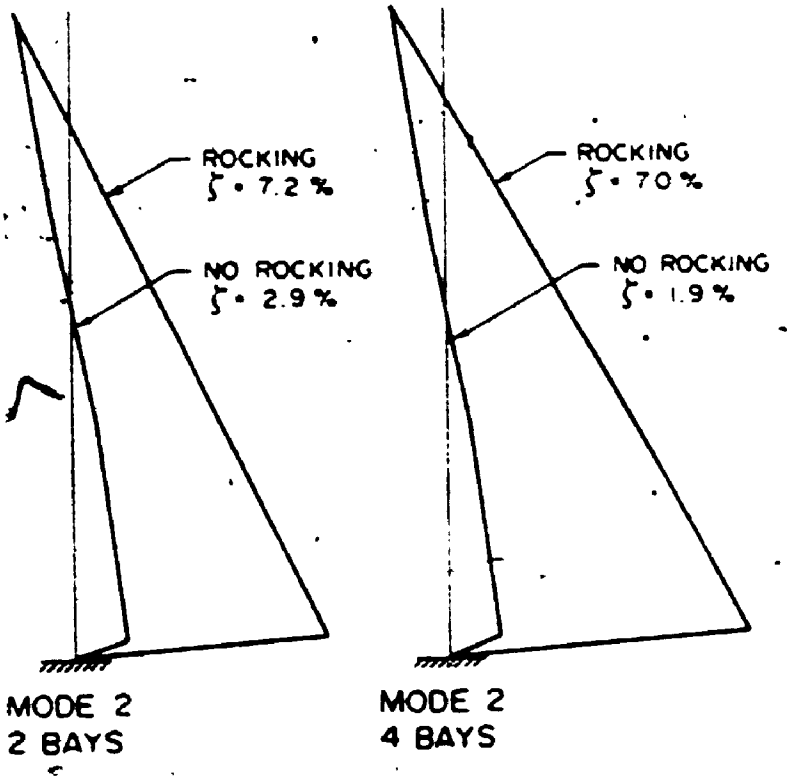

FIGURE 5.8 Influence of rocking on the second mode properties of the three-storey buildings

The shape of the second mode is favourable because it results in a small participation factor. This is desirable because the higher mode frequencies are shifted closer to the peak of the earthquake spectrum. In the highest mode, the foundation vibrates and the structure is almost motionless. This mode is heavily damped due to foundation damping.

The second mode shapes normalized to unity at the top of the building are shown in Figure 5.8. The modal coordinate corresponding to horizontal translation at the level of the isolator is much larger for rocking than in the absence of rocking. This factor, together with the larger vertical deformation of the isolators, combines to more effectively reduce the frequencies and provide higher damping in the second mode. To examine the effect of the vertical flexibility on the isolators in more detail, their damping ratio was increased to 30% in vertical translation. The results in the first and second modes are displayed in Tables 5.4 and 5.5 for the three storey and five storey frames respectively. For the isolated case, the first mode damping is approximately equal to the damping of the isolator in sliding. However, the second mode damping is increased which indicates that rocking is influential even in the isolated case (i.e. with vertically stiff isolators). For the rocking isolators, the damping in the first mode is significantly greater than in the isolated case. For the second mode, the more significant increase in damping occurs with the four bay, wider building. These results indicate that the use of discrete vertical dampers, in buildings on rocking isolators, can be quite beneficial. Such a system, designed by GERB was tested and found to be efficient (Hüffmann, 1984).

TABLE 5.4 Damped natural frequencies (Hz) and damping ratios (%) of base isolated three storey buildings with the vertical damping ratio increased from 7.2% to 30% (large strain; isolated: $k_v = 200\ k_h$, rocking: $k_v = 2\ k_h$)

		Mode	1		2	
		Base	Hz	%	Hz	%
BAYS	Two	Isolated	0.52	7.2	2.79	14.7
		Rocking	0.36	21.7	0.76	16.5
	Four	Isolated	0.52	7.1	4.29	5.3
		Rocking	0.45	15.0	0.74	22.1

TABLE 5.5 Damped Natural Frequencies (Hz) and Damping Ratios (%) of Base-Isolated Five-Storey Buildings With the Vertical Damping Ratio Increased From 7.2% to 30% (large strain, isolated: $k_v = 200\ k_h$, rocking: $k_v = 2\ k_h$)

		Mode	1		2	
		Base	Hz	%	Hz	%
BAYS	TWO	Isolated	0.51	7.3	2.64	9.3
		Rocking	0.27	25.3	0.81	12.3
	FOUR	Isolated	0.51	7.0	3.03	4.7
		Rocking	0.37	19.7	0.77	16.7

The bearing pressure under the inner 4 m by 4 m footings of the five storey-four bay building is 112 KPa. The allowable bearing capacity is increased to 300 KPa and consequently the footings' size is decreased to 2.5 m by 2.5 m. The analysis was repeated for the case of no rocking with soil-structure interaction. The modal damping ratios and the fundamental frequency are the same (as in Table 5.3) while the second mode frequency was reduced slightly to 2.95 Hz.

The effect of base isolation on structural damping is shown in Table 5.6 for the five storey-four bay frame. The isolator damping is set to zero and the damping ratio of the structural members is 1%. The structural damping is small in the first mode for both rocking and no rocking and in the second mode for rocking. Figures 5.9 and 5.10 show the first two modes for the five storey building on rocking isolators and vertically stiff isolators respectively, for small strain, evaluated using the PAFEC finite element program. Rotations and translations are included in the analysis. Some flexing of the superstructure occurs but the general trend is one of a rigid body on springs; except with vertically stiff isolators and the second mode for which considerable deformation of the superstructure occurs. These mode shapes and the reduction in structural damping suggest a simplified analysis may be adequate.

5.7 APPROXIMATE ANALYSIS

In order to obtain the preliminary estimate of the first natural frequency, the buildings can be modelled as a rigid body sliding on the isolators. The circular frequency is given by

TABLE 5.6 Structural Damping of Five-Storey-Four-Bay Frame When Base-Isolated With No Damping in the Base Isolators and 1 Per Cent Damping in the Structural Members

Base	Structural Damping %	Mode 1	Mode 2	Mode 3	Mode 4	Mode 5	Mode 6
Small Strain	Rocking	0.2	0.1	1.0	1.0	1.0	1.1
	Isolated	0.2	0.8	1.0	1.0	1.0	1.0
Large Strain	Rocking	0.1	0.0	1.0	1.0	1.2	1.3
	Isolated	0.1	0.8	1.0	1.0	1.1	1.2
Fixed		1.0	1.0	1.0	1.0	1.0	1.0

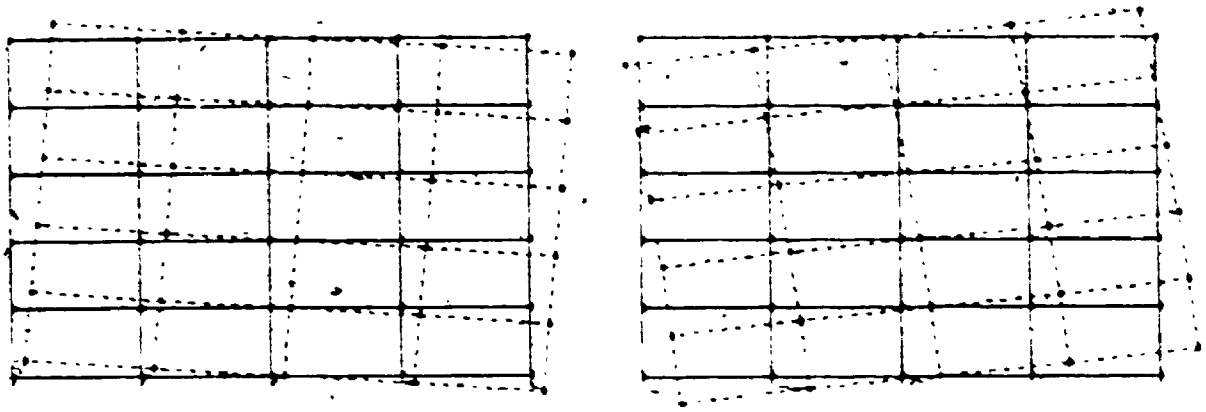

FIGURE 5.9 First and second mode shapes for the five-storey frame with rocking for small strain

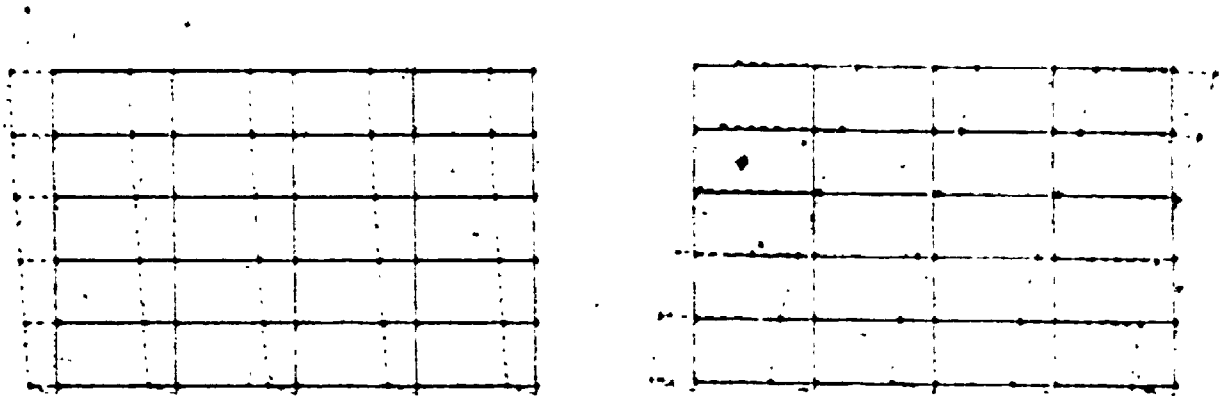

FIGURE 5.10 First and second mode shapes for the five-storey frame with no rocking for small strain

$$\omega_1 = \sqrt{k/M} = \sqrt{a\ Wt/M} = \sqrt{ag} \qquad (5\text{-}35)$$

where $k = a\ Wt$ is the horizontal stiffness of the isolators, Wt is the weight of the building and M its mass, a is a coefficient and g is the acceleration due to gravity (9.81 m/s^2). The cyclic frequency is then

$$f_1 = 0.498\ \sqrt{a} \qquad (5\text{-}36)$$

For small strain, a = 5 while for large strain a = 1.13. Therefore, f_1 = 1.11 Hz for small strain and f_1 = 0.53 Hz for large strain. These values compare well with 1.07 Hz and 0.52 Hz for the three storey building and 0.98 Hz and 0.51 Hz for the five storey building, values found in the more accurate analysis.

In order to account for the effect of rocking, the buildings can be analyzed approximately as a rigid block on springs featuring two degrees-of-freedom at the centre of mass, i.e. a horizontal translation and a rotation. Such analysis was employed by Kelly and Pan (1984). The stiffness matrix is given by

$$[k] = \begin{bmatrix} k_{uu} & k_{u\psi} \\ k_{\psi u} & k_{\psi\psi} \end{bmatrix} \qquad (5\text{-}37)$$

The sliding stiffness is, as before,

$$k_{uu} = a\ Wt \qquad (5\text{-}38)$$

and the rocking stiffness is

$$k_{\psi\psi} = \Sigma k_v\ d^2 + k_{uu}\ y_c^2 \qquad (5\text{-}39)$$

where k_v is the vertical stiffness of the isolator, d is the horizontal distance of the isolator from the centre of mass and y_c is the vertical distance from the centre of mass to the mid-height of the isolator. The rocking stiffness of the individual isolators is neglected. The cross stiffness terms are

$$k_{uv} = k_{vu} = -k_{uu}\, y_c \qquad (5\text{-}40)$$

For the case of soil interaction, foundation stiffness can be added to k_v and k_{uu}.

Incorporating both mass and mass moment of inertia, this analysis yields the first and second mode shapes and frequencies given in Table 5.7. The modal damping is equal to the damping ratio assigned to the isolators.

The fundamental frequencies compare well with those obtained previously. For the rocking isolators, the second natural frequencies are fairly close. For the isolated condition, the second natural frequencies differ substantially from those of the plane frame. The differences can be attributed to the flexing and shearing of the frame members. The modal damping ratios compare well except in the second mode for the isolated condition where the rigid body damping is substantially higher than the accurate value. For the second mode and the isolated condition, the building rocks about a point quite close to its centre of mass while for the rocking condition, the centre of rotation is located above the centre of mass.

linearization, a direct solution of the equations of motion can be obtained by employing the Fast Fourier Transform (FFT) technique. This approach is useful when soil-structure interaction is included since the soil impedances are frequency dependent.

6.2 CHARACTERISTICS OF EARTHQUAKES

The response of a given structure depends upon the characteristics of the earthquake ground motion. The most important of these are the intensity, frequency content, and the duration of the strong motion part of the signal. The effect of intensity is straightforward, and is usually specified by the maximum input acceleration. The earthquake spectrum describes the distribution of energy with frequency. The structural response is determined by the amount of energy close to the natural frequency of vibration. The extent of damage depends upon the number of cycles of loading and therefore on the duration of the motion. These characteristics, in turn, are dependent on the characteristics of the earthquake at its source, the source-to-site transmission and attenuation (wave reflection and refraction, and energy dissipation) and the modifying effects of the local-site conditions.

There are two approaches to determining the design earthquake. The first approach is to determine the distance to a potential fault of the site and the expected magnitude of the earthquake. Then an existing earthquake record of similar fault distance and magnitude must be selected. Some modifications may be performed on the selected record. The second approach is to develop a design response spectrum which is

5.8 PILE FOUNDATIONS

In some cases, piles may be used in conjunction with base isolators with the isolators resting on a rigid pile cap. Such an arrangement was chosen to support a building of the Okamura Corporation in Tsukuba Science City in Japan. Piles are quite flexible in the horizontal direction and if they are friction piles, even in rocking. To examine their effect on the five storey building, wooden piles with an average diameter of 254 mm are assumed in groups of four supporting each column. The four piles are connected by a 2 m square, 45 cm thick rigid reinforced concrete pile cap. The soil is assumed to have a shear wave velocity of 150 m/s at the pile tip with shear modulus diminishing parabolically upwards. The impedance functions were established for the fundamental circular frequency using the program DYNA (Novak et al., 1983) with pile-soil-pile interaction accounted for.

With these data the pile foundation horizontal stiffness turns out to be seven times lower than the horizontal stiffness of the spread footing but this is still about ten times more than the horizontal stiffness of the isolators. The soil-pile-structure interaction effect reduced the first mode damping to 6.4% from 6.9%.

5.9 FREE VIBRATION ANALYSIS WITH DYNAMIC INTERACTION OF FOOTINGS

The five storey-four bay plane frame is analyzed considering footing-soil-footing interaction. The size of the individual footings is 2.5 m x 2.5 m corresponding to a bearing stress of approximately 300 KPa. The natural frequencies of the structure for large strains with vertically

stiff isolators is 0.51 Hz and 3.00 Hz (Table 5.3, isolated + soil) in the first and second modes respectively. The corresponding dimensionless frequencies, a_0, are 0.03 and 0.16. The shear wave velocity is 150 m/s and the damping ratio, β, is 0.05 ($\tau = 0.10$).

The evaluation of the vertical complex compliance is done using subroutine FZGZ provided by L. Gaul. The vertical compliance matrix is computed for the system of equally spaced footings and inverted to give the vertical impedance matrix. The horizontal impedance matrix is established approximately as the product of the vertical impedance matrix and the ratio of the horizontal to vertical impedances of an individual footing computed by the equations of Pais and Kausel (Chapter 4).

The complex eigenvalue analysis was performed with soil impedances for the first and second modes in turn. Table 5.8 lists the natural frequencies and modal damping. The effect of dynamic interaction of the footings is slight.

TABLE 5.8 Damped natural frequencies (Hz) and damping ratios (%) for the first two modes of the base-isolated five storey building with dynamic interaction of 2.5 m by 2.5 m footings

Mode	1		2	
	Hz	%	Hz	%
a_o = 0.03 (mode 1)	0.51	7.0	2.95	2.3
a_o = 0.16 (mode 2)	0.51	6.9	2.95	3.1

CHAPTER 6

SEISMIC ANALYSIS OF BASE-ISOLATED BUILDINGS

6.1 INTRODUCTION

The effectiveness of base isolation in reducing the seismic loading on a building can be examined by subjecting an unisolated and a base-isolated building to earthquake excitation and comparing the building accelerations. For the unisolated building, the input (ground) acceleration is amplified up the building; for the base-isolated building the accelerations are expected to be approximately the same at all levels.

Time history analysis of buildings with non-linearities is usually expensive and is reserved for a final analysis. For a preliminary analysis of base-isolated buildings, an equivalent linear stiffness and viscous damping can be used in a time history analysis of the multi-degree-of-freedom system thereby reducing the computer time. The 'effective amplitude' for the secant modulus linearization and the ductility ratio for the Iwan linearization are obtained by firstly analyzing the building as a sliding mass on the isolators. Also, advantage may be taken of the fact that the non-linearity is localized in a base-isolated building and simple yielding in shear occurs in the isolators, to further reduce the computing time of the multi-degree-of-freedom system. The accuracy of the procedure is verified. No attempt is made to quantify the reduction in computer costs versus general analyses.

The equations of motion are solved by numerical integration and soil-structure interaction is not considered. With equivalent

linearization, a direct solution of the equations of motion can be obtained by employing the Fast Fourier Transform (FFT) technique. This approach is useful when soil-structure interaction is included since the soil impedances are frequency dependent.

6.2 CHARACTERISTICS OF EARTHQUAKES

The response of a given structure depends upon the characteristics of the earthquake ground motion. The most important of these are the intensity, frequency content, and the duration of the strong motion part of the signal. The effect of intensity is straightforward, and is usually specified by the maximum input acceleration. The earthquake spectrum describes the distribution of energy with frequency. The structural response is determined by the amount of energy close to the natural frequency of vibration. The extent of damage depends upon the number of cycles of loading and therefore on the duration of the motion. These characteristics, in turn, are dependent on the characteristics of the earthquake at its source, the source-to-site transmission and attenuation (wave reflection and refraction, and energy dissipation) and the modifying effects of the local-site conditions.

There are two approaches to determining the design earthquake. The first approach is to determine the distance to a potential fault of the site and the expected magnitude of the earthquake. Then an existing earthquake record of similar fault distance and magnitude must be selected. Some modifications may be performed on the selected record. The second approach is to develop a design response spectrum which is

used directly or from which an acceleration time history is generated for a dynamic analysis. In this study the second approach is employed, whereby the response spectrum of the soil deposit is selected and from which an artificial time history is generated.

6.3 THE SIMULATED EARTHQUAKE

The artificial earthquake motion is generated using the program SIMQKE (Vanmarke et al., 1969). The signal is formed by superpositioning a series of sinusoids with random phase angles. The amplitudes of the components are determined from the selected stationary spectral density function. The stationary motion is multiplied by a deterministic intensity function to simulate the transient character of real earthquakes. The simulated motion is then

$$a(t) = I(t) \sum_{i=1}^{n} A_i \sin(\omega_i t + \phi_i) \qquad (6\text{-}1)$$

where $a(t)$ is the nonstationary acceleration process, $I(t)$ is the deterministic intensity function, A_i is the amplitude, ϕ_i is the phase angle and ω_i is the frequency of the ith contributing sinusoid. A description of the selected parameters follows.

The Kanai-Tajimi stationary filtered white noise spectrum of ground acceleration is (Tajimi, 1960)

$$S_{\ddot{u}g}(\omega) = \frac{S_o[1 + 4\xi_g^2 (\frac{\omega}{\omega_g})^2]}{[1-(\frac{\omega}{\omega_g})^2]^2 + 4\xi_g^2 (\frac{\omega}{\omega_g})^2} \qquad (6\text{-}2)$$

in which S_o is the white noise spectral amplitude (bedrock), ω_g is the resonant frequency of the transfer function of the overlying soil which

is characteristic of the ground frequency and ξ_g is the characteristic damping ratio of the soil. For firm soil conditions, the suggested values are 15.6 rad/sec for ω_g and 0.6 for ξ_g. The variance of ground acceleration is (Penzien and Liu, 1969)

$$\sigma^2_{\ddot{u}g} = \int_0^\infty S_{\ddot{u}g}(\omega)d\omega = \frac{\pi S_o \omega_g}{4\xi_g}(1 + 4\xi_g^2) \qquad (6\text{-}3)$$

Then, the normalized spectral density function is,

$$S^n_{\ddot{u}g} = \frac{S_{\ddot{u}g}}{\sigma^2_{\ddot{u}g}} = \frac{[1+4\xi_g^2(\frac{\omega}{\omega_g})^2]}{[1-(\frac{\omega}{\omega_g})^2]^2 + 4\xi_g^2(\frac{\omega}{\omega_g})^2} \frac{4\xi_g}{\pi\omega_g(1+4\xi_g^2)} \qquad (6\text{-}4)$$

and is shown in Figure 6.1.

The r.m.s. ground acceleration of 610 mm/sec^2 (2.0 ft/sec^2) and the peak acceleration of 0.3g are chosen which corresponds to the El Centro 1940 earthquake (Housner and Jennings, 1964 and Clough and Penzien, 1975). The duration is taken as 30 seconds. The compound intensity function for the nonstationary process is shown in Figure 6.2. The resulting simulated earthquake signal is shown in Figure 6.3.

6.4 EQUATIONS OF MOTION

The equations of motion are solved numerically using Newmark's Beta method. The matrix equation of motion at time t_i is

$$[m]\{\ddot{u}_i\} + [c]\{\dot{u}_i\} + \{F_i\} = \{P_i\} \qquad (6\text{-}5)$$

where $\{\dot{u}_i\}$ and $\{\ddot{u}_i\}$ are the vectors of relative velocity and acceleration respectively, $[m]$ and $[c]$ are the mass and damping matrices respectively, $\{F_i\}$ is the restoring force vector, and $\{P_i\}$ is the load

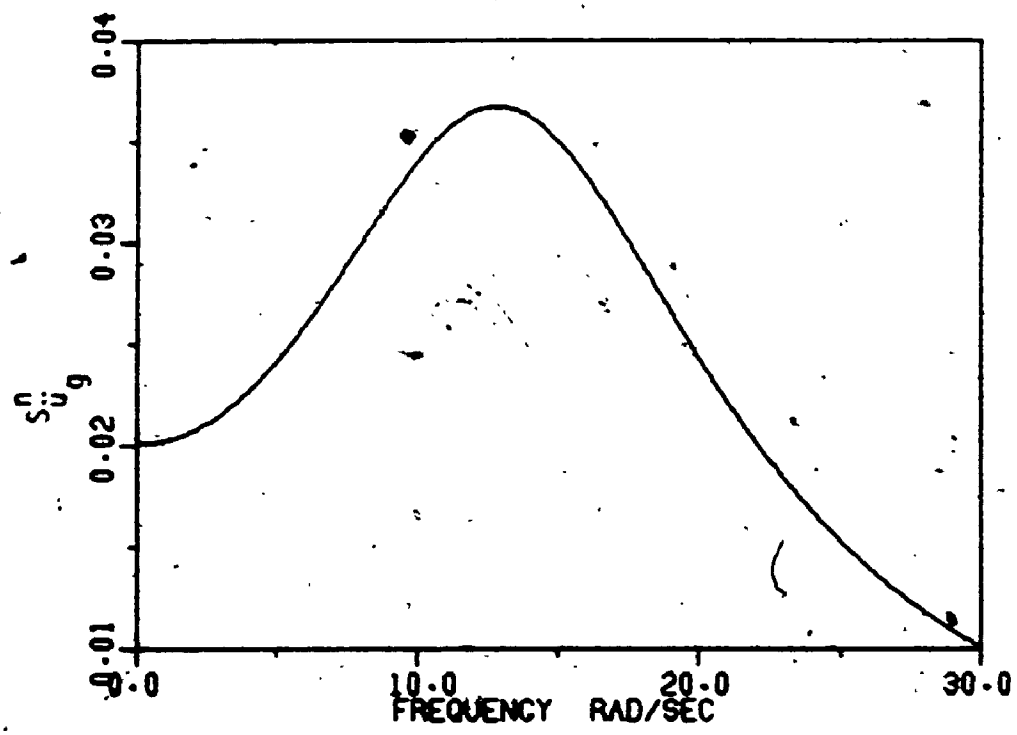

FIGURE 6.1 Normalized Kanai-Tajimi power spectral density function of ground acceleration (ω_g = 15.6 rad/sec, ζ_g = 0.6)

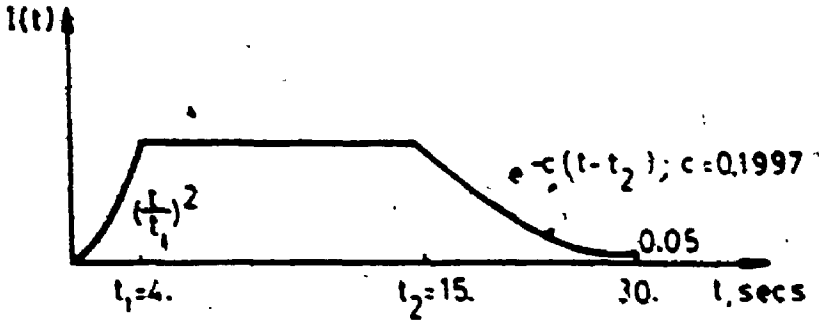

FIGURE 6.2 Intensity function I(t) for the non-stationary process a(t)

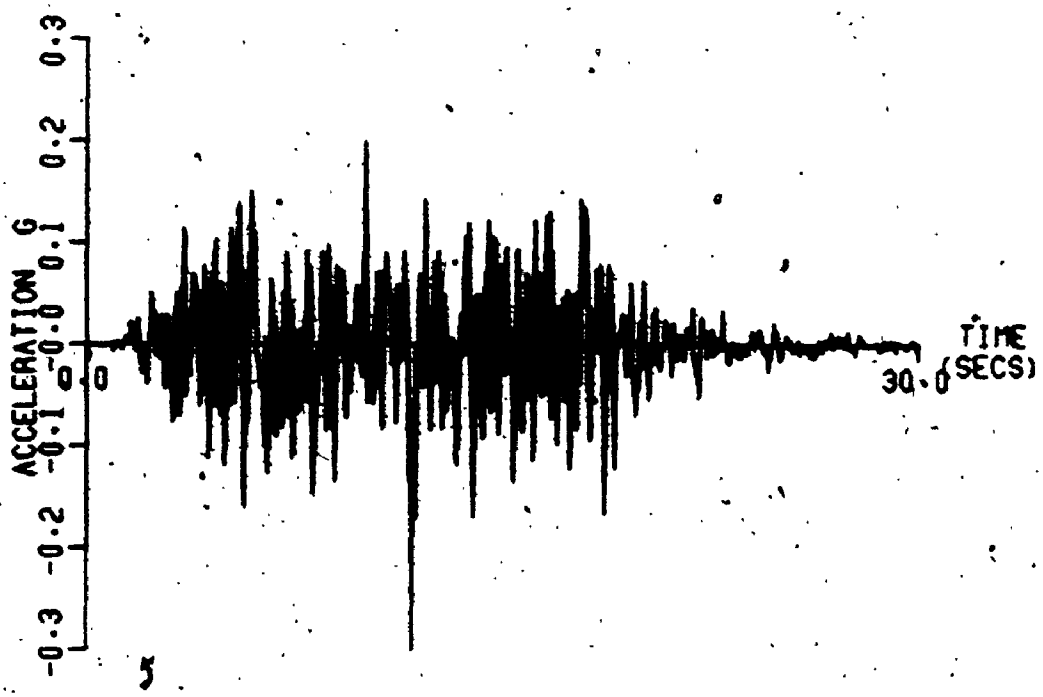

FIGURE 6.3 The artificial earthquake time history

vector which is equal to the product of the floor mass and the ground acceleration at time t_i. At time $t_{i+1} = t_i + \Delta t$ the equation of motion is given by

$$[m]\{\ddot{u}_i+\Delta\ddot{u}\} + [c]\{\dot{u}_i+\Delta\dot{u}\} + \{F_{i+1}\} = \{P_{i+1}\} \qquad (6\text{-}6)$$

The incremental form of the equations of motion is

$$[m]\{\Delta\ddot{u}\} + [c]\{\Delta\dot{u}\} + \{F_{i+1}\} - \{F_i\} = \{\Delta P\} \qquad (6\text{-}7)$$

These equations are solved by assuming the stiffness and damping properties remain constant during the small time increment, Δt. The mass of the system remains constant. The incremental restoring force depends on the hysteretic behaviour of the system. Newmark (1959) suggested the following relations for the velocity and displacement at time t_{i+1}

$$\{\dot{u}_{i+1}\} = \{\dot{u}_i\} + [(1-\gamma)\{\ddot{u}_i\} + \gamma\{\ddot{u}_{i+1}\}]\Delta t \qquad (6\text{-}8)$$

and

$$\{u_{i+1}\} = \{u_i\} + \Delta t\{\dot{u}_i\} + (\tfrac{1}{2} - \beta)(\Delta t)^2\{\ddot{u}_i\} + \beta(\Delta t)^2\{\ddot{u}_{i+1}\} \qquad (6\text{-}9)$$

The parameter γ controls the artificial (numerical) damping. For γ less than 1/2, negative damping is produced while for γ greater than 1/2 the damping is positive. For no artificial damping, γ is equal to 1/2 which is the value used in this study. The parameter β determines the variation of the acceleration within the time step. Linear variation of the acceleration is assumed for which $\beta = 1/6$. For the linear acceleration method the critical time step for numerical stability of the solution is

$(\Delta t)_{cr} = 0.551\ T_n$; T_n being the smallest period of the structure. A commonly used time step is $\Delta t = T_n/10$. For the base-isolated buildings the fundamental elastic period is 1 second approximately. A time step of 0.02 seconds is used. Considering that the response is dominated by the first mode, the time step is 1/50 of the elastic period and is adequate.

The incremental velocity and displacement are

$$\{\Delta\dot{u}\} = [(1-\gamma)\{\ddot{u}_i\} + \gamma\{\ddot{u}_{i+1}\}]\Delta t$$

$$= \{\ddot{u}_i\}\Delta t + \gamma\{\Delta\ddot{u}\}\Delta t \qquad (6\text{-}10)$$

and

$$\{\Delta u\} = \{\dot{u}_i\}\Delta t + 1/2\ \{\ddot{u}_i\}(\Delta t)^2 + \beta\{\Delta\ddot{u}\}(\Delta t)^2 \qquad (6\text{-}11)$$

From which the incremental acceleration is

$$\{\Delta\ddot{u}\} = \frac{1}{\beta(\Delta t)^2}\{\Delta u\} - \frac{1}{\beta\Delta t}\{\dot{u}_i\} + \frac{1}{2\beta}\{\ddot{u}_i\} \qquad (6\text{-}12)$$

and the incremental velocity can be restated as

$$\{\Delta\dot{u}\} = \frac{\gamma}{\beta\Delta t}\{\Delta u\} - \frac{\gamma}{\beta}\{\dot{u}_i\} + (\frac{\gamma}{2\beta} - 1)\Delta t\{\ddot{u}_i\} \qquad (6\text{-}13)$$

Defining the vectors $\{Q_i\}$ and $\{R_i\}$, at time t_i, as

$$\{Q_i\} = \frac{1}{\beta\Delta t}\{\dot{u}_i\} + \frac{1}{2\beta}\{\ddot{u}_i\} \qquad (6\text{-}14)$$

and

$$\{R_i\} = \frac{\gamma}{\beta}\{\dot{u}_i\} + (\frac{\gamma}{2\beta} - 1)\Delta t\{\ddot{u}_i\} \qquad (6\text{-}15)$$

then, Equations (6-12) and (6-13) are rewritten as

$$\{\Delta\ddot{u}\} = \frac{1}{\beta(\Delta t)^2}\{\Delta u\} - \{Q_i\} \tag{6-16}$$

and

$$\{\Delta\dot{u}\} = \frac{\gamma}{\beta\Delta t}\{\Delta u\} - \{R_i\} \tag{6-17}$$

Substituting (6-16) and (6-17) in the incremental equation of motion, (6-7), gives

$$\frac{1}{\beta(\Delta t)^2}[m]\{\Delta u\} - [m]\{Q_i\} + \frac{\gamma}{\beta\Delta t}[c]\{\Delta u\}$$

$$- [c]\{R_i\} + \{F_{i+1}\} - \{F_i\} = \{\Delta P\} \tag{6-18}$$

which can be written in the pseudostatic form

$$[K_e]\{\Delta u\} = \{\Delta P_e\} \tag{6-19}$$

in which the effective stiffness matrix is

$$[K_e] = \frac{1}{\beta(\Delta t)^2}[m] + \frac{\gamma}{\beta\Delta t}[c] + [k_i] \tag{6-20}$$

and the effective load vector is

$$\{\Delta P_e\} = \{\Delta P\} + [m]\{Q_i\} + [c]\{R_i\} \tag{6-21}$$

At time t_{i+1}, the displacement is, $\{u_{i+1}\} = \{u_i\} + \{\Delta u\}$ and the acceleration and velocity are computed using equations (6-16) and (6-17) as $\{\ddot{u}_{i+1}\} = \{\ddot{u}_i\} + \{\Delta\ddot{u}\}$ and $\{\dot{u}_{i+1}\} = \{\dot{u}_i\} + \{\Delta\dot{u}\}$ respectively.

In Equation (6-18) the incremental restoring force is computed, using the tangent stiffness at time t_i, as

$$\{F_{i+1}\} - \{F_i\} = [k_i]\ \{\Delta u\} \qquad (6\text{-}22)$$

Consequently, at the end of the time step (t_{i+1}) a residual (out-of-balance) force occurs which must be corrected by imposing total dynamic equilibrium or else erroneous results are obtained. The correction to the displacement, velocity and acceleration vectors is done iteratively. The out-of-balance force at the end of the time step is computed for the jth iteration as

$$\{P_r\}^j = \{P_{i+1}\} - [m]\cdot\ddot{u}_{i+1}^{j-1} - [c]\cdot\dot{u}_{i+1}^{j-1} - \{F_{i+1}\}^{j-1} \qquad (6\text{-}23)$$

in which $\{P_{i+1}\}$ is the external load vector at time t_{i+1}. The correction to the incremental displacement, $\{\varepsilon u\}^j$, is computed from

$$[K_e]^j\ \{\varepsilon u\}^j = \{P_r\}^j \qquad (6\text{-}24)$$

for which the effective stiffness matrix is updated at each iteration. The corrected incremental displacement is $\{\Delta u\}^j = \{\Delta u\}^{j-1} + \{\varepsilon u\}^j$. Then, the corrected displacement, velocity and acceleration are computed. It is usual to carry out the iterative process until the out-of-balance force, or the vector norm of the correction to the displacements, is small. However, for the building considered, the nonlinearity is localized and rigid floor diaphragms are assumed. The iteration convergence is checked, using the displacement of the base isolator, as $|\varepsilon u^j(bi)|/|u_i^j(bi)| \leq 0.001$. The updating of the effective stiffness matrix at each iteration corresponds to the Newton-Raphson technique which is depicted in Figure 6.4 for yielding of the isolators. Then, only one iteration is required. Apart from numerical stability

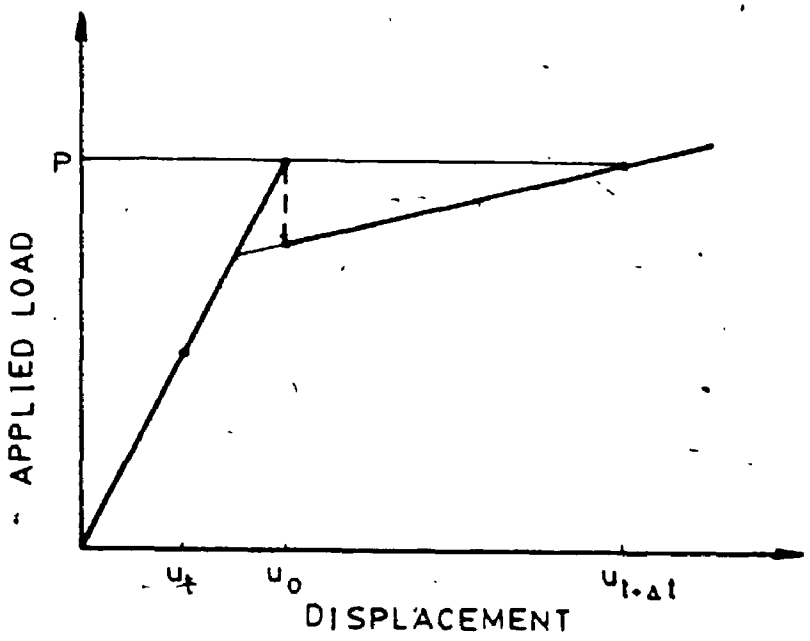

FIGURE 6.4 Newton-Raphson technique for correcting out-of-balance forces (yielding of the isolator)

considerations, a small time step is needed to follow the unloading behaviour accurately. The 0.02 sec time step is considered adequate for this purpose and was checked by using a time step of 0.01 sec. No appreciable change in the results occurred.

Only the effect of horizontal ground acceleration is studied. Therefore, the external load vector is given by the product of the mass of each floor and the ground acceleration, $\ddot{u}_g(t)$. The number of equations to be solved is reduced by using condensed mass, stiffness and damping matrices as in the free vibration analysis. The process of updating the effective stiffness matrix at each iteration is simplified by forming two effective stiffness matrices outside the iteration loop corresponding to the two possible states of the bilinear isolators (elastic and post-elastic); the isolators are assumed to yield and unload together.

6.5 DISCUSSION AND RESULTS

The five storey building, described in Chapter 5 (Figure 5-2), is analyzed. Firstly, the structure is analyzed with a fixed base (unisolated) assuming that the members remain linear. The damping ratio of the superstructure and the isolator in the elastic range is taken as 2%. The peak acceleration at roof level is 0.77g. The frame is next analyzed with the isolators, having the properties described in Chapter 5, and the bilinear hysteretic loop is followed. In this case, the peak acceleration at roof level is reduced to 0.34g. Therefore, the seismic forces on the building are considerably reduced. The unisolated and isolated roof acceleration time histories are shown in Figure 6.5. The beneficial

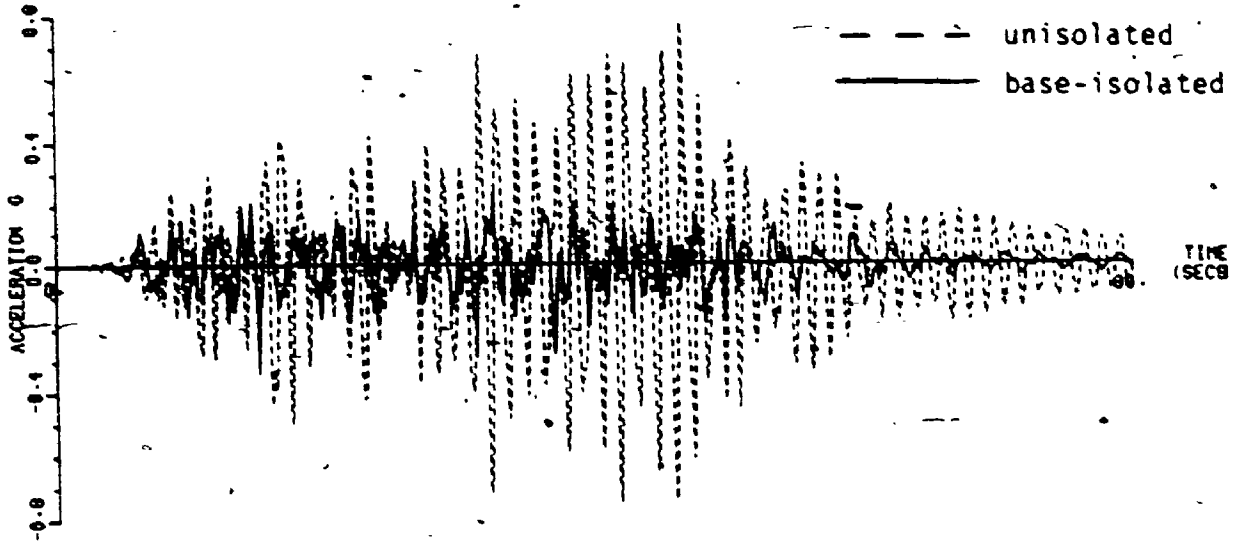

FIGURE 6.5 Roof accelerations of the unisolated and base-isolated buildings

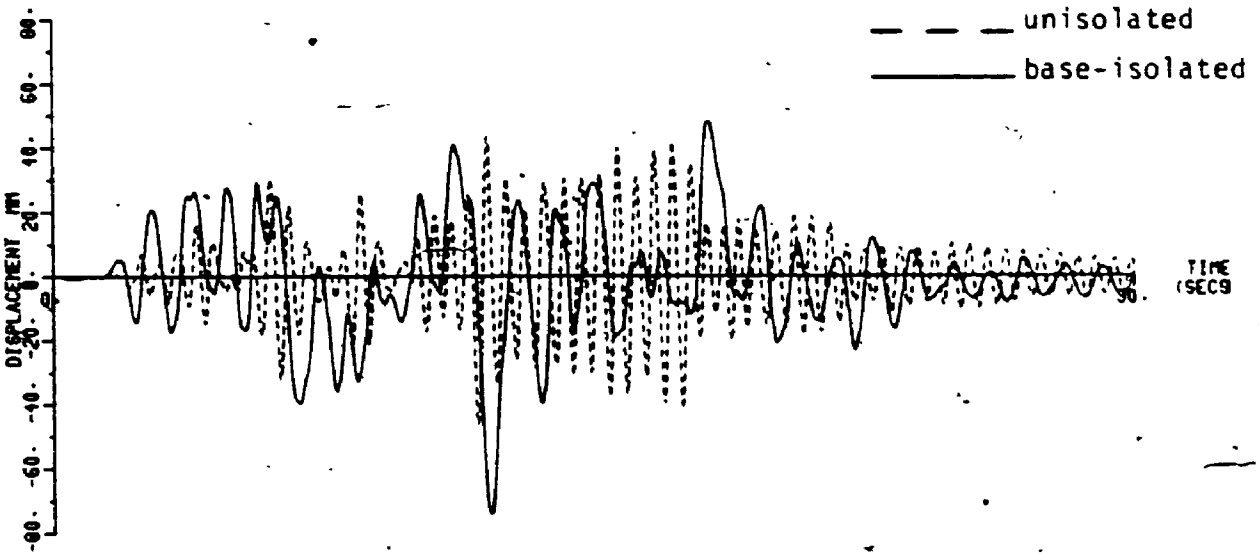

FIGURE 6.6 Roof displacements of the unisolated and base-isolated buildings

effect of base isolation is clearly demonstrated. The relative displacements are compared in Figure 6.6 where the reduction in the frequency of the base isolated building is quite apparent but the displacements are increased from 46 mm to 74 mm. For the isolated building, the acceleration and displacement at the level of the isolators are 0.25g and 64 mm respectively. This displacement must be accommodated by the isolators as well as the utility connections and the accesses to the building.

The adequacy of a simple single degree-of-freedom model is examined by analyzing the building as a sliding rigid mass. For this case, the peak displacement is 63 mm and the peak acceleration is 0.29g which compare well with the peak roof displacement of 74 mm and the peak roof acceleration 0.34g by the frame analysis.

The single degree-of-freedom analysis was repeated using equivalent linear isolator properties based on the secant modulus (Chapter 3) corresponding to several fractions of the peak amplitude (63 mm). An effective amplitude of 80 per cent of the peak amplitude results in a peak displacement of 62 mm and peak acceleration of 0.28g. The associated damping ratio is 22.6% and the equivalent linear stiffness is 1.79 times the weight of the building per metre of displacement. The response of the frame using these parameters results in a peak roof displacement and acceleration of 72 mm and 0.31g respectively. The roof accelerations and displacements using the bilinear hysteretic loop and the secant modulus linearization are compared in Figures 6.7 and 6.8 respectively. The appropriateness of this simplified method is quite evident.

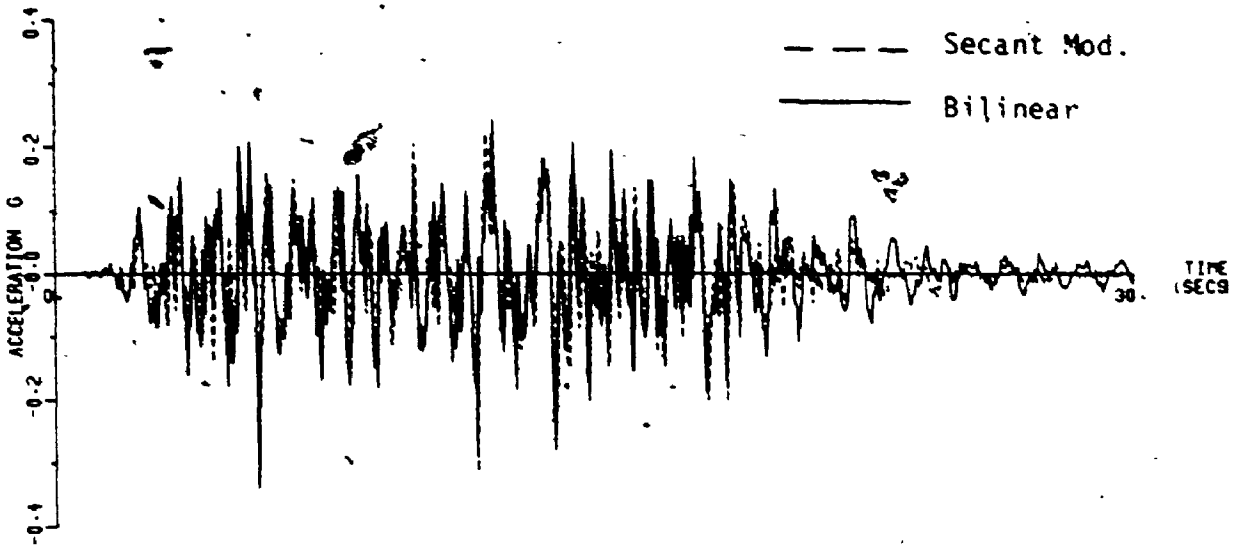

FIGURE 6.7 Roof accelerations using the secant modulus linearization (80 per cent effective amplitude) and the bilinear hysteretic loop

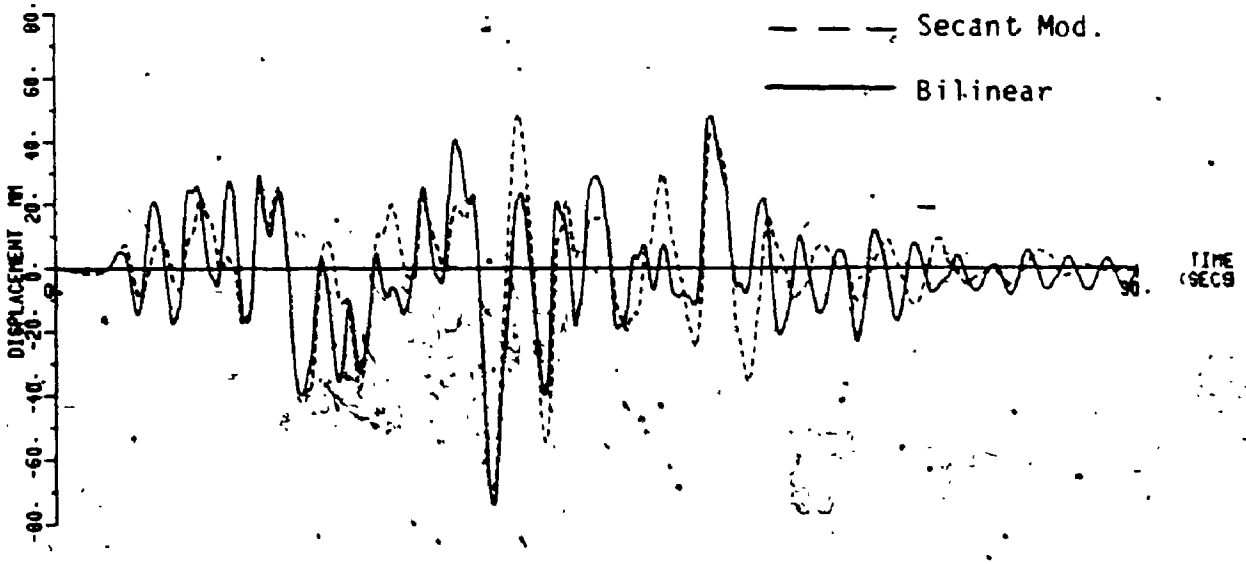

FIGURE 6.8 Roof displacements using the secant modulus linearization (80 per cent effective amplitude) and the bilinear hysteretic loop

A maximum displacement of 63 mm (sliding mass) and a yield displacement of 10 mm were used in the computation of the equivalent linear parameters by Iwan's method (Chapter 3). The equivalent linear stiffness is 2.01 times the weight of the building per metre of displacement. For 2 per cent viscous damping associated with small displacements, the equivalent viscous damping ratio is 12.9%. The peak roof displacement and acceleration are 80 mm and 0.33g respectively. The roof acceleration and displacement are compared with the accurate values in Figures 6.9 and 6.10. The agreement is very good. A comparison of Figures 6.8 and 6.10 reveals that the secant modulus linearization provides a better matching of the peaks.

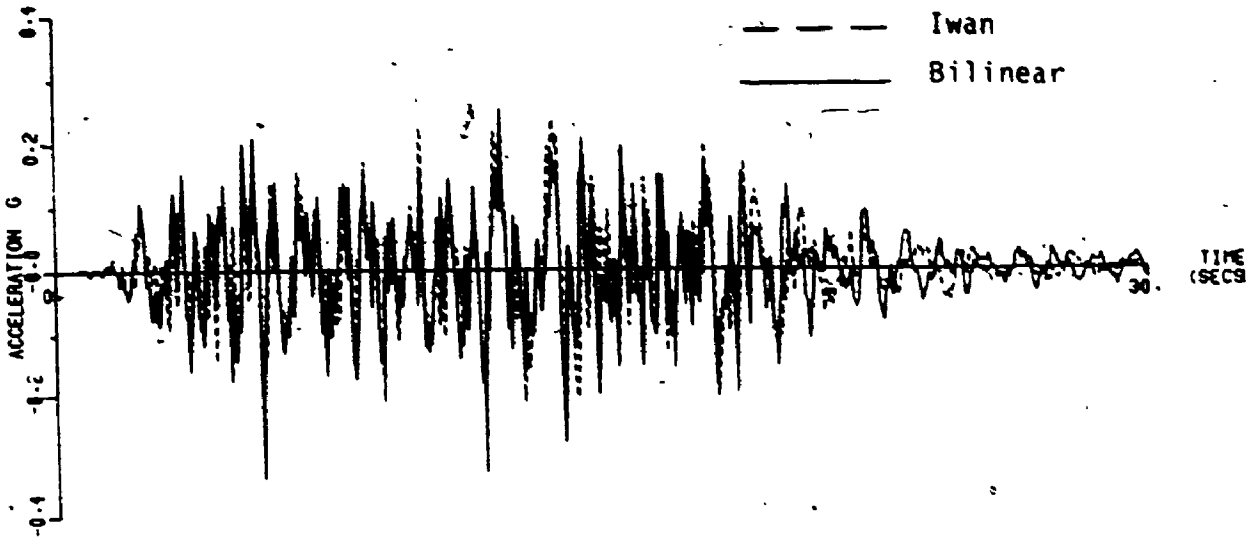

FIGURE 6.9 Roof accelerations using Iwan's linearization and the bilinear hysteretic loop

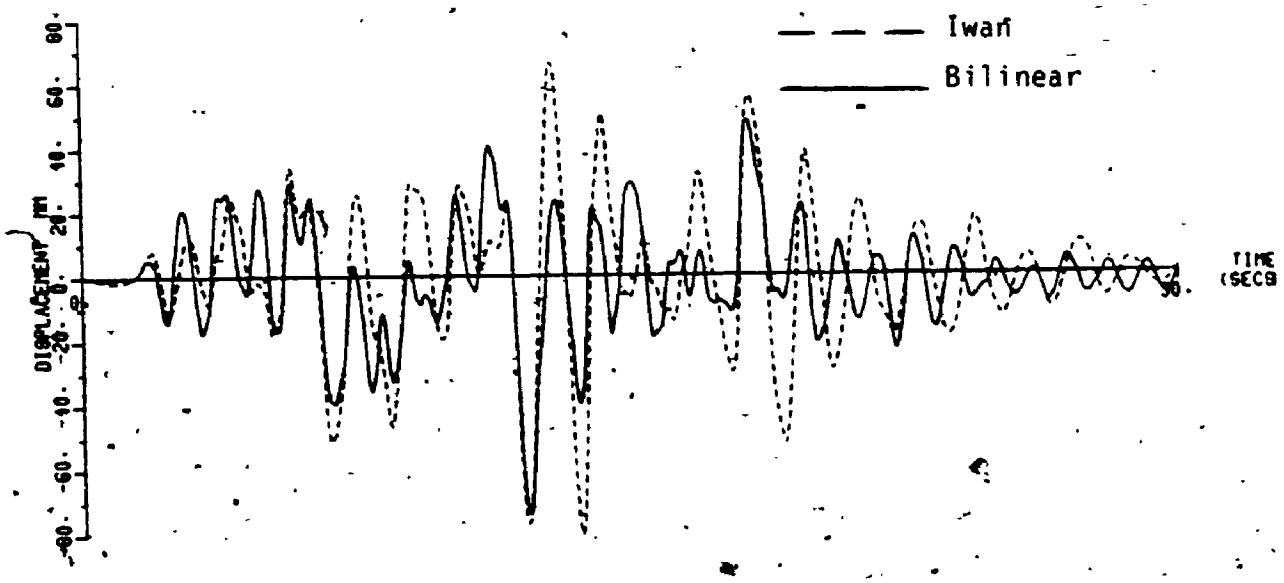

FIGURE 6.10 Roof displacements using Iwan's linearization and the bilinear hysteretic loop.

CHAPTER 7

EXPERIMENTAL INVESTIGATION OF WIND FORCES ON BASE-ISOLATED BUILDINGS

7.1 INTRODUCTION

The methods for wind effects prediction are well established but they are based on research that was mostly concerned with tall buildings. The question therefore arises as to whether these procedures are also adequate for low-rise base-isolated buildings whose fundamental frequencies are much lower than those of conventional buildings of similar size. In this study, the focus is on low-rise buildings and the characteristics of the turbulent air flow close to the ground. The models are tested in three terrain types namely, open, suburban and urban. The models, experimental procedures and results are described in the following sections.

7.2 MODEL LAWS

The wind force acting on a building depends on the aerodynamic shape and the following physical parameters: the air density, ρ, the wind velocity, U, a characteristic dimension, D, the viscosity of air, μ, and a characteristic frequency, f (Whitbread, 1965; Simiu, 1985). Dimensional analysis reveals that the force coefficient (generally $F/\rho U^2 D^2$) is a function of the dimensionless numbers fD/U and $\mu/\rho UD$ if gravitational effects are neglected.

The dimensionless number, fD/U, is the reduced frequency and is denoted by n. Its reciprocal, U/fD, is the reduced velocity. The

Reynolds number is $\rho UD/\mu$ or UD/ν, where ν is the kinematic viscosity. Other dimensionless numbers associated with the above parameters are the Strouhal number and the Rossby number ($U/f_c D$) which requires scaling the Coriolis parameter, f_c. Neither are considered in the ensuing discussion. These similarity laws must be adhered to in making prototype predictions from model test results.

For sharp-edged bodies the separation points are fixed and therefore the drag on the body is only slightly influenced by the Reynolds number. However, if there is a long afterbody, reattachment occurs and the drag coefficient is reduced (wake width is reduced). The drag on the body is then dependent on the Reynolds number.

The necessity for the dimensionless numbers in the model and the prototype to be the same leads to several scaling considerations. The length scale is defined as

$$\lambda_L = \frac{D_m}{D_p} \tag{7-1}$$

which sets the ratio of model to prototype dimensions (m refers to the model and p to the prototype). The velocity scale is

$$\lambda_V = \frac{U_m}{U_p} \tag{7-2}$$

where U_m is the wind tunnel velocity and U_p is the natural wind velocity. The density scale is

$$\lambda_\rho = \frac{\rho_m}{\rho_p} \tag{7-3}$$

which is unity for tests using air under atmospheric conditions. The similitude of the reduced frequency requires that

$$\left(\frac{fD}{U}\right)_m = \left(\frac{fD}{U}\right)_p \tag{7-4}$$

therefore the frequency scale, λ_f, is

$$\lambda_f = \frac{f_m}{f_p} = \frac{\lambda_v}{\lambda_L} \tag{7-5a}$$

or

$$f_m = \frac{f_p}{\lambda_L}\frac{U_m}{U_p} \tag{7-5b}$$

The reciprocal of the frequency scale is the time scale, λ_T. Reynolds number scaling requires that

$$\left(\frac{UD}{\nu}\right)_m = \left(\frac{UD}{\nu}\right)_p \tag{7-6}$$

For model and prototype in air under atmospheric conditions $\nu_m = \nu_p$ and therefore Equation (7-6) becomes

$$\lambda_V = 1/\lambda_L \tag{7-7}$$

which may not be achieved. It is therefore considered necessary to violate Reynolds number scaling, which should only induce errors when the model is tested with its long dimension downwind (reattachment of flow). The dimensions of the model are therefore determined by the length scale, λ_L, which is governed by the scaling of the boundary layer thickness and the integral length scale of the wind turbulence (Davenport and Isyumov, 1968).

The forces and moments acting on the prototype are determined from the tests on a stationary rigid model by the force and moment coefficients defined generally as

$$\text{Force coefficient, } C_F = \frac{F}{\frac{1}{2}\rho U_r^2 A} \tag{7-8}$$

and

$$\text{Moment coefficient, } C_M = \frac{M}{\frac{1}{2}\rho U_r^2 AH} \tag{7-9}$$

where F is the base shear force, M is the base overturning moment, U_r is a reference wind velocity, and A and H are the frontal area and height of the building respectively.

In relating the wind tunnel force and wind spectra to the full-scale force and wind spectra, it is necessary to match the reduced frequencies, Equation (7-4), or use the frequency scale, Equation (7-5). The three similarity conditions defined by Equations (7-4), (7-8) and (7-9) are the relationships to be used in transfering wind tunnel forces to full-scale values.

7.3 DESCRIPTION OF EXPERIMENTS

7.3.1 Boundary Layer Wind Tunnel (BLWT I)

The experiments were conducted in the smaller boundary layer wind tunnel of The Boundary Layer Wind Tunnel Laboratory at The University of Western Ontario. The working section of this wind tunnel is approximately 24.4 m long, 2.4 m wide and has an adjustable height, variable from 1.7 m at the entrance to 2.3 m at the end. The wind velocity is adjustable to a maximum of 15 m/s. The turbulent boundary layer develops as the air flows over the roughness elements on the wind tunnel floor to the test area 20.7 m from the entrance. A rough carpet simulates open

terrain while suburban and urban terrains are simulated by randomly spaced foam blocks (25 mm high for suburban and 25-100 mm high for urban). A 0.25 m high grid of horizontal bars (trip) is used at the entrance to the test section for all three exposures to enhance the turbulence scales. This arrangement generates boundary layers that approximately match the turbulence intensity, mean velocity profiles and wind spectra of the natural wind. The boundary layer thickness determines a geometric scale of 1:400. A more detailed description of this wind tunnel is provided by Davenport and Isyumov (1968).

For the three types of boundary layers (terrains), all the flow characteristics were measured that are needed to calculate the wind forces. These include the mean wind profiles, turbulence intensities, power spectra of velocity fluctuations and normalized cross spectra (coherence functions).

The flow characteristics of the boundary layers generated in the suburban and urban exposures correspond to rather homogeneous environments. Local irregularities in the vicinity of the building can have a marked effect but such factors cannot be generally quantified.

7.3.2 Base Balance

In the second series of experiments, models constructed on the geometric scale of 1:400 were used to directly measure the wind forces acting on the buildings. Assuming a quasi-steady behaviour, i.e. the independence of the wind forces on the motion of the building (aerodynamic damping is negligible), the wind forces can be established using rigid,

extremely light models mounted on a special base balance. The base balance is very rigid and thus has very high natural frequencies and yet is very sensitive. It measures all static and dynamic components of the resultant wind forces acting on the model, except the vertical one. Two horizontal base shears, two overturning moments and the torque are measured (Figure 7.1). The models are constructed of lightweight white styrofoam. A complete description of the base-balance technique can be found in Tschanz (1982).

The advantage of this technique is that the forces measured on the stationary model are independent of building properties other than shape and can be used to predict the static and dynamic response of the prototype for any structural properties. If the prototype has a triangular mode shape the measured overturning moment corresponds to the generalized force of the prototype. If the prototype mode is uniform in bending and torsion, as it is approximately for a base-isolated building, the measured base shear and torque represent the force and twisting moment on the prototype, respectively. To obtain the data for prototype response prediction the mean values, root-mean-square values (r.m.s.) and power spectral densities of all force components were established for different exposures (turbulence characteristics) and for different angles of attack. The models are symmetrical about both axes, therefore the measurements were taken through 90 degrees in increments of 10°. The analog signals from the balance transducers were first amplified and then filtered. The low pass filters are set at 50 Hz to remove the acoustical wave generated by the fan blades (58 Hz) and the noise at higher frequencies. The filtered signal is digitized, processed and stored by a PDP 11/23

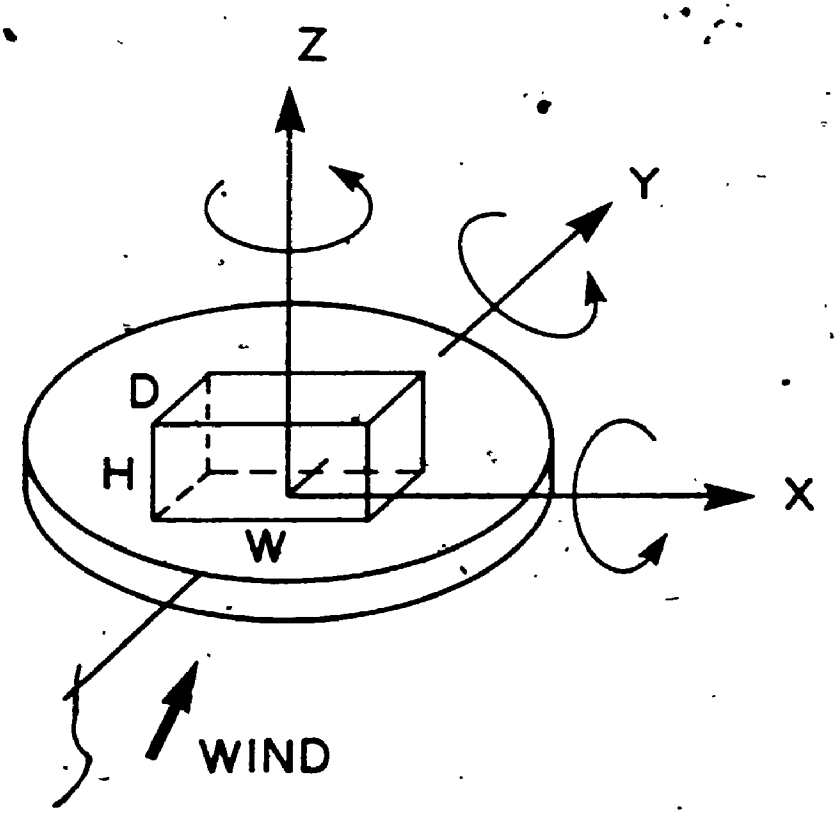

FIGURE 7.1 Schematic of model on the force balance and measured force components

workstation. A data acquisition program on this computer continuously controls the wind tunnel velocity, executes the sampling and rotates the model to the next test position. The entire process is fully automated. The gradient wind velocity was set to 12.2 m/s (40 ft/s). For a velocity scale, λ_V, of 1:4 and a length scale, λ_L, of 1:400, the time scale, λ_L/λ_V, is 1:100. Therefore, the experimental sampling period of 60 seconds corresponds to full-scale sampling of about 1 2/3 hours.

7.3.3 Models

Three models of prototype buildings, denoted A, B and C, were tested. The full-scale dimensions are listed in Table 7.1 and the model dimensions are given in Table 7.2. The dimensions in the narrow direction correspond to the plane frames analyzed in Chapter 5. Plate 7.1a shows Model A in the wind tunnel with urban exposure, Plate 7.1b shows Model B in suburban exposure, and Plate 7.1c shows Model C in suburban exposure. Models B and C were tested in all three exposures (open, suburban and urban) while Model A which is twice the width of Model B was tested in open and urban exposures.

7.3.4 Measurement of Wind Parameters

The mean wind profile was measured at the position corresponding to the centre of the upstream face of Models A and B. The measurements were done using two hot-wire anemometers with the lower probe starting at 6 mm (0.25 in) above the tunnel floor. The mean and r.m.s. wind velocity were measured using a 30 second sampling period at 6 mm (0.25 in) intervals for the first 51 mm (2 in) above the starting position then

TABLE 7.1 DIMENSIONS OF PROTOTYPE BUILDINGS

Building	Width		Depth		Height	
	m	ft	m	ft	m	ft
A	120	393.72	30	98.43	20	65.62
B	60	196.86	30	98.43	20	65.62
C	84.6	277.57	24.6	80.71	10.25	33.63

TABLE 7.2 DIMENSIONS OF MODELS

Model	Width		Depth		Height		Aspect
	mm	in	mm	in	mm	in	Ratio
A	300	11.81	75	2.95	50	1.97	6:1.5:1
B	150	5.91	75	2.95	50	1.97	3:1.5:1
C	212	8.35	62	2.44	26	1.02	8.25:2.4:1

(a)

(b)

(c)

PLATE 7.1 MODELS IN THE WIND TUNNEL
(a) Model A - urban exp.
(b) Model B - suburban exp.
(c) Model C - suburban exp.

at 13 mm (0.5 in) intervals for the second 51 mm (2 in) and thereafter at 102 mm (4 in) intervals. The experimental sampling period corresponds to full-scale sampling of about 50 minutes.

The auto-spectra and coherences were established by means of a Hewlett Packard Structural Dynamics Analyzer for both vertical and horizontal directions using two hot-wire anemometers. All measurements were done at a position corresponding to the upstream face of Models A and B. For the vertical measurements, the reference position (uppermost position) was 51 mm (2 in) above the tunnel floor; the second probe was located at points 13 mm (0.5 in), 25 mm (1 in) and 38 mm (1.5 in) above the tunnel floor in turn. For the horizontal measurements, the reference position was 76 mm (3 in) to the right (facing the intake) of the wind tunnel centreline and two sets of measurements at elevations of 25 mm (1 in) and 51 mm (2 in) above the tunnel floor were obtained. The second probe was positioned at points 76 mm (3 in), 152 mm (6 in), 229 mm (9 in) and 305 mm (12 in) away from the reference probe, in turn..

7.4 PRESENTATION AND DISCUSSION OF EXPERIMENTAL RESULTS

7.4.1 Mean Wind Profile

The variation in the mean wind velocity with height, for the three exposures, is shown in Figures 7.2, 7.3 and 7.4. In these figures, the full lines are the theoretical variation of the mean velocity obtained by fitting the experimental data points with the empirical power law (Davenport, 1961)

$$\bar{U}(z) = \bar{U}_g \left(\frac{z}{z_g}\right)^{\alpha} \qquad (7\text{-}10)$$

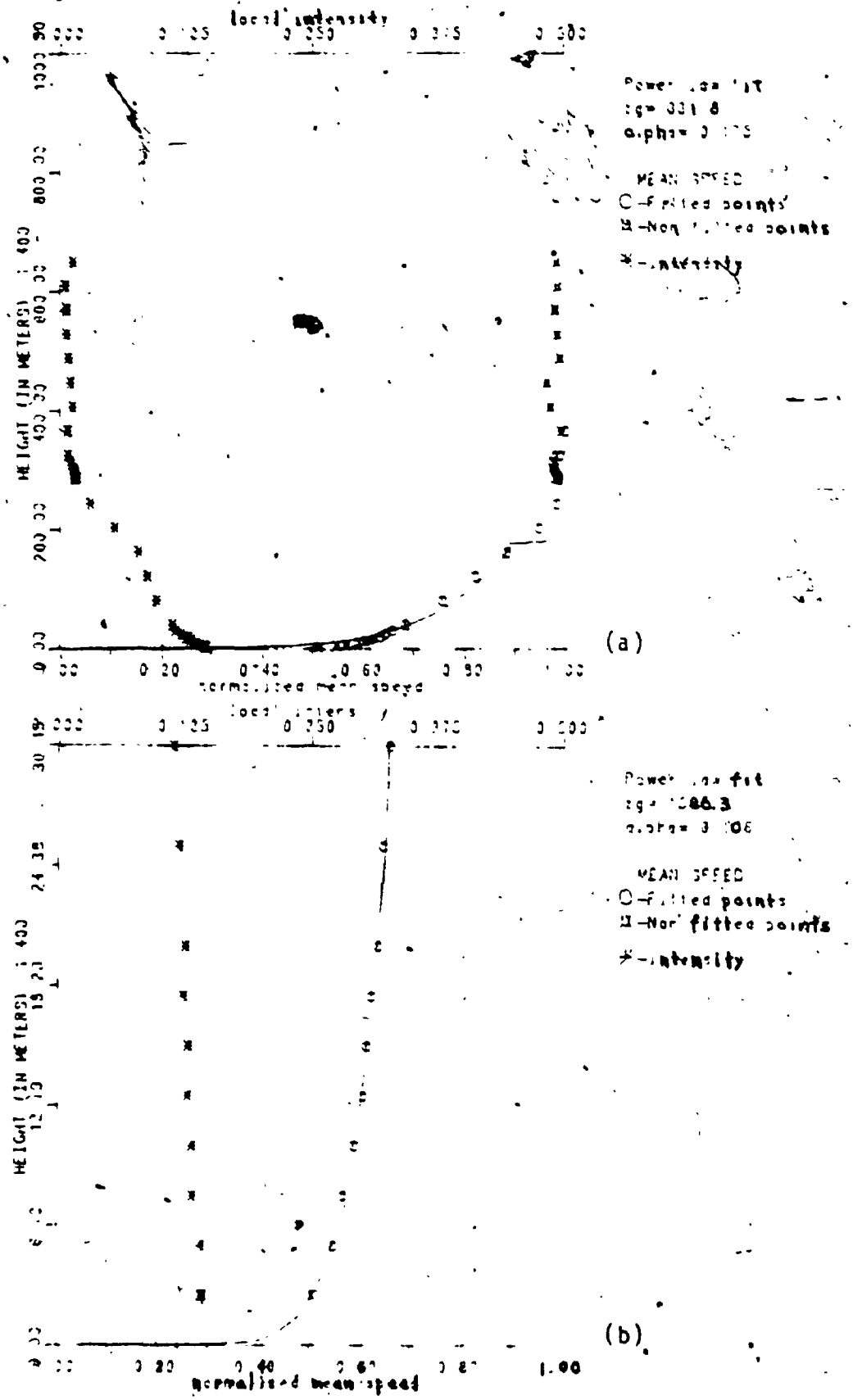

FIGURE 7.2 Mean wind profile and turbulence intensity for open exposure (a) whole profile and (b) lowest 30 m

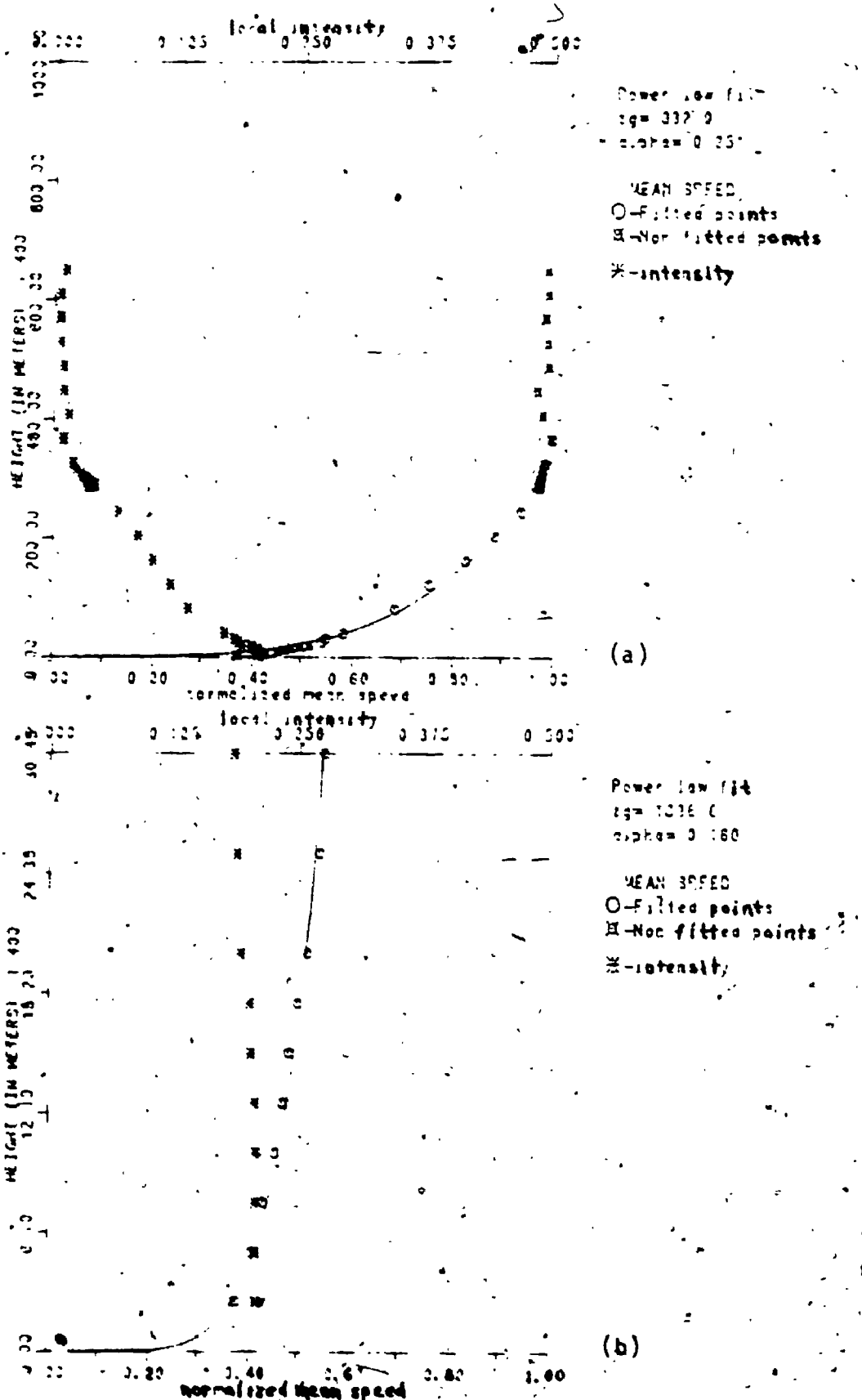

FIGURE 7.3 Mean wind profile and turbulence intensity for suburban exposure (a) whole profile and (b) lowest 30 m

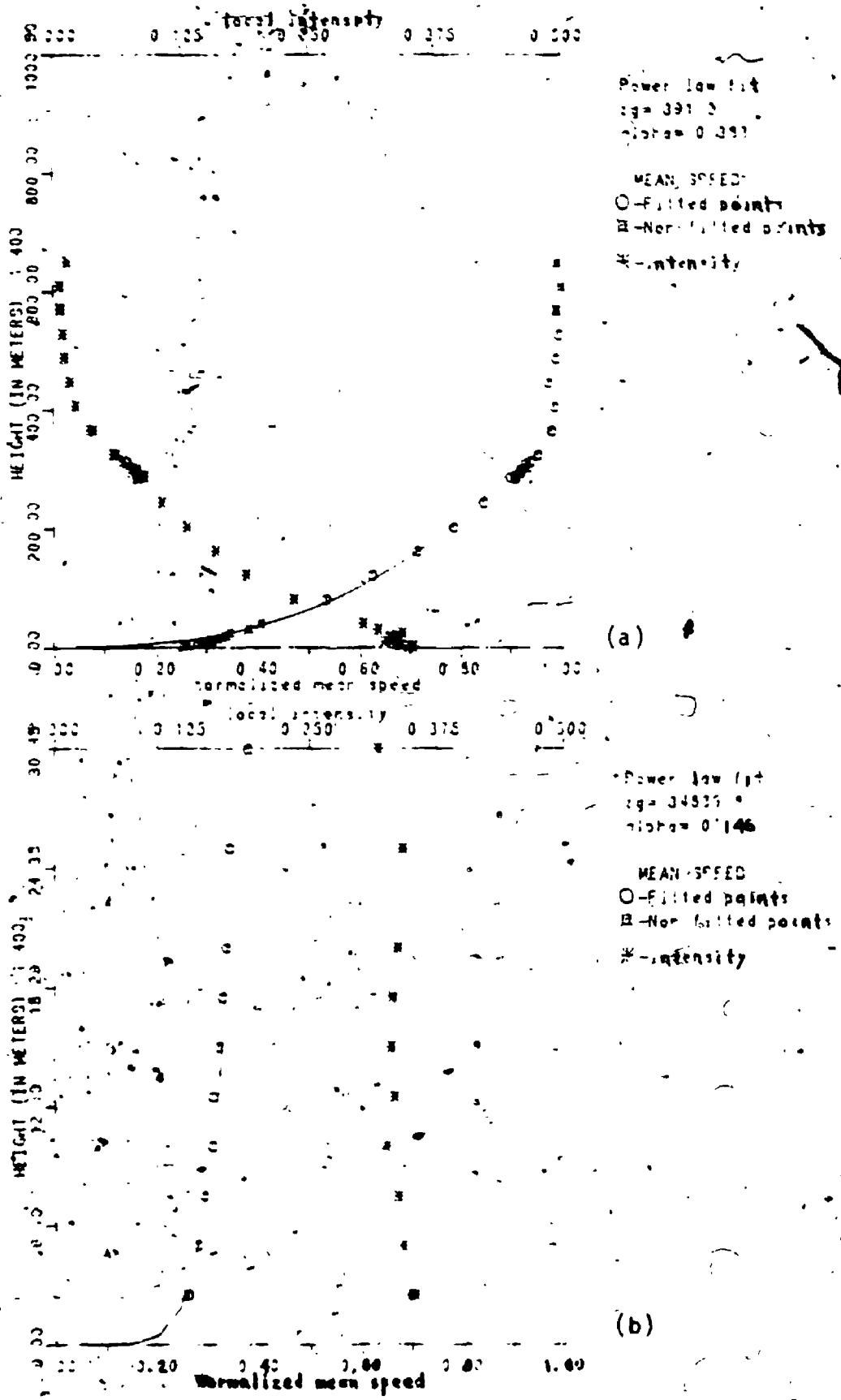

FIGURE 7.4 Mean wind profile and turbulence intensity for urban exposure (a) whole profile (b) lowest 30 m

where $\bar{U}(z)$ and $\bar{U}_g$ are the mean velocities at the elevation z and the gradient height, Z_g respectively and α is an exponent less than unity. Figures (b) depict the profile for the lowest 30 m. The theoretical fit is excellent particularly for the lowest 30 m (full-scale), the region of particular interest in this study. Both the exponent and the gradient height increase with increasing terrain roughness. The logarithmic law is an alternative expression for the wind profile near the ground and is given by

$$\bar{U}(z) = \frac{u_*}{k} \ln\left(\frac{z}{Z_o}\right) \qquad (7\text{-}11)$$

where u_* is the friction velocity which is a function of the surface shear stress, τ_o, and the air density, ρ ($u_* = \sqrt{\tau_o/\rho}$). The roughness length, Z_o, characterizes the extent of the surface roughness but is considerably less than the actual size of the roughness elements. The von Karman constant, k, is approximately 0.4. Typical values of the parameters for the power and logarithmic laws are given in Table 7.3. The wind profile parameters measured for the whole boundary layer are listed in Table 7.4 and for the lowest 30 m in Table 7.5. The values shown in Table 7.5 differ from those for the whole profile which suggests that the entire mean wind profile is not well suited for the lowest part of the boundary layer. The gradient heights in Table 7.5 are hypothetical resulting from the optimum fit. This is particularly obvious for the urban exposure.

The variation in the mean wind velocity and, therefore, the mean forces is slight over the lowest 30 m. Most base-isolated buildings are about 5 storeys high (20 m) or less. Thus, the mean velocity can be

TABLE 7.3 Typical Values of Parameters for the Power and Logarithmic Laws (Davenport, 1977)

Terrain	Z_g (m)	Z_o (cm)	α
Open	300	1-10	0.16
Suburban	400	30-100	0.28
Urban	500	100-500	0.40

TABLE 7.4 Power Law and Logarithmic Law Parameters for the Whole Boundary Layer by Figures 7.2 to 7.4

Terrain	Z_g (m)	Z_o (cm)	α_1
Open	332	2.3	.175
Suburban	332	44.7	.251
Urban	391	-	.383

TABLE 7.5 Power Law Parameters of Mean Wind Profile for Lowest 30 m by Figures 7.2 to 7.4

Terrain	Z_g (m)	α_2
Open	1565	.106
Suburban	1337	.160
Urban	34836	.145

assumed to be constant and equal to its value at the roof level for the practical analysis of the alongwind response.

7.4.2 Turbulence Intensity

Also shown in Figures 7.2 through 7.4 is the turbulence intensity defined at any level z by

$$I_u(z) = \frac{\sigma_u(z)}{\bar{U}(z)} \qquad (7\text{-}12)$$

where $\sigma_u(z)$ is the r.m.s. wind velocity fluctuation. The turbulence intensity is approximately equal to the power law exponent, α. Turbulence intensity variation over the whole profile is quite marked but over the lowest 30 m it is practically constant and may be taken as equal to its value at a suitable height such as 10 m.

7.4.3 Spectrum of Longitudinal Wind Velocity

The power spectrum defines the distribution of the energy of the wind fluctuations with frequency. The area under the spectrum is equal to the variance and the auto-covariance (correlation) function and the wind spectrum form a Fourier Transform pair. The peak of the velocity spectrum is at approximately 1 cycle per minute.

Power spectra of the longitudinal wind velocity fluctuations were measured at elevations corresponding to 5.1 m, 10.2 m, 15.2 m and 20.3 m (full-scale) in the three exposures along the vertical centreline of the wind tunnel. Evaluated in dimensionless form, the spectra for the three exposures are shown in Figures 7.5 through 7.7 plotted versus frequency

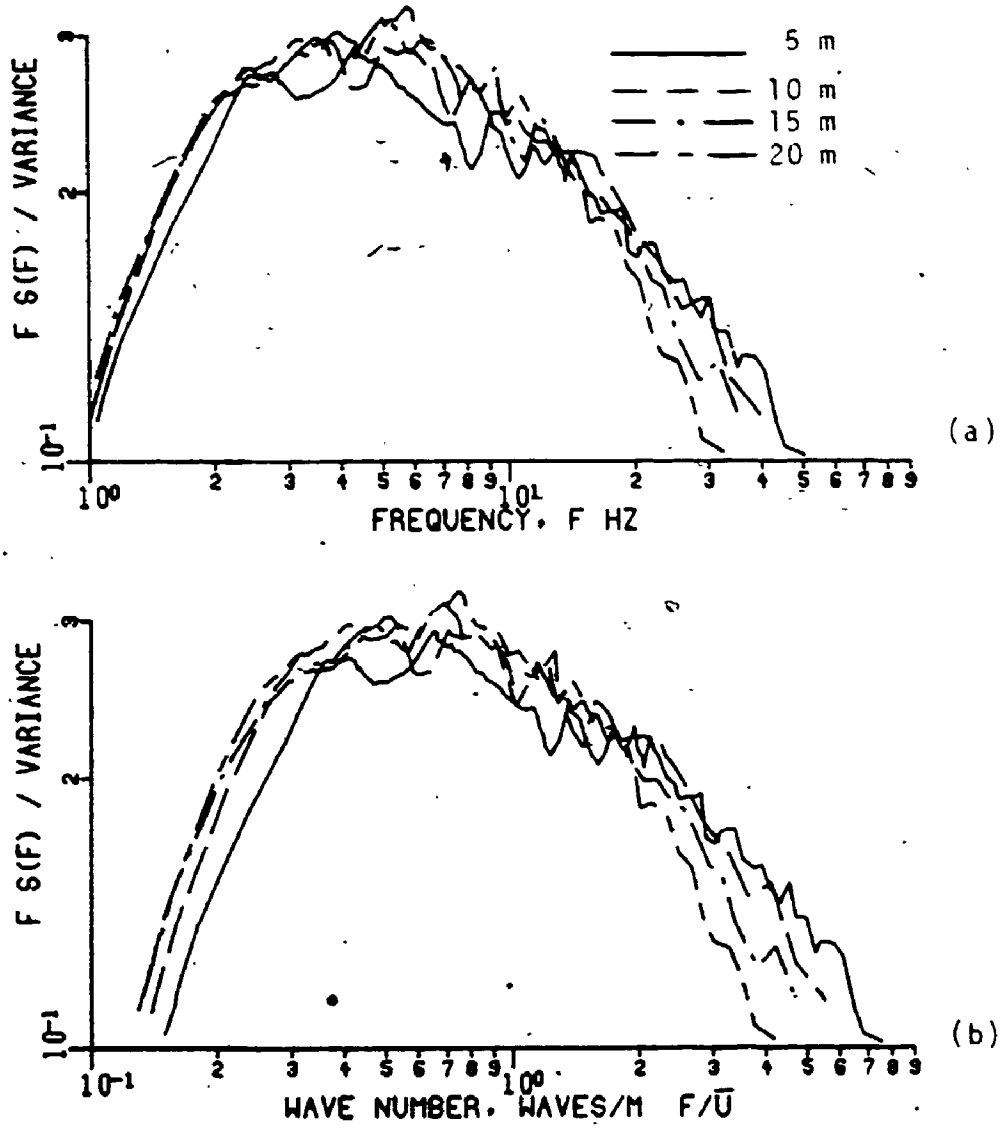

FIGURE 7.5 Measured wind spectra - open exposure
(a) vs frequency (b) vs wave number

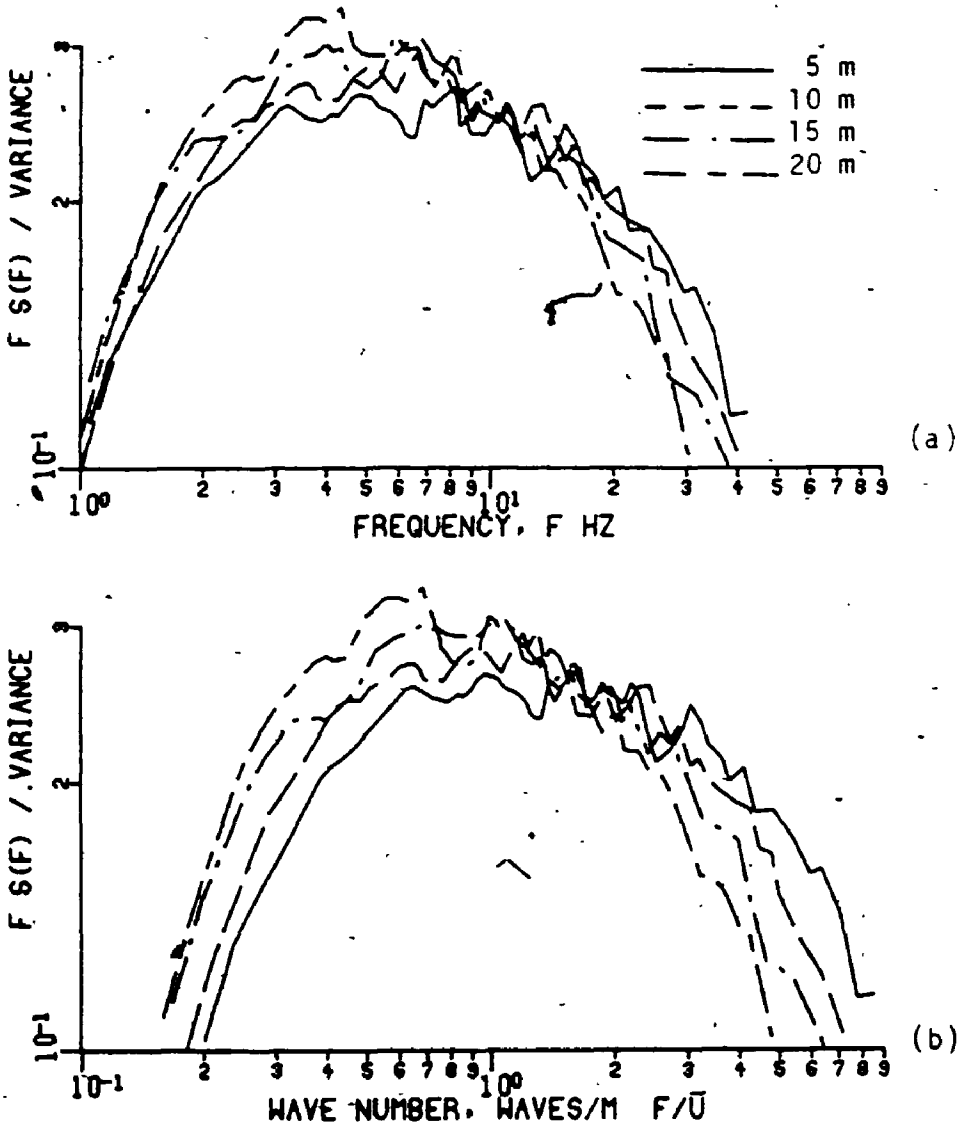

FIGURE 7.6 Measured wind spectra - suburban exposure
(a) vs frequency (b) vs wave number

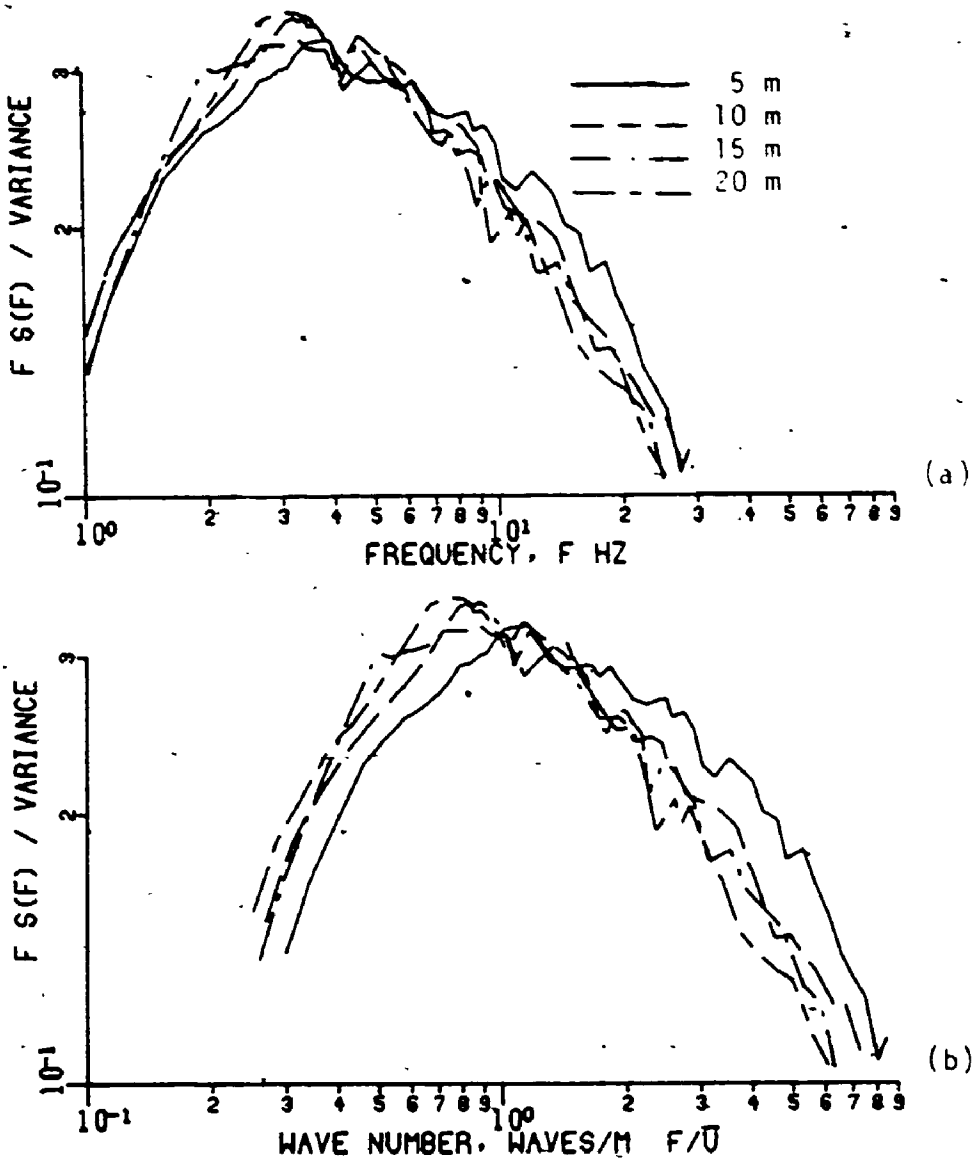

FIGURE 7.7 Measured wind spectra - urban exposure
(a) vs frequency (b) vs wave number

(a) and wavenumber (b). The spectral peaks are almost coincident along the frequency axis indicating that the spectrum varies slightly over the height considered. The spectra shift to the left along the wavenumber axis (larger wavelength), with increased elevation, implying that the length scale of turbulence increases upward as the eddies are allowed 'room to grow'. The spectral maximum also increases with height and the spectrum becomes more pointed. It is emphasized that the logarithmic spectrum does not show the true distribution of energy with frequency as its ordinates are multiplied by frequency.

For the purpose of later structural response analysis, the measured spectra are fitted with an analytical expression. In the inertial subrange, Kolmogorov's second hypothesis states that the energy spectrum is determined by the wavelength ($\bar{U}/f$) and the rate of viscous dissipation of energy. Therefore, the variation of the spectral ordinate with frequency is

$$S_u(f) \propto f^{-5/3} \qquad (7\text{-}13)$$

Several spectra of this form have been suggested. Davenport's spectrum (1961) is

$$f\frac{S_u(f)}{\sigma_u^2} = \frac{2/3\ n^2}{(1+n^2)^{4/3}} \qquad (7\text{-}14)$$

where the reduced frequency $n = fL/\bar{U}_{10}$, with the length scale $L = 1200$ m, $\bar{U}_{10}$ is the mean velocity at 10 m, f is the cyclic frequency and σ_u^2 is the variance. Harris (1971) modified Davenport's spectrum so that there is a value at zero frequency (giving an integral length scale). The expression for the spectrum is

$$f\frac{S_u(f)}{\sigma_u^2} = \frac{0.6n}{(2+n^2)^{5/6}} \qquad (7\text{-}15)$$

in which the length scale, L = 1800 m. Simiu (1975) suggested the expression

$$f\frac{S_u(f)}{\sigma_u^2} = \frac{100/3\ n}{(1+50n)^{5/3}} \qquad (7\text{-}16),$$

which is a modified form of the equation proposed by Kaimal et al. (1972) such that the variance $\sigma_u^2 = 6.0\ u_*^2$. Thus, the basic form of the spectrum is well established.

A model chosen for fitting the dimensionless spectra to measured data is that of Olsen et al. (1984), i.e.

$$f\frac{S_u(f)}{\sigma_u^2} = \frac{A\ n^{\gamma}}{(1+Bn^{\theta})^{\Omega}} \qquad (7\text{-}17)$$

where the reduced frequency is $n = f.z/\bar{U}(z)$, $\bar{U}(z)$ is the mean wind velocity at height z and A, B, γ, Ω and θ are fitting parameters. On a log-log plot of the spectrum, γ represents the low frequency slope while the high frequency slope is given by $\gamma-\Omega\theta$. The values of Ω, θ and γ influence the pointedness (or bluntness) of the spectrum. The position of the spectrum is determined by the parameters A and B.

The spectrum may then be subjected to several theoretical considerations. For the spectrum to conform to Kolmogorov's law in the inertial subrange, the slope of the high frequency asymptote must be

$$\gamma - \Omega\theta = -2/3 \qquad (7\text{-}18)$$

and the ordinate of the dimensionless spectrum is

$$f \frac{S_u(f)}{\sigma_u^2} = C\, n^{-2/3} \qquad (7\text{-}19)$$

in which C is a constant of proportionality.

For the position of the measured spectral maximum, n_m, to coincide with the maximum of the model, the following relationship must hold

$$n_m = \left(\frac{1.5\gamma}{B}\right)^{1/\theta} \qquad (7\text{-}20)$$

which is obtained by differentiating Equation (7-17) with respect to the reduced frequency, n. Substituting the expression for n_m in Equation (7-17) gives the value of the spectral maximum, S_m, as

$$\left(f \frac{S_u(f)}{\sigma_u^2}\right)_{max} = S_m = A\left(\frac{1.5\gamma}{B}\right)^{\gamma/\theta}(1+1.5\gamma)^{-\Omega} \qquad (7\text{-}21)$$

The integral of the dimensionless spectrum must equal unity, therefore

$$\int \frac{S_u(f)}{\sigma_u^2}\, df = 1.0 \qquad (7\text{-}22)$$

which implies, by integrating Equation (7-17), that

$$1.0 = AB^{-\gamma/\theta}\left(\frac{1}{\theta}\right) \frac{\Gamma(\gamma/\theta)\Gamma\left(\frac{2}{3\theta}\right)}{\Gamma(\Omega)} \qquad (7\text{-}23)$$

As pointed out by Harris (1971), in relation to Davenport's spectrum, it is desireable that the spectrum has a value at zero frequency. This is required to define the integral time and length scales. Therefore, the parameter γ is set equal to unity and $\Omega = 5/3\theta$. Another form of the characteristic length scale corresponds to the peak of the logarithmic spectrum, $f\, S_u(f)$,

$$L = \bar{U}(z)/f_m \tag{7-24}$$

where f_m is the frequency associated with the spectral peak. If, instead of the height z, this length scale is used in the normalization for the reduced frequency, then at the peak

$$n_m = \frac{f_m L}{\bar{U}(z)} = 1 \tag{7-25}$$

Substituting for n_m in Equation (7-20) with $\gamma=1$, the value of B becomes 1.5.

The high frequency portion of the dimensionless spectrum can be approximated by

$$f\frac{S_u(f)}{\sigma_u^2} = \frac{A}{B^{\Omega}} n^{-2/3} = \kappa f^{-2/3} \tag{7-26}$$

where

$$\kappa = \frac{A}{1.5^{5/3\theta}} \left(\frac{L}{\bar{U}(z)}\right)^{-2/3} \tag{7-27}$$

Rearranging this equation gives the length scale

$$L = \bar{U}\left[\frac{\kappa}{A} 1.5^{5/3\theta}\right]^{-3/2} \tag{7-28}$$

for which the spectral model conforms to Kolmogorov's law. The final expression for the dimensionless spectrum becomes

$$f\frac{S_u(f)}{\sigma_u^2} = \frac{An}{(1+1.5n^{\theta})^{5/3\theta}} \tag{7-29}$$

in which the reduced frequency is $n = fL/\bar{U}(z)$ and the length scale, L, is computed from Equation (7-28).

The unknown parameters are A and θ. The proportionality constant, κ, is determined by optimization of the spectral points in the high frequency region. The parameter A is expressed in terms of θ using Equation (7-23). The length scale, L, is given by Equation (7-28) which allows the computation of the reduced frequency in terms of θ. The parameter, θ, is then computed by optimization of the measured spectral values. Once θ is determined, A and L are computed. The parameters established in this way are listed in Table 7.6. The measured spectra and theoretical fitted spectra for the three exposures are shown in Figures 7.8 through 7.10. The area under the normalized fitted spectra in open exposure varies from 0.97 to 1.03 (integrated numerically from 0 to 200 Hz), a difference of 6 per cent. The spectral peaks on a log-log plot correspond to the drooping portions of the spectral density functions and the spread is much less pronounced. Consequently, the differences in the areas are small.

Harris (1971) has shown that the time scale of turbulence is

$$T = \frac{1}{4\sigma_u^2} S_u(o) \qquad (7\text{-}30)$$

which is obtained by integrating the auto-correlation function (normalized auto-covariance). The integral length scale, ℓ, is

$$\ell = \bar{U}(z)\ T = \frac{\bar{U}(z)}{4\sigma_u^2} S_u(o) \qquad (7\text{-}31)$$

From Equation (7-29), the value of the spectrum at zero frequency is

$$S_u(o) = \sigma_u^2 \frac{L}{\bar{U}(z)} A \qquad (7\text{-}32)$$

TABLE 7.6 PARAMETERS A, θ, L, ℓ AND σ_u FOR THE DIMENSIONLESS WIND SPECTRUM (values in parentheses are full-scale, length scale 1:400)

Terrain	Elev. in (m)	K	A	θ	L(m)	ℓ(m)	σ_u(m/s)	$I_u=\sigma(z)/\bar{U}(z)$
Open	.5 (5.08)	1.29	.62	1.85	1.30 (520)	(80.6)	.95	.142
	1.0 (10.16)	1.31	.58	2.26	1.36 (544)	(78.9)	.96	.134
	1.5 (15.24)	1.23	.57	2.50	1.56 (624)	(88.9)	.97	.130
	2.0 (20.32)	1.16	.57	2.57	1.80 (720)	(102.6)	.98	.127
Mean			.59	2.30	1.51 (602)			
Std.Dev.			.02	.28	.20 (78.3)			
C.O.V.			.04	.12	.13			
Suburban	.5 (5.08)	1.37	.64	1.75	.88 (352)	(56.3)	1.03	.208
	1.0 (10.16)	1.39	.59	2.10	.95 (380)	(56.1)	1.15	.207
	1.5 (15.24)	1.30	.57	2.38	1.12 (448)	(63.8)	1.19	.202
	2.0 (20.32)	1.20	.57	2.70	1.41 (564)	(80.4)	1.21	.192
Mean			.59	2.23	1.09 (436)			
Std.Dev.			.03	.35	.20 (81.7)			
C.O.V.			.05	.16	.19			
Urban	.5 (5.08)	1.16	.57	2.63	.86 (344)	(49.0)	1.16	.340
	1.0 (10.16)	1.02	.57	2.71	.96 (384)	(54.7)	1.22	.325
	1.5 (15.24)	0.97	.57	2.89	1.03 (412)	(58.7)	1.29	.330
	2.0 (20.32)	0.92	.57	2.95	1.22 (488)	(69.5)	1.38	.336
Mean			.57	2.80	1.02 (407)			
Std.Dev.			0	.13	.13 (52.6)			
C.O.V.			0	.05	.13			
Overall Mean			.58	2.44	1.21 (483)			

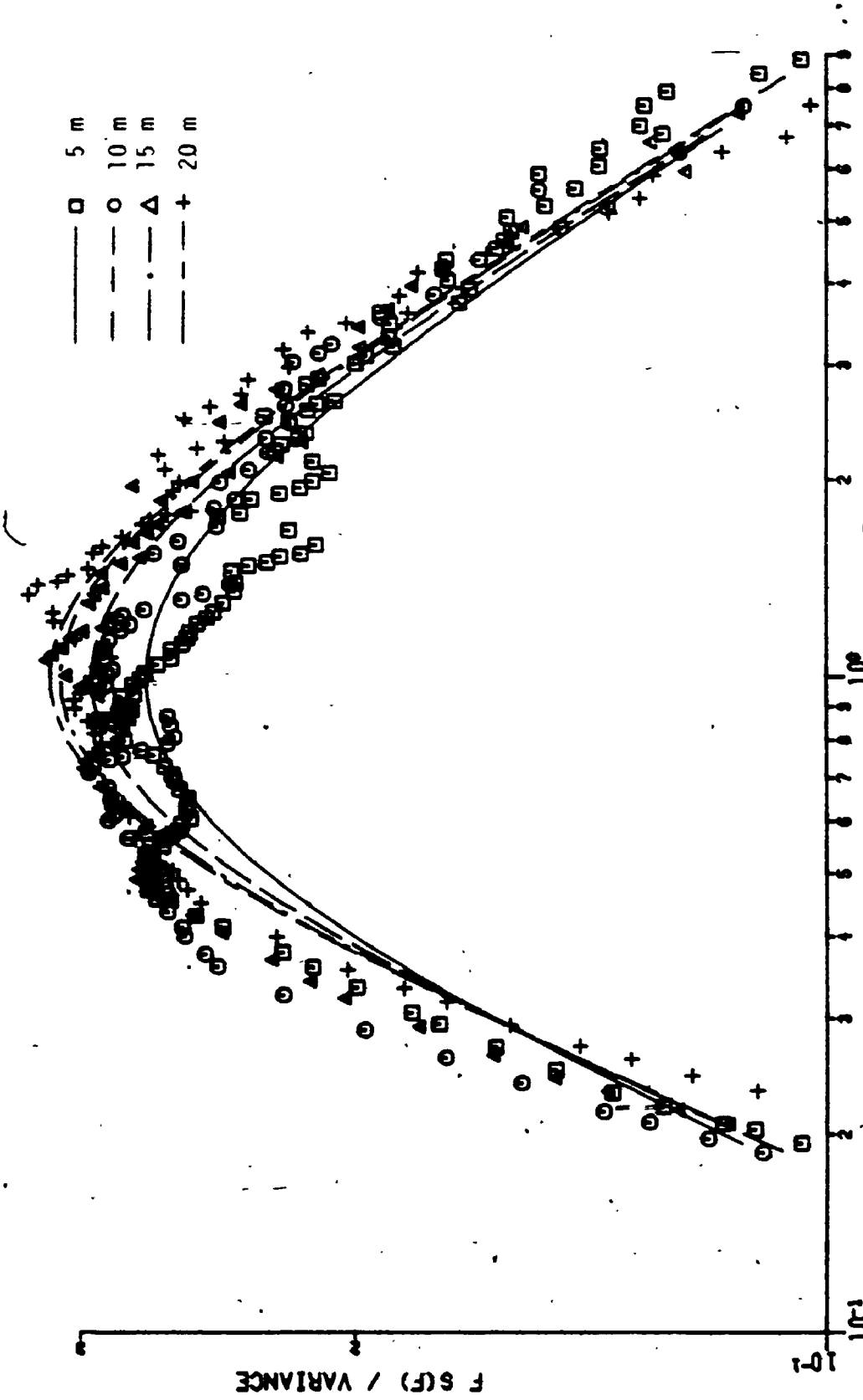

FIGURE 7.8 Measured spectra and theoretical fitted spectra - open exposure

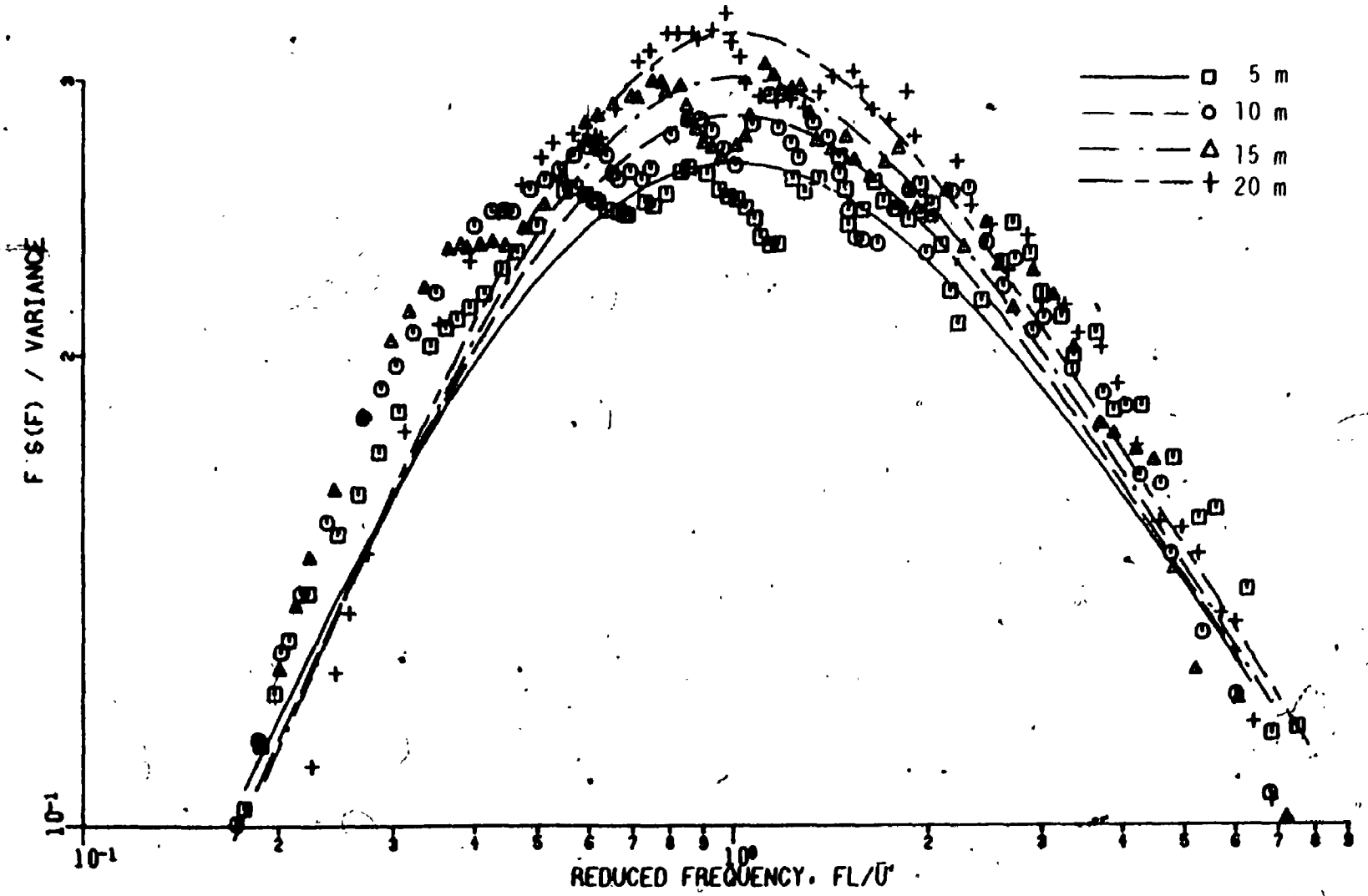

FIGURE 7.9 Measured spectra and theoretical fitted spectra - suburban exposure

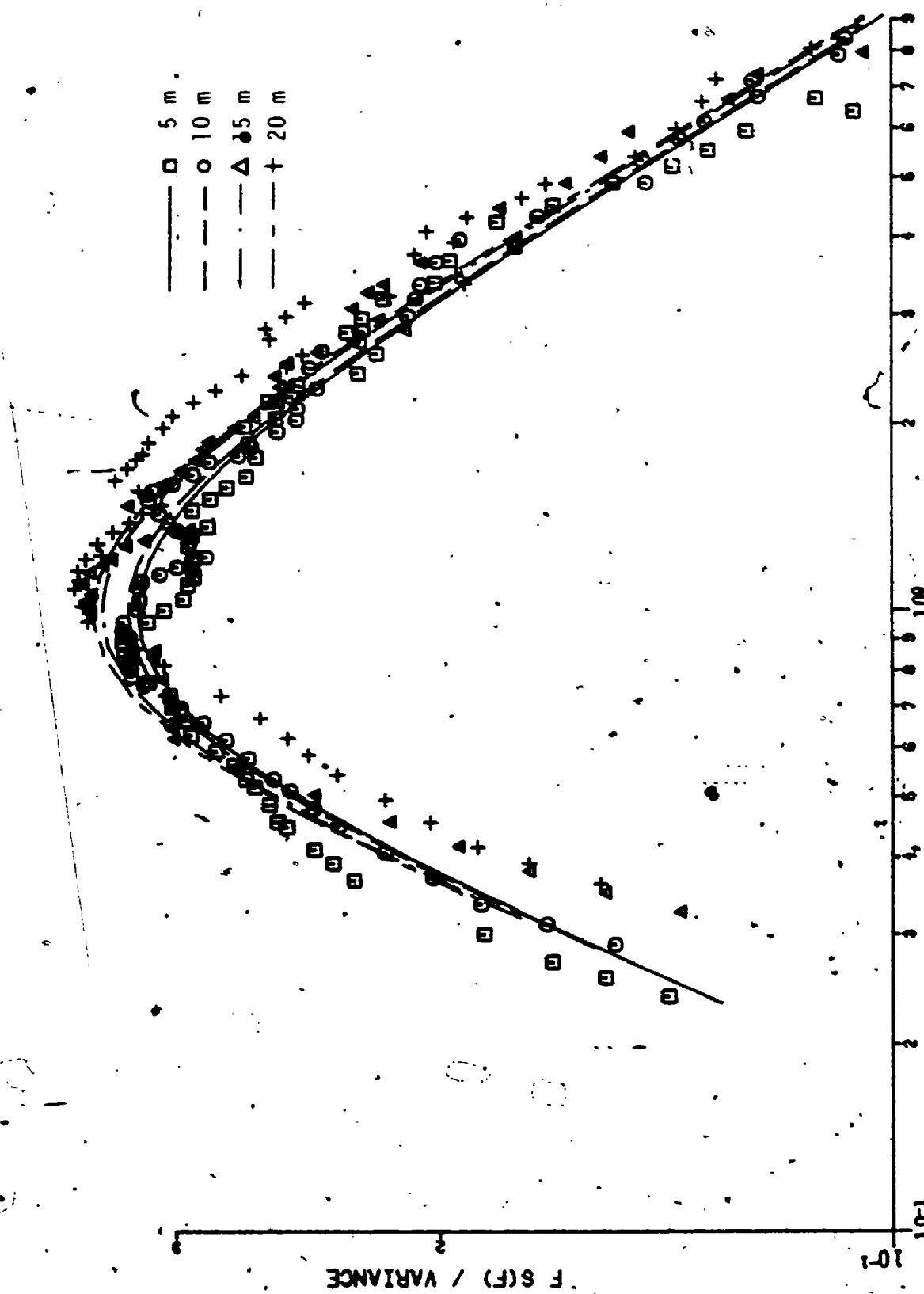

FIGURE 7.10 Measured spectra and theoretical fitted spectra - urban exposure

Then the integral length scale is related to the length scale L by

$$\ell = \frac{A}{4} L \qquad (7\text{-}33)$$

For an approximate value of A equal to 0.6 gives $\ell = 0.15L$. This compares well with the relationship derived on the assumption of an exponentially decaying auto-correlation function (Pasquill, 1962) which is

$$\ell = \frac{1}{2\pi} L = 0.159\ L \qquad (7\text{-}34)$$

The integral length scales (full-scale) are listed in Table 7.6. Values of the length scale, L, derived from the reduced frequency corresponding to spectral peaks are, according to Berman (1965)

$$L = 200\ z^{0.25} \qquad (7\text{-}35)$$

and, according to Fichtl and McVehil (1970)

$$L = 600\ m \qquad (7\text{-}36)$$

Berman's expression which is based on spectra from many locations, with roughness lengths varying from 1 cm to 100 cm, compares well with the suburban exposure length scales (Table 7.6). The length scale of 600 m is close to the values for the open exposure. Equation (7-36) was derived from data obtained in open terrain.

The fitted parameters of the dimensionless wind spectra do not vary much with height and thus the mean value of these parameters can be quite appropriate for evaluating the dimensionless spectrum. The theoretical spectra, calculated using the mean values, along with the measured spectra are plotted in Figure 7.11 for all three exposures. In computing

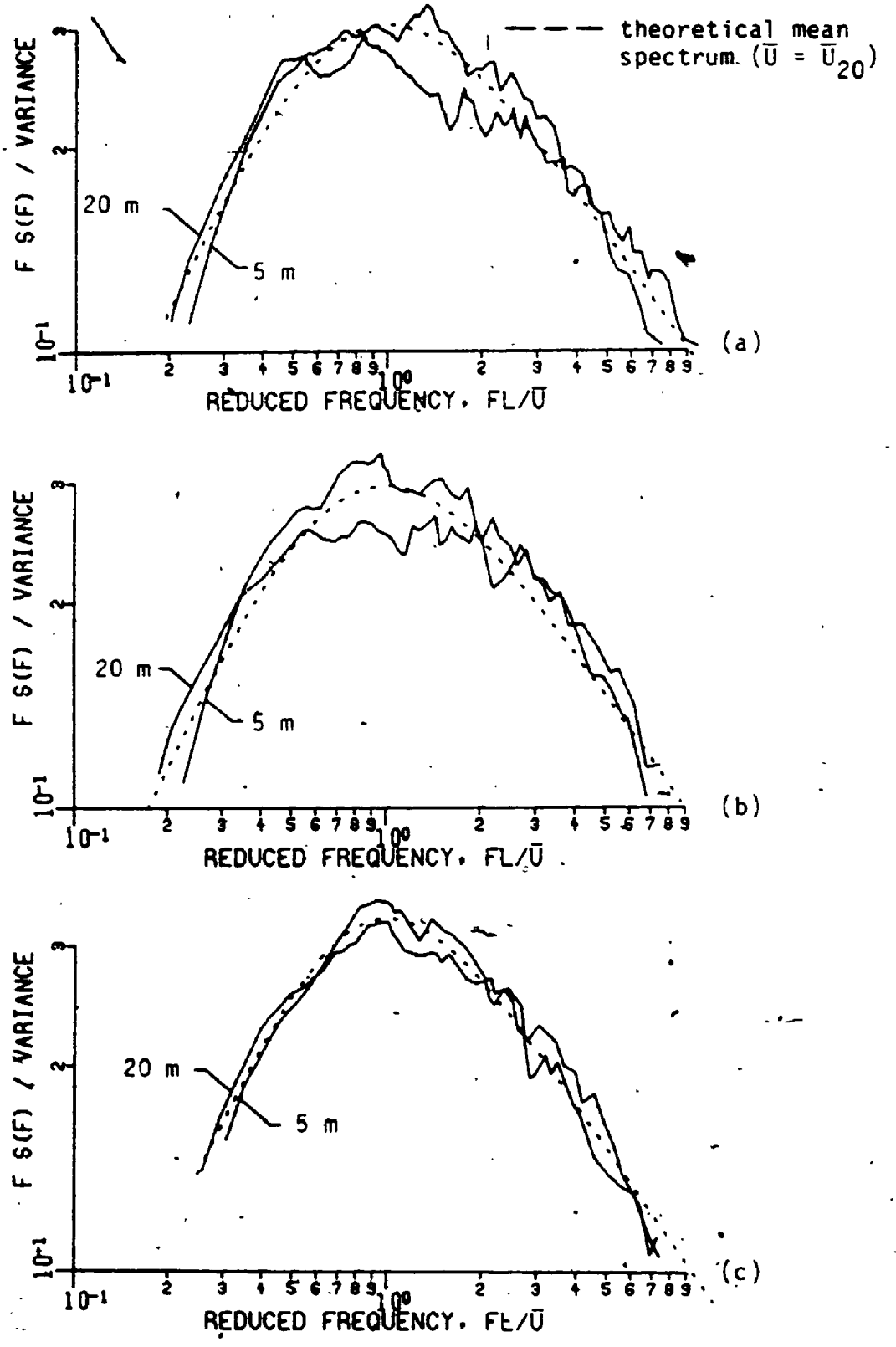

FIGURE 7.11 Measured spectra and theoretical mean spectrum (a) open exp. (b) suburban exp. (c) urban exp.

the reduced frequency for the fitted spectrum, the mean wind velocity at 20 m is used. The elevation of 20 m is adopted since this is the common roof level expected for base-isolated buildings and the wind velocity at this level varies less with terrain roughness than at the usual 10 m. The mean spectrum fits within the range of spectra very well.

To indicate the comparison of other theoretical spectra with the measured ones, Figure 7.12 shows, for open and urban exposures, the wind tunnel spectra at elevations of 5.1 m and 20.3 m, the mean fitted spectrum, Harris's spectrum and the ESDU spectrum (1986) versus full-scale frequencies. A length scale of 400 is applied to the wind tunnel spectra. The ESDU spectrum is height dependent and is presented for an elevation of 10 m although this spectrum is recommended for elevations greater than 20 m above the general level of obstructions. For the open exposure, the ESDU spectrum is close to the wind tunnel spectra for the higher frequencies while there is some difference in the spectral maxima. For the urban exposure, Harris's spectrum matches the wind tunnel spectra better than the ESDU spectrum. Similar differences in the spectral maxima and their position were found by Flaga and Wrana (1987) for spectra at 10 m elevation. Thus, the length scale of 400 is suitable for full-scale computations.

Finally, the mean fitted spectra for all three exposures and the spectrum using the overall mean of the parameters are shown in Figure 7.13. The spectra collapse in both the high frequency and low frequency regions. The differences occur in the spectral maxima which result in only a small difference in the variance. Therefore, one spectrum using

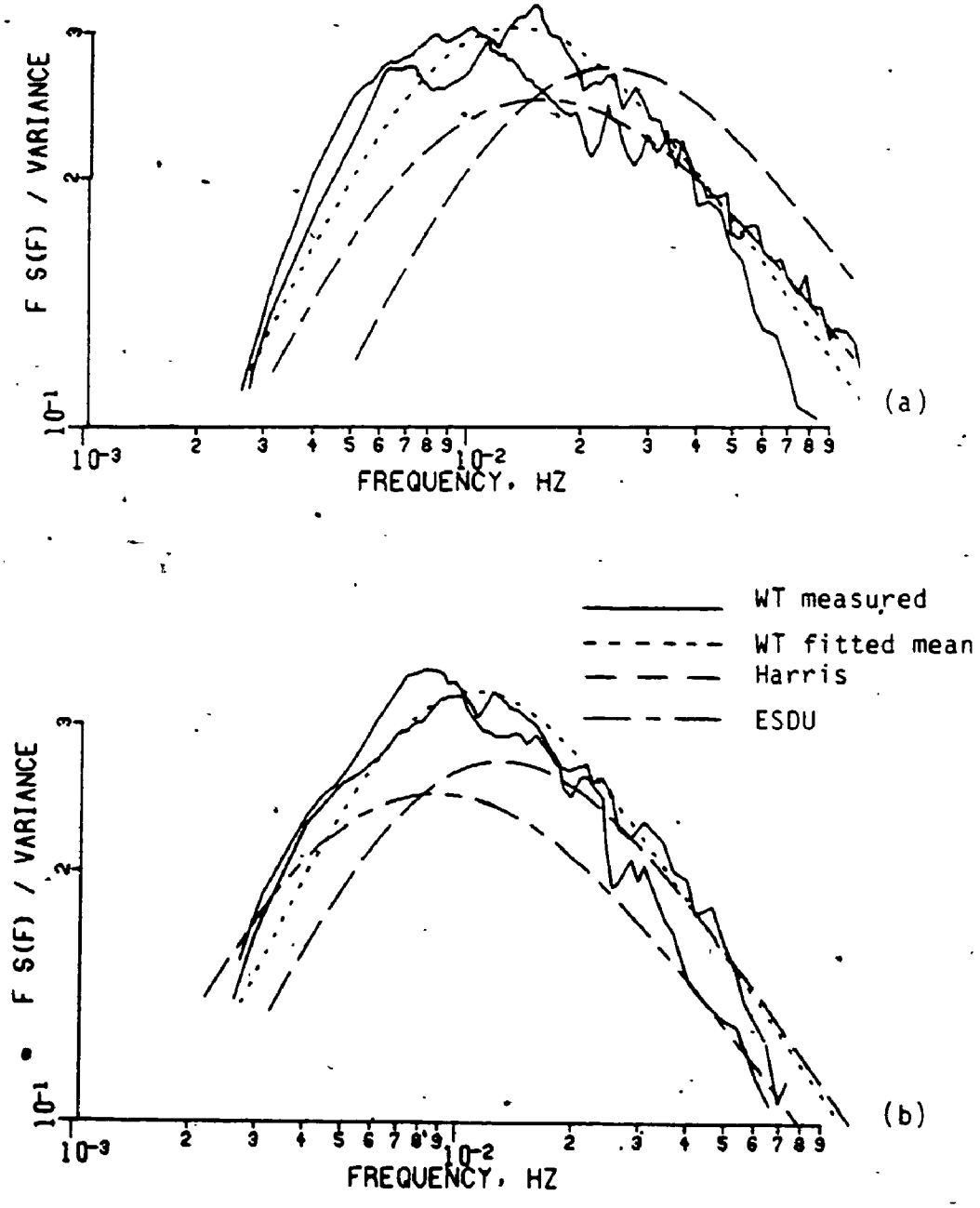

FIGURE 7.12 Wind tunnel spectra, Harris's spectrum and ESDU spectrum (full-scale frequencies) (a) open exp. (b) urban exp.

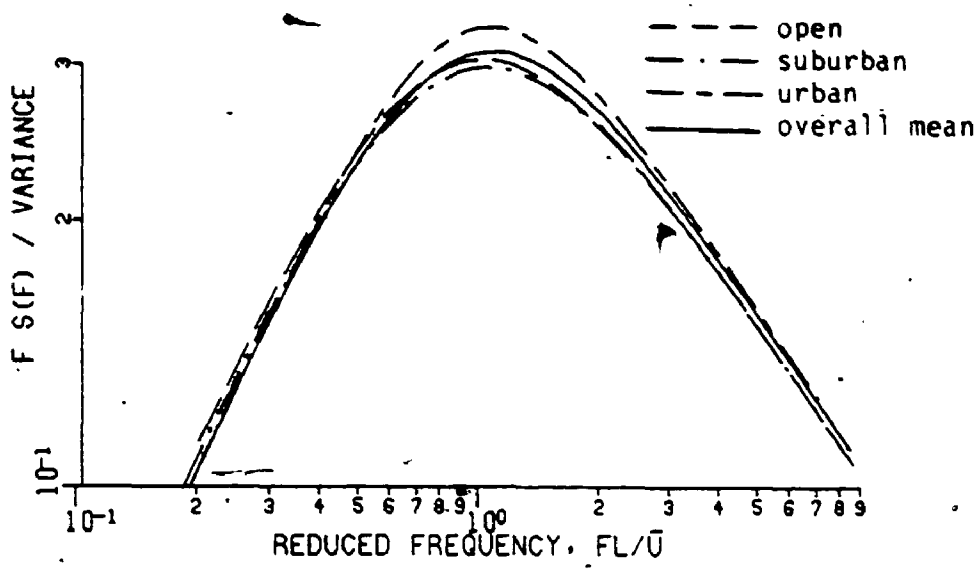

FIGURE 7.13 Mean and overall mean wind tunnel spectra

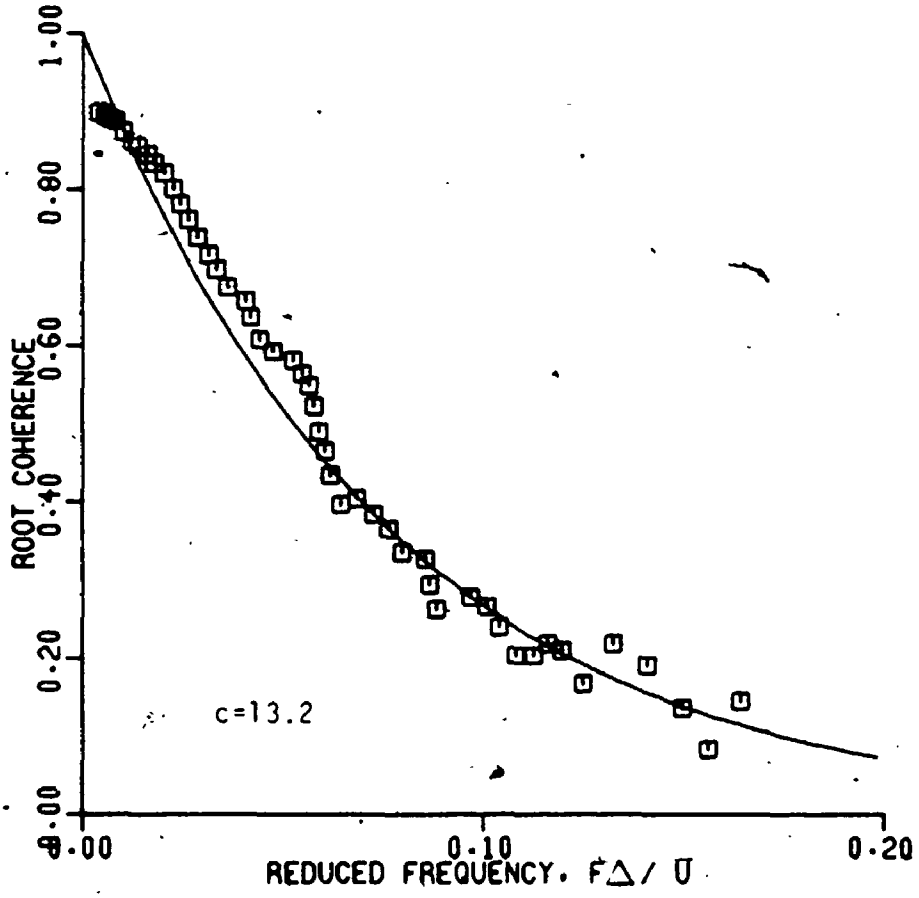

FIGURE 7.14 Fit of root coherence function to the coherence in urban exp. (separation Δ=1.5 in, lower probe at 0.5 in above floor)

the overall mean of the parameters can be considered to be adequate for all three exposures. The overall means of the spectrum parameters are $A = 0.58$, $\theta = 2.44$ and $L = 483$ m in full-scale.

7.4.4 Horizontal and Vertical Coherences

The coherence functions describe the spatial correlation of the frequency components of the wind velocity at two positions. The coherence is defined as

$$\text{coh}(f) = \frac{|S_{12}(f)|^2}{S_1(f)S_2(f)} \qquad (7\text{-}37)$$

in which $S_1(f)$ and $S_2(f)$ are the local spectra at positions 1 and 2 respectively and $S_{12}(f)$ is the cross-spectrum of the longitudinal wind velocity at positions 1 and 2. The magnitude of the cross spectrum is given by

$$|S_{12}(f)|^2 = C_{o_{12}}^2(f) + Q_{u_{12}}^2(f) \qquad (7\text{-}38)$$

where $C_{o_{12}}(f)$ is the co-spectrum (real part), and $Q_{u_{12}}(f)$ is the quad-spectrum (imaginary part). An often used empirical expression for the root coherence is

$$\sqrt{\text{coh}(f)} = e^{-c\frac{\Delta f}{\bar{U}}} \qquad (7\text{-}39)$$

where Δ is the absolute value of the separation and f is the frequency. For horizontal separations, $\bar{U}$ is the mean velocity at the elevation under consideration while for vertical separations $\bar{U}$ is the average of the mean velocities at positions 1 and 2. Values of the decay coefficient,

c, commonly used are between 6 and 10 for vertical separation and between 10 and 16 for horizontal separation.

The decay coefficients for the coherences measured in the wind tunnel were determined by optimization. The decay coefficients established are listed in Table 7.7. The fit of Equation (7-39) to the data is shown for one case in Figure 7.14. The trend is for the decay coefficient to decrease and the correlation to increase as the terrain becomes rougher, indicating that larger eddies are formed. The decay coefficient is actually dependent on both the separation and the elevation. An expression reflecting these dependencies was proposed by Panofsky and Dutton (1984); it is

$$c = c_o + c_m \frac{\Delta}{z} \qquad (7\text{-}40)$$

where Δ/z is the normalized separation. The values of c_o and c_m are obtained from a best fit to Equation (7-40).

More extensive measurements of coherence were done by Ng (1986) in the larger wind tunnel at The University of Western Ontario. The variation of the decay coefficients with normalized separation is shown in Figures 7.15 and 7.16. The symbols indicate the measured values while the lines represent theoretical fits. The trends of both data sets are similar throughout and the agreement is good in some cases. The measurements by Ng incorporate many more data points. The values of c_o and c_m to be used in the response calculations are; therefore, computed from a weighted average of those obtained by the present study and the study by Ng. The weighting is based on the number of reliable data points in

TABLE 7.7 Measured Decay Coefficients (distances in mm)

(a) Horizontal Separation - c_y

Exp.	Δy / z	38	76	152
open	25	-	23.	54.
	51	-	18.5	-
suburban	25	-	30.	50.
	51	-	27.	-
urban	25	-	12.3	26.
	51	9.3	14.8	-

(b) Vertical Separation (z_1 = 51 mm) - c_z

Exp.	z_2	$\bar{z}$	Δz	c_z
open	38	44	13	12.4
	25	38	25	14.8
	13	32	38	18.6
suburban	38	44	13	11.1
	25	38	25	13.3
	13	32	38	16.2
urban	38	44	13	9.2
	25	38	25	11.4
	13	32	38	13.2

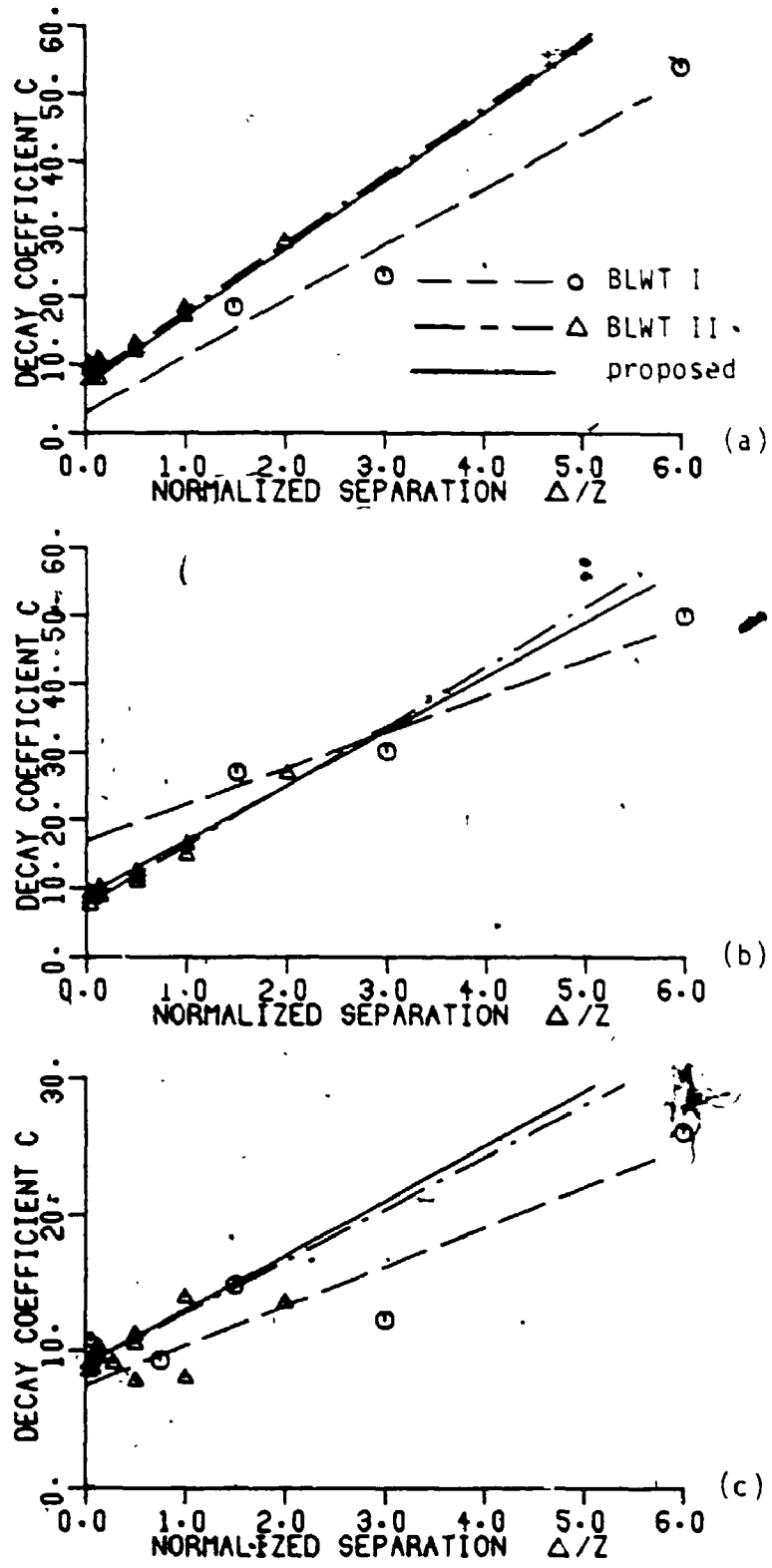

FIGURE 7.15 Coherence decay coefficient, c_y vs normalized horizontal separation (a) open exp. (b) suburban exp. (c) urban exp. (separation = Δ, elevation = z)

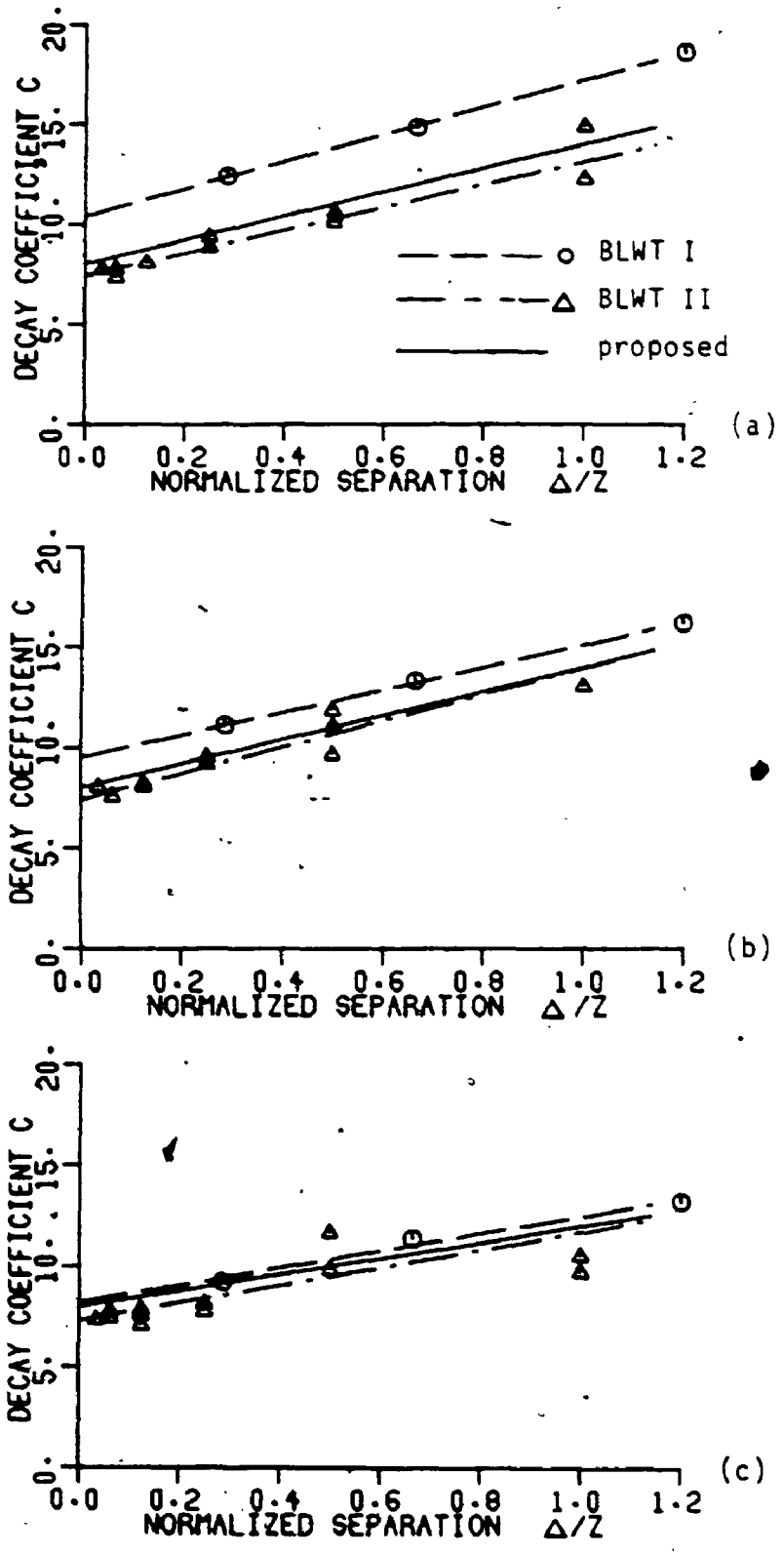

FIGURE 7.16 Coherence decay coefficient, c_z, vs normalized average vertical separation (a) open exp. (b) suburban exp. (c) urban exp. (separation = Δ, average elevation = z)

each case. The final values are listed in Table 7.8. Figures 7.15 and 7.16 also show the variation of the decay coefficient based on these proposed values. It is worth noting that the variations in the decay constants c with Δ/z are quite strong. The code data such as those of the NBCC are based on decay coefficients independent of Δ/z.

7.4.5 Flow Over Low-Rise Buildings

As the flow encounters the building in its path, part of the air is deflected upwards; some of the air flows around the sides; and the other part deflects downward forming vortices which eventually flow around the sides (horse-shoe vortices). Pressures develop on the windward face and suctions on the leeward face. The streamlines separate from the front roof edge (Figure 7.17) where a shear layer separates the outer region from the inner (wake) region. Large negative pressures (suctions) are created which decrease downstream. When the roof is long, streamwise, compared to the height of the building, reattachment of the flow occurs with associated zero or positive pressures. Figures 7.18 and 7.19 show examples of the pressure contours and trends in the pressure distribution on the roofs of low-rise models. The flow from the upper third of the building goes over the roof. In doing so, it displaces the flow having more kinetic energy (mean wind profile increases with height) which lowers the separation streamline. The difference in kinetic energy increases as the terrain roughens leading to lower streamlines, smaller suctions and earlier reattachment.

The pressure distribution on the roof is important not only for the

TABLE 7.8 Decay Coefficient Parameters c_o and c_m

Direction		Lateral			Vertical		
Exposure		Open	Suburban	Urban	Open	Suburban	Urban
BLWT I (present study)	c_o	3.	17.	7.5	10.4	9.5	8.2
	c_m	8.2	5.3	2.9	6.8	5.6	4.3
BLWT II (Ng)	c_o	7.8	7.6	9.	7.4	7.4	7.3
	c_m	10.	8.7	3.8	5.7	6.5	4.4
Proposed	c_o	7.	9.	9.	8.	8.	8.
	c_m	10.	8.	4.	6.	6.	4.

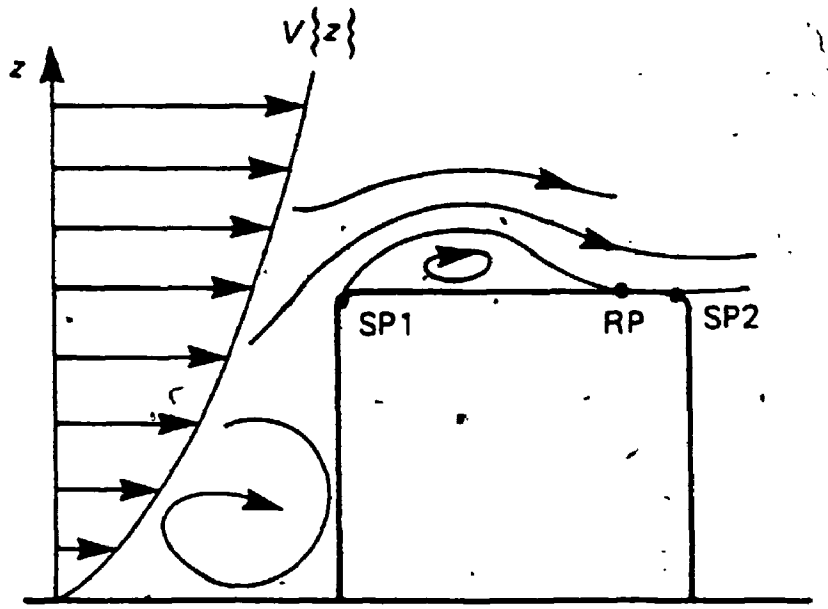

FIGURE 7.17 Separation and reattachment of flow over a roof (Cook, 1985)

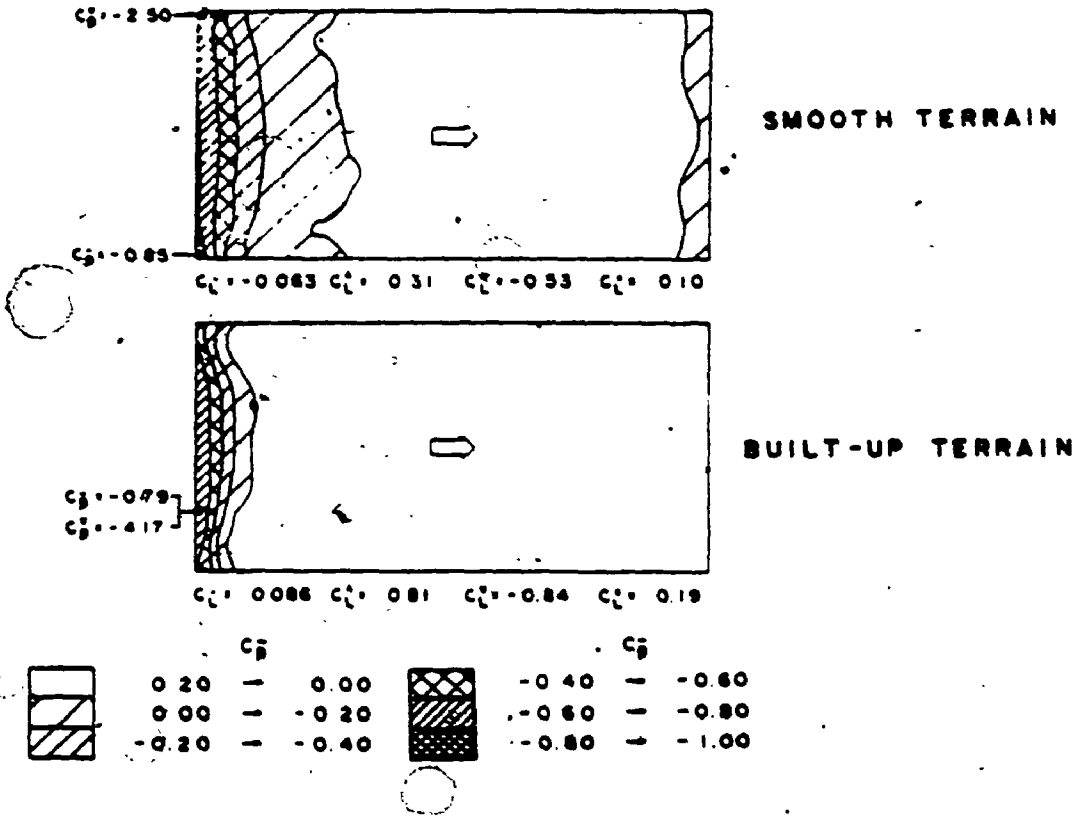

FIGURE 7.18 Contours of mean roof pressure coefficients (Davenport and Surry, 1974)

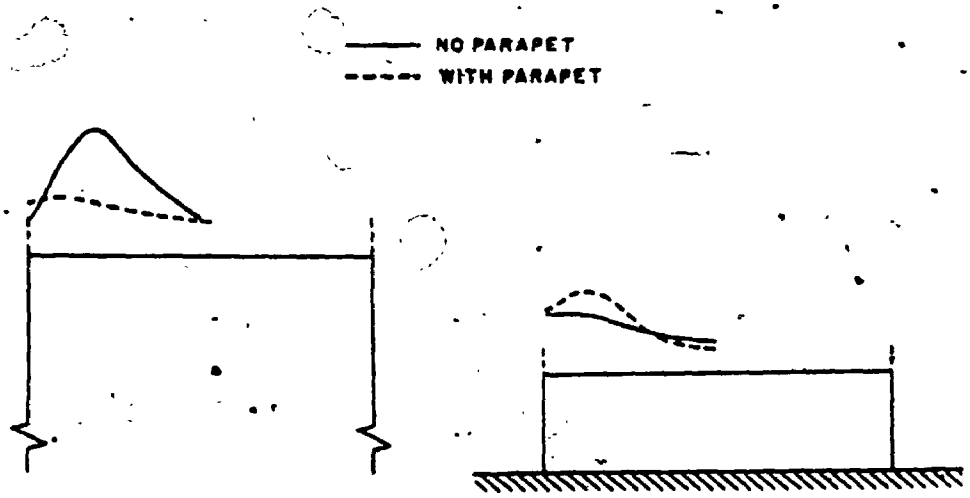

FIGURE 7.19 Trends in the mean pressure over low buildings (Lythe and Surry, 1983)

roof itself but for the whole building because its nonuniformity results in overturning moments as discussed later herein.

7.4.6 Drag Coefficients and Effective Heights

7.4.6.1 Drag Coefficients

Apart from a small Reynolds number effect, the force coefficients measured on the balance are equal to full-scale values. The total mean base shear in the y direction is

$$\bar{S}_y = \frac{1}{2} \rho C_D W \int_0^H \bar{U}^2(z)\, dz \qquad (7\text{-}41)$$

in which C_D is the drag coefficient, W the width and H the height of the building. The mean wind velocity at elevation z, below the height of the building, may be expressed as

$$\bar{U}(z) = \bar{U}_H \left(\frac{z}{H}\right)^{\alpha_2} \qquad (7\text{-}42)$$

where $\bar{U}_H = \bar{U}(z=H)$ is the mean velocity at the roof level of the building and the power law exponent, α_2, expresses the variation of the mean wind profile over the lowest 30 m of the boundary layer. Substituting Equation (7-42) in Equation (7-41) and integrating, the total mean base shear becomes

$$\bar{S}_y = \frac{1}{2} \rho C_D W H \bar{U}_H^2 \frac{1}{(2\alpha_2+1)} \qquad (7\text{-}43)$$

The mean base shear actually measured is defined in terms of the gradient wind velocity $\bar{U}_g$ and base shear coefficient C_{sy} as

$$\bar{S}_y = \frac{1}{2} \rho C_{sy} W H \bar{U}_g^2 = \frac{1}{2} \rho C_{sy} W H \bar{U}_H^2 \left(\frac{Z_g}{H}\right)^{2\alpha_1} \qquad (7\text{-}44)$$

in which α_1 is the power law exponent for the whole boundary layer. Comparing Equations (7-43) and (7-44), the drag coefficient, C_D, is obtained from the measured shear force coefficient as

$$C_D = C_{sy} (2\alpha_2+1)\left(\frac{Z_g}{H}\right)^{2\alpha_1} \qquad (7\text{-}45)$$

The variation of the force coefficients (shear, moment and torque) with the angle of attack (azimuth angle) are shown in Appendix I. The drag coefficient, C_D, is plotted for all three models in Figure 7.20. The maximum value is about 1.3 except for Model C in urban exposure for which the maximum is about 1.6. The value recommended for rectangular buildings in the NBCC (1985) is 1.3 which agrees with the measured data.

7.4.6.2 Effective Heights

The total mean overturning moment due to forces in the y direction is

$$\bar{M}_y = \frac{1}{2} \rho C_D W \int_0^H z \bar{U}^2(z) dz \qquad (7\text{-}46)$$

which, upon substitution of Equation (7-42) and integration reduces to

$$\bar{M}_y = \frac{1}{2} \rho C_D W H^2 \bar{U}_H^2 \frac{1}{(2\alpha_2+2)} \qquad (7\text{-}47)$$

Dividing the overturning moment by the base shear gives the effective height at which the drag force can be thought of as acting, that is

$$H_e = \frac{\bar{M}_y}{\bar{S}_y} = H \frac{(2\alpha_2+1)}{(2\alpha_2+2)} \qquad (7\text{-}48)$$

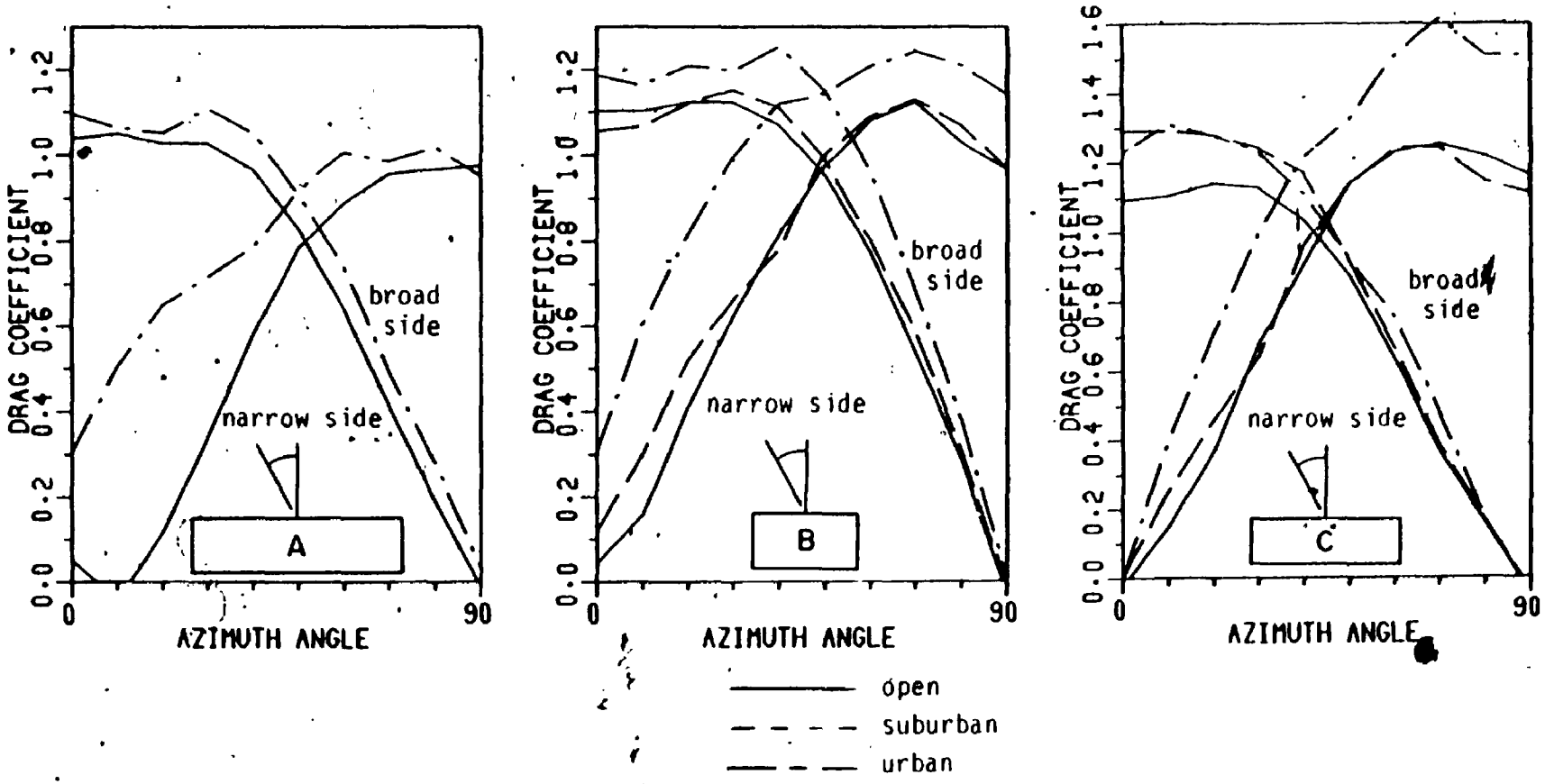

FIGURE 7.20 Variation of drag coefficient with azimuth angle

Therefore, the effective height depends only on the building height, H and the wind profile exponent, α_2. For open exposure, α_2 = 0.106 and H_e = 0.55H. A similar result was obtained by Tschanz (1982) in the wind tunnel and by Joubert et al. (1967) in full-scale measurements. However, for lower buildings the effective height can be greater because the overturning moment from the non-uniform pressure distribution (mostly suction) on the roof is not included in Equations (7-47) and (7-48).

The effective heights are obtained for the models considered by dividing the moment coefficients by the shear coefficients. These are plotted in Figures 7.21 through 7.23 for the three models. The effective heights on the broad side of Models A and B are greater than 0.55H. The effective heights on the narrow side of Models A and B (long afterbody) and on both sides of Model C (lower model) are greater than unity. This means that the drag force has to be applied above the roof level in order to account for the total overturning moment from the drag as well as suction on the roof. For the long afterbody, reattachment of the flow on the roof increases the unbalanced force on the roof which, together with its greater eccentricity, contributes significantly to the overturning moment. For the lowest model, C, the flow is deflected only slightly and reattachment occurs closer to the windward edge which results in effective heights greater than unity for both sides.

For base-isolated buildings, the effect of the uplift forces on the roof increases the axial forces on the isolators. Consider the three storey building shown in Figure 5.1 which corresponds to Model C. With axially soft isolators (k_v=2k_h), the building response also increases

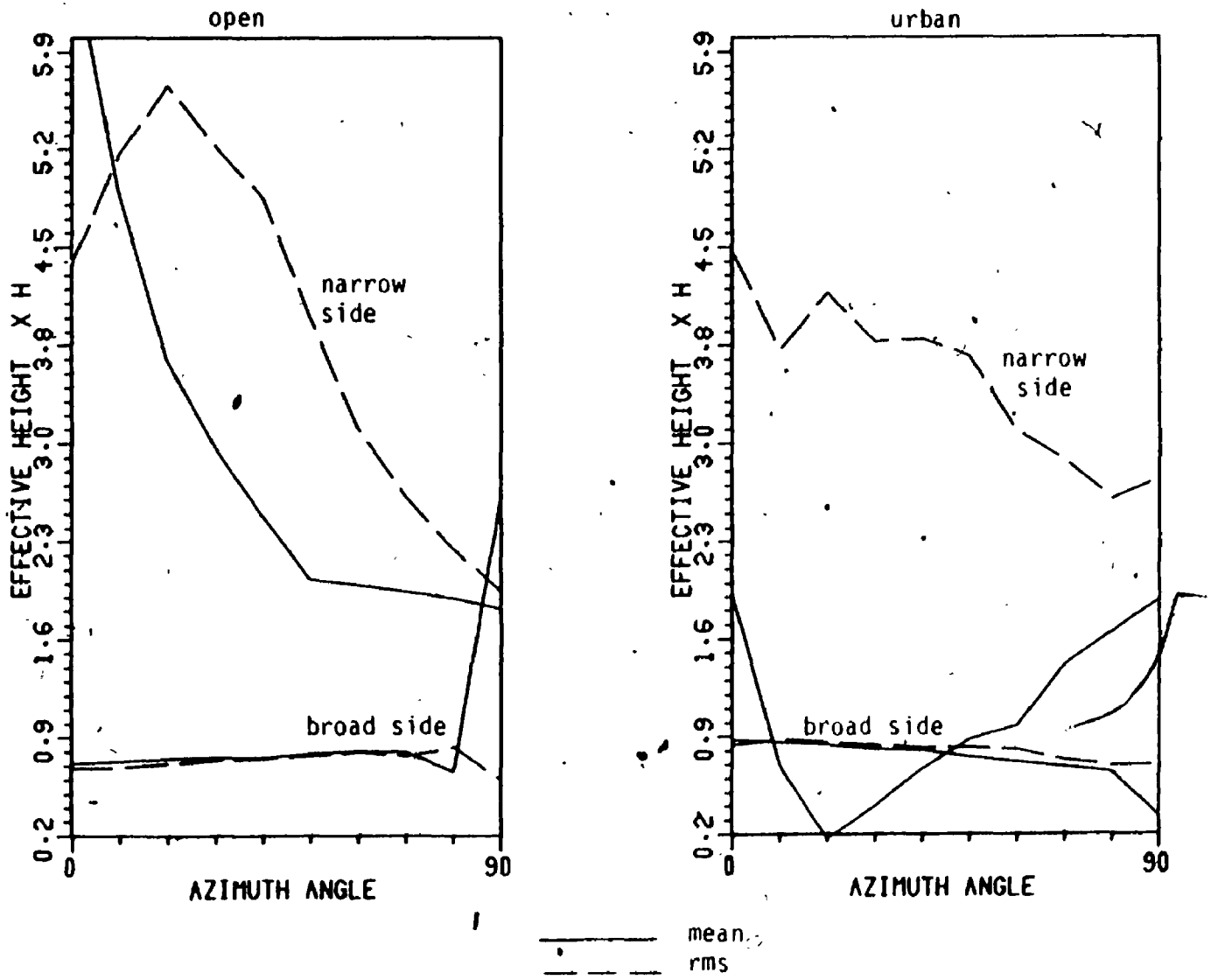

FIGURE 7.21 Effective height of the resultant force on Model A

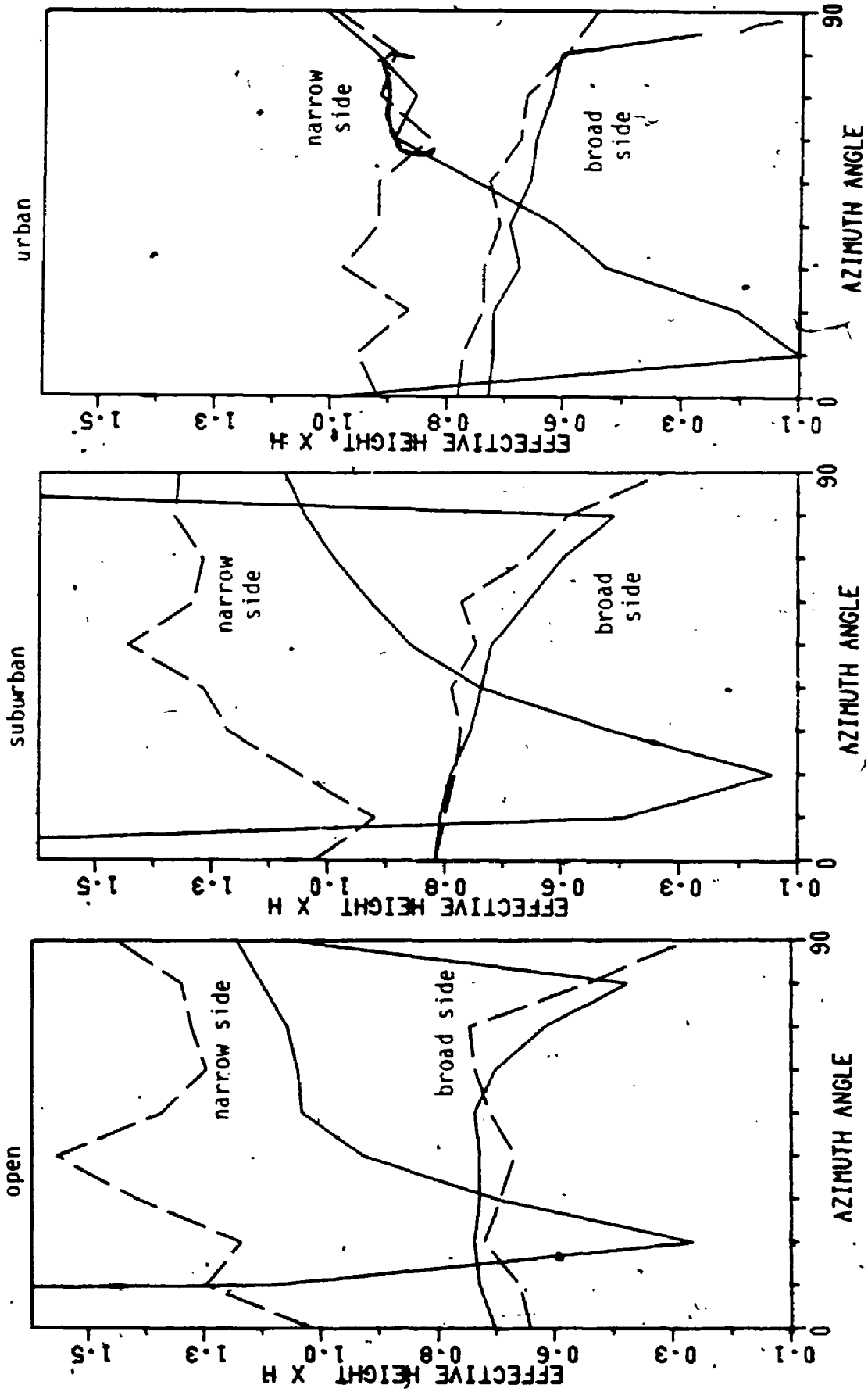

FIGURE 7.22 Effective height of the resultant force on Model B

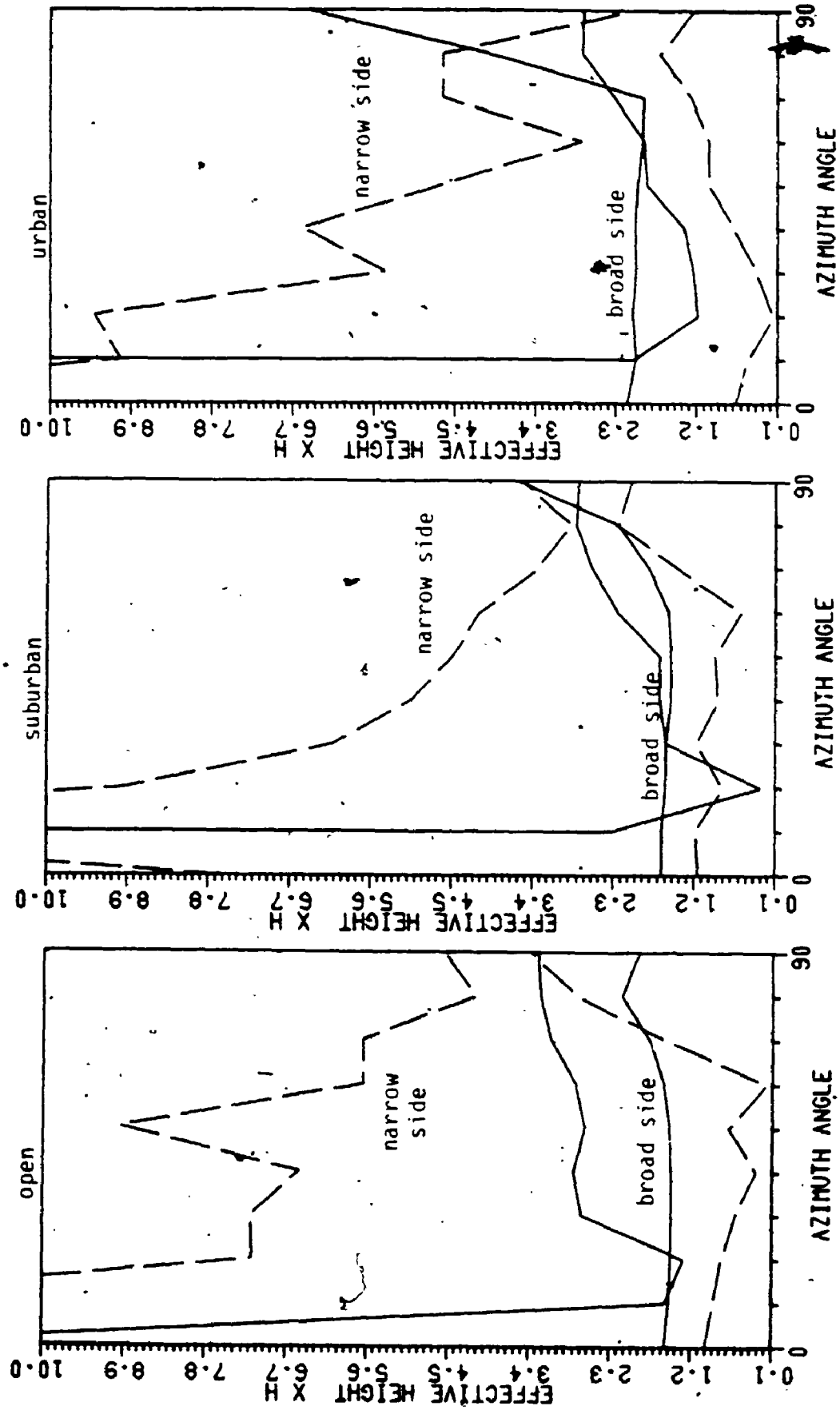

FIGURE 7.23 Effective height of the resultant force on Model C

due to rocking unless the damping is increased sufficiently by rocking. For an estimate of the increase in axial load, the building is idealized as a rigid body on springs. The building is subjected to the peak overturning wind moment in a plane normal to the broad side, assuming a peak factor $g_p = 3.8$. On the outer bearing, the axial loads due to wind are 20% of the seismic load (Figure 5.1) and 16% of the gravity load (assuming office loads and the dead load in Figure 5.1 minus a seismic live load of 1 KN/m^2). The axial loads for the building corresponding to Model B are 12% of the seismic load (Figure 5.2) and 10% of the gravity load on the outer bearing. In the above, the dead load is the same on the outer and inner bearings. If the dead load on the outer bearings is less, then these percentages increase.

CHAPTER 8

RESPONSE OF BASE-ISOLATED BUILDINGS TO WIND LOADING

8.1 INTRODUCTION

The response of base-isolated buildings to gusting wind can be predicted theoretically if the characteristics of the turbulent wind in the lowest part of the boundary layer are known. Such data were established in Chapter 7.

The existing procedures for the prediction of structural response to gusting wind were found to be adequate for tall buildings (Loh and Isyumov, 1985) but their adequacy for low-rise base-isolated buildings has not been verified. Differences in the flow characteristics as well as the modal properties exist for these two types of buildings. For example, the procedure for computing the wind load in the NBCC uses a triangular mode shape while base-isolated buildings slide on vertically stiff but horizontally soft isolators with a uniform or nearly uniform mode shape. The fundamental frequency of the base-isolated building is lowered being approximately 1 Hz for displacements less than the yield displacement. The lower frequency makes the building more sensitive to dynamic wind loading than conventional buildings of comparable size. The theory for the alongwind response to gusting wind was formulated previously (Davenport, 1967; Vickery, 1971; Yang and Lin, 1981 and Solari, 1982) and is well established. Some account for the correlation of wind pressures on all faces of the building while others assign all

wind pressures to the projected area of the building. The latter, simpler, assumption is adopted here because the differences in the results are small. The characteristics of the lower part of the boundary layer ascertained in the experimental part of the study are incorporated in the theory.

The adequacy of existing codes for the evaluation of wind loading on base-isolated buildings is examined. Such a verification is desireable because the wind velocity spectra and coherences found suitable for base-isolated buildings as well as their vibration modes differ from those assumed in the codes.

8.2 EVALUATION OF ALONGWIND RESPONSE

The alongwind velocity component is expressed as

$$U(y,z,t) = \bar{U}(z) + u(y,z,t) \qquad (8\text{-}1)$$

in which $\bar{U}(z)$ is the mean velocity and $u(y,z,t)$ is the fluctuating velocity component varying in both space and time. The pressure at any point (y,z) on the face of the building is

$$p(y,z,t) = \frac{1}{2} \rho C_p(y,z) U^2(y,z,t)$$

$$= \frac{1}{2} \rho C_p(y,z) \bar{U}^2 (1 + \frac{u}{\bar{U}})^2$$

$$= \bar{p}(y,z) + p(y,z,t) \qquad (8\text{-}2)$$

Since $(u/\bar{U})^2$ is much smaller than unity, this term is neglected. Then,

the mean wind pressure is

$$\bar{p}(y,z) = \frac{1}{2} \rho C_p(y,z) \bar{U}^2(z) \tag{8-3}$$

and the fluctuating pressure is

$$p(y,z,t) = \rho C_p(y,z) \bar{U}(z) u(y,z,t) \tag{8-4}$$

In Equations (8-2) to (8-4), ρ is the air density and $C_p(y,z)$ is the pressure coefficient.

The mean force acting on the structure is

$$\bar{Q} = \int^A \frac{1}{2} \rho C_p(y,z) \bar{U}^2(z) \, dA \tag{8-5}$$

and the fluctuating force is

$$Q(t) = \int^A \rho C_p(y,z) \bar{U}(\bar{z}) u(y,z,t) \, dA \tag{8-6}$$

The drag coefficient is defined as

$$C_D = \frac{\bar{Q}}{\int^A \frac{1}{2} \rho \bar{U}^2(z) \, dA} = \frac{\bar{Q}}{\frac{1}{2} \rho W \int_0^H \bar{U}^2(z) dz} \tag{8-7}$$

where, W is the width of the building and the pressure coefficient $C_p(y,z)$ is averaged over the face of the building and set equal to C_D. Denote the dimensionless coordinate $Z = z/H$, H being the height of the building and express the mean velocity by the power law relationship

$$\bar{U}(z) = \bar{U}_H \left(\frac{z}{H}\right)^{\alpha} = \bar{U}_H Z^{\alpha} \tag{8-8}$$

in which $\bar{U}_H$ is the mean wind velocity at the top of the building and α

expresses the variation of the mean wind profile over the height of the building. Then, the mean force becomes

$$\bar{Q} = \frac{1}{2} \rho C_D W H \int_0^1 \bar{U}^2(z)\, dZ = \frac{1}{2} \rho C_D W H \bar{U}_H^2 \int_0^1 Z^{2\alpha}\, dZ \qquad (8\text{-}9)$$

and the fluctuating force is

$$Q(t) = \rho C_D \bar{U}_H \int_0^H \int_0^W Z^{\alpha} u(y,z,t) dydz \qquad (8\text{-}10)$$

Introducing the dimensionless coordinate $Y = y/W$, Equation (8-10) becomes

$$Q(t) = \rho C_D W H \bar{U}_H \int_0^1 \int_0^1 Z^{\alpha} u(y,z,t)\, dYdZ \qquad (8\text{-}11)$$

In order to compute the dynamic response using modal analysis, the generalized (modal) force is required. The modal force is the summation of the product of the wind force and modal coordinate over the face of the building. The mode shape in translation varies with height only and is constant across the building at a particular elevation. The mean generalized force in mode j is

$$\bar{F}_j = \int_0^W \int_0^H \bar{p}(y,z)\, \phi_j(z)\, dydz \qquad (8\text{-}12)$$

and using Equation (8-9), this becomes

$$\bar{F}_j = \frac{1}{2} \rho C_D W H \bar{U}_H^2 \int_0^1 Z^{2\alpha}\, \phi_j(z)\, dZ \qquad (8\text{-}13)$$

where $\phi_j(z)$ is the modal coordinate in mode j at the height $z = ZH$. The fluctuating generalized force in mode j is

$$F_j(t) = \int_0^W \int_0^H p(y,z,t)\, \phi_j(z)\, dydz \qquad (8\text{-}14)$$

and using Equation (8-11), this expands to

$$F_j(t) = \rho\, C_D\, W\, H\, \bar{U}_H \int_0^1\int_0^1 Z^{\alpha}\, u(y,z,t)\, \phi_j(z)\, dY dZ \qquad (8\text{-}15)$$

It is desireable to evaluate the response in terms of the statistical parameters of the force, namely the mean, standard deviation and the power spectral density. The fluctuating force is represented by its spectral density function through the Fourier transform of the cross-correlation function (cross-covariance function). The cross-correlation function of the fluctuating force is

$$R_Q(\tau) = \overline{Q(t)Q(t+\tau)} = \int_A\int_A \overline{p(y_1,z_1,t)p(y_2,z_2,t+\tau)}\, dA_1 dA_2 \qquad (8\text{-}16)$$

where the fluctuating pressure $p(y_i,z_i,t)$, given by Equation (8-4), represents the random pressure at position (y_i,z_i) and τ is the time shift. The two sided spectrum of the load is

$$S_Q(f) = 2\int_{-\infty}^{\infty} R_Q(\tau)\, e^{-i2\pi f\tau} d\tau$$

$$= 2\int_{-\infty}^{\infty}\int_A\int_A \overline{p(y_1,z_1,t)p(y_2,z_2,t+\tau)}\, dA_1 dA_2$$

$$e^{-i2\pi f\tau} d\tau \qquad (8\text{-}17)$$

Changing the order of integration, S_Q is rewritten as

$$S_Q(f) = \int_0^H\int_0^H\int_0^W\int_0^W S_{p_1p_2}(y_1,y_2,z_1,z_2,f)\, dy_1 dy_2 dz_1 dz_2 \qquad (8\text{-}18)$$

where the cross-spectrum of the pressure at positions (y_1,z_1) and (y_2,z_2) is

$$S_{p_1p_2}(y_1,y_2,z_1,z_2,f) = 2\int_{-\infty}^{\infty} \overline{p(y_1,z_1,t)p(y_2,z_2,t+\tau)}\, e^{-i2\pi f\tau} d\tau \qquad (8\text{-}19)$$

Using Equations (8-4) and (8-11), the spectrum of the force is expressed directly in terms of the cross-spectrum of the alongwind velocity component as

$$S_Q(f) = \rho^2 C_D^2 W^2 H^2 \bar{U}_H^2 \int\int\int\int_0^1 S_u(y_1,z_1,y_2,z_2,f) Z_1^\alpha Z_2^\alpha dY_1 dY_2 dZ_1 dZ_2 \qquad (8\text{-}20)$$

The spectrum of the generalized fluctuating force is

$$S_{F_j}(f) = \rho^2 C_D^2 W^2 H^2 \bar{U}_H^2 \int\int\int\int_0^1 S_u(y_1,z_1,y_2,z_2,f) Z_1^\alpha Z_2^\alpha \phi_j(z_1)\phi_j(z_2)\, dZ_1 dZ_2 dY_1 dY_2 \qquad (8\text{-}21)$$

The cross-spectrum of the wind velocity is expressed as

$$S_u(y_1,z_1,y_2,z_2,f) = \sqrt{S_u(z_1,f)S_u(z_2,f)} \cdot R(y_1,z_1,y_2,z_2,f) \qquad (8\text{-}22)$$

in which $S_u(z,f)$ is the local spectrum and the normalized cross-spectrum, $R(y_1,z_1,y_2,z_2,f)$ is defined by the root coherence function proposed by Vickery (1971)

$$R(y_1,z_1,y_2,z_2,f) = \exp\left\{\frac{-f\sqrt{c_y^2(y_1-y_2)^2 + c_z^2(z_1-z_2)^2}}{\frac{1}{2}[\bar{U}(z_1)+\bar{U}(z_2)]}\right\} \qquad (8\text{-}23)$$

Using the dimensionless coordinates, the root coherence function becomes

$$R(Y_1,Z_1,Y_2,Z_2f) = \exp\left\{\frac{-f\sqrt{c_y^2W^2(Y_1-Y_2)^2 + c_z^2H^2(Z_1-Z_2)^2}}{\frac{1}{2}\bar{U}_H(Z_1^\alpha + Z_2^\alpha)}\right. \qquad (8\text{-}24)$$

The decay coefficient for horizontal separation is

$$c_y = c_o + c_m \frac{|y_1 - y_2|}{\bar{z}} = c_o + 2c_m \frac{W}{H} \frac{|Y_1 - Y_2|}{(Z_1 + Z_2)} \tag{8-25a}$$

and for vertical separation

$$c_z = c_o + c_m \frac{|z_1 - z_2|}{\bar{z}} = c_o + 2c_m \frac{|Z_1 - Z_2|}{(Z_1 + Z_2)} \tag{8-25b}$$

where the parameters c_o and c_m are as described in Chapter 7.

The normalized wind spectrum, $S_u(f)/\sigma^2(z)$, is taken to be height independent as discussed in Chapter 7. Then, the spectrum of the generalized force follows from Equation (8-21) and Equation (8-22) as

$$S_{F_j}(f) = \rho^2 C_D^2 W^2 H^2 I_u^2 \bar{U}_H^4 \frac{S_u(f)}{\sigma_u^2(z)} \chi^2(f;W,H,\bar{U}_H) \tag{8-26}$$

in which the function $\chi^2(f,W,H,\bar{U}_H)$, often called the joint acceptance function, is

$$\chi^2(f,W,H,\bar{U}_H) = \int_0^1 \int_0^1 \int_0^1 \int_0^1 Z_1^{2\alpha} Z_2^{2\alpha} \phi_j(z_1)\phi_j(z_2) R(Y_1,Z_1,Y_2,Z_2,f) dZ_1 dZ_2 dY_1 dY_2 \tag{8-27}$$

and for turbulence intensity, $I_u = \sigma_u(z)/\bar{U}(z)$, the r.m.s. wind velocity is

$$\sigma_u(z) = I_u \bar{U}_H Z^{\alpha} \tag{8-28}$$

The integral in Equation (8-27) is evaluated numerically. Its evaluation is discussed further in Section 8.2.1. The variance of the generalized force is

$$\sigma_{F_j}^2 = \int_0^\infty S_{F_j}(f)\, df$$

$$= \rho^2 C_D^2 W^2 H^2 I_u^2 \overline{U}_H^4 \int_0^\infty \frac{S_u(f)}{\sigma_u^2(z)} \chi^2(f,W,H,\overline{U}_H) df \qquad (8\text{-}29)$$

For the buildings considered, the dominant contribution to the response is in the first vibration mode. The generalized stiffness of the first mode is

$$K_1 = M_1 \omega_1^2 \qquad (8\text{-}30)$$

where M_1 is the first mode generalized mass and ω_1 is the fundamental angular frequency. The mean tip deflection is

$$\overline{x} = \overline{F}_1 / K_1 \qquad (8\text{-}31)$$

in which $\overline{F}_1$, the mean generalized force, is evaluated from Equation (8-13). The variance of the tip dynamic response, assuming $\phi_1(H) = 1$, is

$$\sigma_x^2 = \int_0^\infty S_x(f) df = \frac{1}{K_1^2} \int_0^\infty S_{F_1}(f) |H_1(f)|^2 \, df \qquad (8\text{-}32)$$

where $|H_1(f)|^2$ is the mechanical admittance function of the first mode expressed

$$|H_1(f)|^2 = \frac{1}{\{[1-(\frac{f}{f_1})^2]^2 + 4\zeta^2(\frac{f}{f_1})^2\}} \qquad (8\text{-}33)$$

f_1 is the fundamental frequency and ζ is the modal damping ratio (first mode). The integral in Equation (8-32) can be evaluated analytically or numerically. Here it is approximated by two components; a quasi-static or background response in which the mechanical admittance function is taken as equal to unity, and a resonant component equal to the area

under the peak of the response spectrum. Then, the variance of the response is written as

$$\sigma_x^2 = \frac{1}{K_1^2}\int_o^{f_1} S_{F_1}(f)df + \frac{1}{K_1^2}\frac{\pi f_1}{4\zeta} S_{F_1}(f_1) \qquad (8\text{-}34)$$

The r.m.s. background response is

$$\sigma_B = \frac{1}{K_1}\sqrt{\int_o^{f_1} S_{F_1}(f)df} \simeq \frac{\sigma_{F_1}}{K_1} \qquad (8\text{-}35a)$$

and the r.m.s. resonant response is

$$\sigma_R = \frac{1}{K_1}\sqrt{\frac{\pi f_1}{4\zeta} S_{F_1}(f_1)} \qquad (8\text{-}35b)$$

The variance of the response is, by summing the squares,

$$\sigma_x^2 = (\sigma_B^2 + \sigma_R^2) = \frac{1}{K_1^2}\left(\sigma_{F_1}^2 + \frac{\pi f_1}{4\zeta} S_{F_1}(f_1)\right) \qquad (8\text{-}36)$$

The expected peak displacement is written as

$$\hat{x} = \bar{x} + g_p \sigma_x \qquad (8\text{-}37)$$

where the peak factor g_p is, (Davenport, 1964)

$$g_p = \sqrt{2 \ln \nu T} + \frac{0.5772}{\sqrt{2 \ln \nu T}} \qquad (8\text{-}38)$$

The peak factor is the ratio of the expected value of the largest peak fluctuating displacement to the r.m.s. displacement occurring in the interval of observation, T (usually 1 hour or 3600 s) and has a value of approximately 3.8. The average fluctuating rate, ν, is (Rice, 1945)

$$\nu = \left[\frac{\int_0^\infty f^2 S_x(f) df}{\int_0^\infty S_x(f) df} \right]^{1/2} \tag{8-39}$$

The product $f^2 S_x(f)$ for low frequencies, corresponding to the quasi-static response, is small compared to the product around the peak of the response spectrum. The former is neglected and the numerator of Rice's formula is approximated by the product of the square of the natural frequency and the area under the spectral peak, then

$$\int_0^\infty f^2 S_x(f) df \approx f_1^2 \sigma_R^2 \tag{8-40}$$

The denominator of Equation (8-39) is the variance of the response. The expression for the average fluctuating rate can be written as

$$\nu = f_1 \sqrt{\frac{\sigma_R^2}{\sigma_B^2 + \sigma_R^2}} \tag{8-41}$$

Accelerations are induced in the building by the motion primarily associated with the resonant displacement since the background response is quasi-static. The frequencies associated with the resonant response vary closely about the natural frequency. Also, viewing the peak resonant displacement cycles as harmonic motion with frequency ω_1, the peak building acceleration becomes

$$\hat{a} = g_p \, \sigma_R \, \omega_1^2 \tag{8-42}$$

The peak factor is computed using an average fluctuation rate for acceleration of

$$\nu_a = \left[\frac{\int_0^\infty f^2 S_{\ddot{x}}(f)df}{\int_0^\infty S_{\ddot{x}}(f)df} \right]^{1/2} \qquad (8\text{-}43a)$$

Since the spectrum of acceleration is assumed to be discrete at the fundamental frequency, f_1, ν_a is approximated by dropping the background component of Equation (8-41), then

$$\nu_a = f_1 \qquad (8\text{-}43b)$$

The gust factor (Davenport, 1967), defined as the ratio of the peak total displacement to the mean displacement, is expressed as

$$G = 1 + g_p \frac{\sigma_x}{\bar{x}} \qquad (8\text{-}44a)$$

The product of the gust factor and the mean force is the equivalent lateral force required to produce the peak displacements and consequently the peak forces in the members of the building. The gust factor is rewritten in the familiar form as (Davenport, 1967 and Vickery, 1971)

$$G = 1 + g_p r(B + \frac{sF}{\zeta})^{1/2} \qquad (8\text{-}44b)$$

where the roughness factor, r, is

$$r = \frac{2I_u}{\int_0^1 Z^{2\alpha}\phi_1(z)dZ} \qquad (8\text{-}45)$$

The background turbulence factor, B, is

$$B = \int_0^{f_1} \frac{S_u(f)}{\sigma_u^2(z)} \chi^2(f,W,H,\bar{U}_H)df \qquad (8\text{-}46)$$

The size reduction factor, s, is the value of the joint acceptance

function, Equation (8-27), at the natural frequency f_1

$$s = \chi^2(f_1, W, H, \bar{U}_H) \tag{8-47}$$

and the gust energy ratio, F, is defined as

$$F = \frac{\pi}{4} f_1 \frac{S_u(f_1)}{\sigma_u^2(z)} \tag{8-48}$$

The normalized wind spectrum, $S_u(f)/\sigma_u^2(z)$, is obtained from Equation (7-37) with the parameters A, θ and L equal to 0.58, 2.44 and 483 m respectively. The peak factor is computed from Equation (8-38) for which the fluctuating rate is, in terms of the above variables,

$$\nu = f_1 \sqrt{\frac{sF}{sF+\zeta B}} \tag{8-49}$$

Using the parameters r, B, s, F and ζ the quantities σ_{F_1}, $\bar{x}$, g_p, σ_x, σ_B, σ_R, $\hat{x}$ and $\hat{a}$ can be evaluated. Thus, the product of the mean force and the gust factor defines the equivalent static wind force that produces a displacement equal to the peak dynamic displacement.

8.2.1 Evaluation of the Joint Acceptance Function (Size Reduction Factor)

The evaluation of the four-fold integral of the joint acceptance function (Equation 8-27) is a key part in the computation of the response. The integral can be evaluated numerically or, in some instances, analytically. An analytical evaluation of the integral was obtained by Davenport (1977) with the introduction of several approximations. Firstly, the root coherence function was expressed similar to Equation (8-24) as

$$R(Y_1, Z_1, Y_2, Z_2, f) = \exp\{-\sqrt{(c_y \frac{fW}{\bar{U}})^2 (Y_1 - Y_2)^2 + (c_z \frac{fH}{\bar{U}})^2 (Z_1 - Z_2)^2}\} \quad (8\text{-}50)$$

The coefficients c_y and c_z defining the decay of the correlation function in the horizontal (lateral) and vertical direction are constant i.e., independent of elevation and separation and $\bar{U}$ is the reference wind velocity assumed to be constant.

An approximation is made for the sum of the squared terms under the square root and the root coherence function is approximated as

$$R = \exp\{-\theta(c_y \frac{fW}{\bar{U}} |Y_1 - Y_2| + c_z \frac{fH}{\bar{U}} |Z_1 - Z_2|)\} \quad (8\text{-}51)$$

where $.71 < \theta < 1.0$ depending on the ratio of the two terms and is given by

$$\theta \simeq \sqrt{1+\lambda^2} / (1+\lambda) \quad (8\text{-}52)$$

in which $\lambda = \frac{c_y W}{c_z H}$. With the above approximation for the root coherence function the four-fold integral can be expressed as the product of two one-dimensional joint acceptance functions: J_y in the direction y and J_z in the direction z. Each joint acceptance function is then approximated by the reciprocal of the sum of the asymptotic values as the reduced frequency $fH/\bar{U}$ or $fW/\bar{U}$ tends to zero and infinity. Then, the expression for the joint acceptance function for a building with a triangular mode shape (vertically) in a flow with mean wind profile variation given by the power law exponent, α; is derived as

$$\chi^2 = J_z J_y = [\frac{1}{(2+\alpha)^2 + (\frac{2\alpha+3}{2})\phi}][\frac{1}{1+0.5r\phi}] \quad (8\text{-}53a)$$

where $\phi = c_z' \frac{fH}{\bar{U}}$ and $r = \frac{c_y' W}{c_z' H}$ and the decay constants c_y and c_z have been adjusted to

$$c_y' = (\frac{4}{\pi})^{\frac{1}{1+\lambda}} c_y \text{ and } c_z' = (\frac{4}{\pi})^{\frac{\lambda}{1+\lambda}} c_z \qquad (8\text{-}53b)$$

in which $\lambda = \frac{c_y W}{c_z H}$.

For a base-isolated building with a uniform mode in a flow with uniform mean wind profile and constant c_y and c_z, the joint acceptance function is given by

$$\chi^2 = [\frac{1}{1+0.5\phi}] [\frac{1}{1+0.5r\phi}] \qquad (8\text{-}54)$$

where ϕ and r are as defined above.

Foutch and Safak (1981) used Davenport's approximation for the root coherence, Equation (8-51), and evaluated the four-fold integral analytically. In their analysis the structure is 'sign-like' with uniform mode shape, the mean wind velocity is constant, and the decay coefficients are also constant. Their expression for the joint acceptance function is

$$\chi^2 = \frac{2}{D_y^2} (e^{-D_y} + D_y - 1)[\frac{2}{D_z^2} (e^{-D_z} + D_z - 1] \qquad (8\text{-}55)$$

in whjch $D_y = \frac{f C_y W}{\bar{U}_o}$, $D_z = \frac{f C_z H}{\bar{U}_o}$ and $\bar{U}_o$ is the mean wind velocity at the centre of the structure.

With the introduction of height and separation dependent coefficients, an analytical derivation of the joint acceptance function becomes

very difficult if at all possible. Therefore, the analytical approach is avoided in this study and the numerical integration procedure is adopted.

Simiu (1975) reduced the four-fold integral to a three-fold integral by replacing the dimensionless variables Y_1 and Y_2 by a single dimensionless variable, g, and obtaining the root coherence function as

$$R(Z_1, Z_2, f, g) = \exp\left\{\frac{-2c_z f\sqrt{(Z_1-Z_2)^2+(\frac{c_y W}{c_z H})^2 g^2}}{\bar{U}(Z_1) + \bar{U}(Z_2)}\right\} \qquad (8\text{-}56)$$

The substitution of the variable g is somewhat suspect. It was tested for a line structure for which the double integral was evaluated analytically and compared with the expression obtained by the single integral using the same substitution. The two expressions were different and gave different results for an example. Further, the four-fold and three-fold integrals were evaluated numerically for Building B and markedly different values were obtained.

Therefore, Simiu's simplification is not adopted. The four-fold integral of Equation (8-27) and the five-fold integral of Equation (8-29) are evaluated numerically using subroutine D01GBF of the Numerical Algorithms Group library (NAG library) which employs an adaptive Monte Carlo method. The accuracy of the evaluation was checked against analytical solutions for line and two-dimensional structures and found to be satisfactory.

8.3 COMPARISON OF MEASURED AND CALCULATED WIND FORCES

Once the wind forces acting on the building are determined, the linear response of the building to these forces can be evaluated using well established principles of structural dynamics. Thus the accuracy of the response depends mainly upon how accurately the forces are evaluated. In particular, the dynamic response to gusting wind depends on the spectrum of the generalized force which is calculated using the local spectra and coherences of the fluctuating wind velocity in the free flow. One check on the reliability of the wind forces used in the response prediction is to compare the total wind forces measured directly on the models by the force balance with the wind forces calculated from the free flow data. Such a comparison is made in Table 8.1 which shows the forces on Building B in open and urban exposures. The agreement between the measured forces and the calculated forces is very good. The forces, calculated using the parameters proposed for practical applications, are conservative.

8.4 EVALUATION OF RESPONSE TO GUSTING WIND AND COMPARISON WITH CODES

The response of the three buildings, A, B and C is computed, for the three exposures, using the theory outlined above and is listed in Tables 8.2, 8.3 and 8.4 respectively. For wind loading the vertically stiff isolators are assumed to remain in the initial elastic range. The modal properties of the buildings are listed in Tables 5.2 and 5.3; the pertinent values are for four bays and small strains. The damping ratio is 2 per cent. The mean wind velocity at roof level, $\bar{U}_H$, given in the

TABLE 8.1 Wind Forces on Building B (N) for $\bar{U}_g$ = 12.19 m/s and Two Exposures

	open		urban	
	mean	rms	mean	rms
$\bar{U}_H$ (m/s)	7.46		3.90	
I_u	.134		.325	
Forces measured using balance coefficients	39530.	7651.	10897.	5564.
Forces calculated with measured parameters (α_2, c_o, c_m, & c_D)	39503.	6994.	10890.	5013.
Forces calculated with proposed parameters (α_2, c_o, c_m, & c_D)	47906.	8138.	14055.	6251.

TABLE 8.2 Response of Building A to Gusting Wind (displacements in mm, $\bar{U}_{10}$(open) = 28.5 m/s; i - isolated, f - fixed)

	open		suburban		urban	
	fixed	isolated	fixed	isolated	fixed	isolated
$\bar{U}_H$ (m/s)	31.4		22.6		18.0	
$\bar{U}_e$ (m/s)	29.3		20.6.		18.0	
I_u	.134		.207		.325	
mean disp. $\bar{x}$	1.28	3.86	.63	1.91	.48	1.46
background disp. σ_B	.19	.52	.14	.41	.19	.53
resonant disp. σ_R	.04	.20	.02	.10	.02	.11
r.m.s. disp. σ_x	.19	.56	.15	.42	.19	.55
peak disp. $\hat{x}$	2.03	6.05	1.19	3.52	1.20	3.53
gust factor C_g	1.59	1.57	1.88	1.84	2.48	2.42
peak accln. $\hat{a}$ %g	.27	.32	.13	.16	.13	.18
peak base shear $\hat{Q}$ (KN)	2765.	2733.	1625.	1589.	1635.	1593.
(σ_R/σ_B)x100	21.	38.	14.	24.	11.	21.
disp. ratio $\hat{x}_i/\hat{x}_f$	2.98		2.96		2.94	
accln. ratio $\hat{a}_i/\hat{a}_f$	1.19		1.23		1.38	

TABLE 8.3 Response of Building B to Gusting Wind (displacements in mm, $\bar{U}_{10}$(open) = 28.5 m/s, i - isolated, f - fixed; f_f = 2.02 Hz, f_i = 0.98 Hz)

	open		suburban		urban	
	fixed	isolated	fixed	isolated	fixed	isolated
$\bar{U}_H$ (m/s)	31.4		22.6		18.0	
$\bar{U}_e$ (m/s)	29.3		20.6		18.0	
I_u	.134		.207		.325	
Mean disp. $\bar{x}$	1.28	3.86	.63	1.91	.48	1.46
Background disp. σ_B	.23	.65	.18	.51	.23	.65
Resonant disp. σ_R	.05	.28	.02	.14	.03	.16
r.m.s. disp. σ_x	.24	.71	.18	.52	.23	.67
Peak disp. $\hat{x}$	2.22	6.65	1.33	3.93	1.35	4.01
Gust factor C_g	1.73	1.72	2.10	2.06	2.80	2.75
Peak accln. $\hat{a}$%g	.37	.45	.18	.23	.19	.25
Peak base shear $\hat{Q}$ (KN)	1510.	1524.	907.	889.	922.	905.
(σ_R/σ_B) %	22.	43.	11.	27.	13.	25.
Disp. ratio $\hat{x}_i/\hat{x}_f$	3.0		2.95		2.97	
Accln. ratio $\hat{a}_i/\hat{a}_f$	1.22		1.28		1.32	

TABLE 8.4 Response of Building C to Gusting Wind (displacements in mm, $\bar{U}_{10}$(open) = 28.5 m/s; i - isolated, f - fixed)

	open		suburban		urban	
	fixed	isolated	fixed	isolated	fixed	isolated
$\bar{U}_e = \bar{U}_H$ (m/s)	28.5		20.2		18.0	
I_u	.134		.207		.325	
mean disp. $\bar{x}$	.33	2.41	.17	1.21	.13	.96
background disp. σ_B	.05	.34	.04	.27	.05	.37
resonant disp. σ_R	.01	.14	.004	.08	.004	.10
r.m.s. disp. σ_x	.05	.37	.04	.28	.05	.39
peak disp. $\hat{x}$	.53	3.88	.32	2.29	.34	2.46
gust factor C_g	1.61	1.61	1.92	1.90	2.58	2.55
peak accln. $\hat{a}$ %g	.16	.28	.08	.15	.09	.19
peak base shear $\hat{Q}$ (kN)	958.	958.	572.	566.	614.	607.
$(\sigma_R/\sigma_B) \times 100$	20.	41.	10.	30.	8.	27.
disp. ratio $\hat{x}_i/\hat{x}_f$	7.32		7.16		7.24	
accln. ratio $\hat{a}_i/\hat{a}_f$	1.75		1.88		2.1	

Tables corresponds to a gradient wind speed of approximately 51 m/s. The computations are based on an equivalent uniform (α_2=0) mean wind velocity $\bar{U}_e$. The integral of the square of this velocity ($\bar{U}_e$) and the integral of the square of the velocity prescribed in the NBCC (non uniform wind profile), over the height of the building, are equal. Only for the urban exposure, the NBCC profile is uniform over the entire height of Buildings A and B.

The peak displacement with an isolated base is about three times, for Buildings A and B, and seven times, for Building C, that obtained with a fixed base. The displacements are less than the 10 mm yield displacement usually prescribed for the isolators. The peak accelerations are increased much less by base isolation than peak displacements. The gust factor varies somewhat with exposure but only slightly with base condition. The peak equivalent base shear is only slightly affected by the isolation. For open exposure, it is 2.6 per cent of the weight of Building B. This is the total force (generalized force) applied in the first vibration mode. For a static structural analysis (e.g. displacement method), the base shear required to give the same displacements would be 3.3 per cent of the weight of Building B.

For comparison, the displacements and accelerations were computed by the NBCC (1985) and the ANSI Code (1982). The results are shown in Table 8.5 for Building B in all three exposures and in Table 8.6 for Building C in suburban exposure. The NBCC gives larger displacements. Smaller background displacements are obtained from the present analysis. The form of the coherence decay parameters, increasing with an increased

TABLE 8.5 Response of Building B Calculated Using NBCC and ANSI Codes (i-isolated, f-fixed; $\bar{U}_{10}$(open) = 28.5 m/s, displacements in mm)

	open		suburban		urban	
	fixed	isolated	fixed	isolated	fixed	isolated
NBCC						
Mean disp. $\bar{x}$	1.34	3.84	.66	1.91	.48	1.46
Background disp. σ_B	.30	.86	.23	.66	.25	.75
Resonant disp. σ_R	.04	.29	.02	.16	.02	.14
r.m.s. disp. σ_x	.30	.91	.23	.68	.25	.76
Peak disp. $\hat{x}$	2.51	7.41	1.53	4.52	1.41	4.30
Gust factor C_g	1.88	1.93	2.31	2.37	2.92	2.95
Peak accln. $\hat{a}$ %g	.32	.47	.16	.25	.12	.20
Peak base shear $\hat{Q}$ (KN)	1630	1673	996	1021	962	975
Hourly mean wind velocity U_H (m/s)	31.4		22.6		18.0	
ANSI						
Mean disp. $\bar{x}$	2.18	6.13	1.21	3.35	-	-
Peak disp. $\hat{x}$	2.60	7.32	1.67	4.60	.84	2.54
Gust factor C_g	1.20		1.38		-	
Peak base shear $\hat{Q}$ (KN)	1655		1040		575	

TABLE 8.6 Response of Building C in Suburban Exposure - NBCC and ANSI Code
($\bar{U}$ = 20.2 m/s, displacements in mm)

	NBCC		ANSI	
	fixed	isolated	fixed	isolated
mean disp. $\bar{x}$	.16	1.21	.15	1.76
background disp. σ_B	.06	.44	-	-
resonant disp. σ_R	.003	.09	-	-
r.m.s. disp. σ_x	.06	.45	-	-
peak disp. $\hat{x}$	.39	2.92	.22	2.62
gust factor C_g	2.38	2.42	-	-
peak base shear $\hat{Q}$ (KN)	771.	720.	646.	

ratio of separation to elevation instead of being constant as assumed in NBCC results in reduced correlations and consequently smaller background responses. This difference in the background displacements translates into a difference in the r.m.s. displacements which when multiplied by the peak factor approximately accounts for the difference in the peak displacements by the Code and the present analysis.

For the ANSI computations, the rational analysis is not used as there are no charts for a width to height ratio greater than one. The gust factors are obtained from Table 8 of the Code. The peak displacements computed using the ANSI Code and NBCC are similar except for the urban exposure where the ANSI specification of the peak load being not less than 0.48 KN/m^2 (10 psf) is invoked. The major reason for this difference is the variation of the mean wind profile with height by ANSI whereas by the NBCC and the present analysis, the mean wind profile is uniform.

8.5 APPROXIMATE EVALUATION OF THE GUST FACTOR

For a detailed analysis, the computation of the response can be facilitated by a set of design charts similar to the procedure in the NBCC. The charts are based on the gust factor approach outlined earlier.

The roughness factor, r, for constant wind profile (α_2=0) reduces to

$$r = \frac{2I_u}{\int_0^1 \phi(z)dZ} \qquad (8\text{-}57)$$

For a triangular mode shape $r = 4I_u$ while for a uniform mode $r = 2I_u$.

The size factor, s, (Equations (8-47), (8-27) and (8-24)) is presented in Figure 8.1 for various width to height (W/H) ratios as a function of the reduced frequency $fH/\bar{U}_H$. The curves are shown for a uniform mode shape. The chart is applicable to any of the three exposures. The decay coefficients, c_o and c_m, are averaged for the three exposures. Values of $c_o = 8$ and $c_m = 7$ are used in the expression for height and separation dependent coherences for horizontal direction while for vertical direction the values are $c_o = 8$ and $c_m = 5$.

The charts for the background turbulence factor, B, (Equations (8-46), (8-27), (8-24) and (7-29)) are shown in Figure 8.2 and are applicable to all three exposures. A power law exponent of $\alpha = 0.14$ is used to relate the wind velocity at 20 m to the wind velocity at roof level. The gust energy ratio (Equation (8-48)) is shown in Figure 8.3 as a function of wave number, $f/\bar{U}_H$. As a check of the charts, the gust factor for Building B in suburban exposure is computed. Table 8.7 shows the procedure. The gust factors agree well with the more accurate ones in Table 8.3.

The gust factors were evaluated for four buildings and are listed in Table 8.8. Buildings A and D have the same dynamic properties as Buildings B and C respectively. Building A is twice as wide as Building B while Building D is only 10 metres wide. As the width of the buildings decreases the gust factor increases. The gust factors for Building D are larger than those for the other buildings. This is due to its small width but the aspect ratio of Building D (1:1) may be rare for a low-rise building. Apart from Building D, the gust factors vary slightly with the type of building and, therefore, approximate values can be recommended

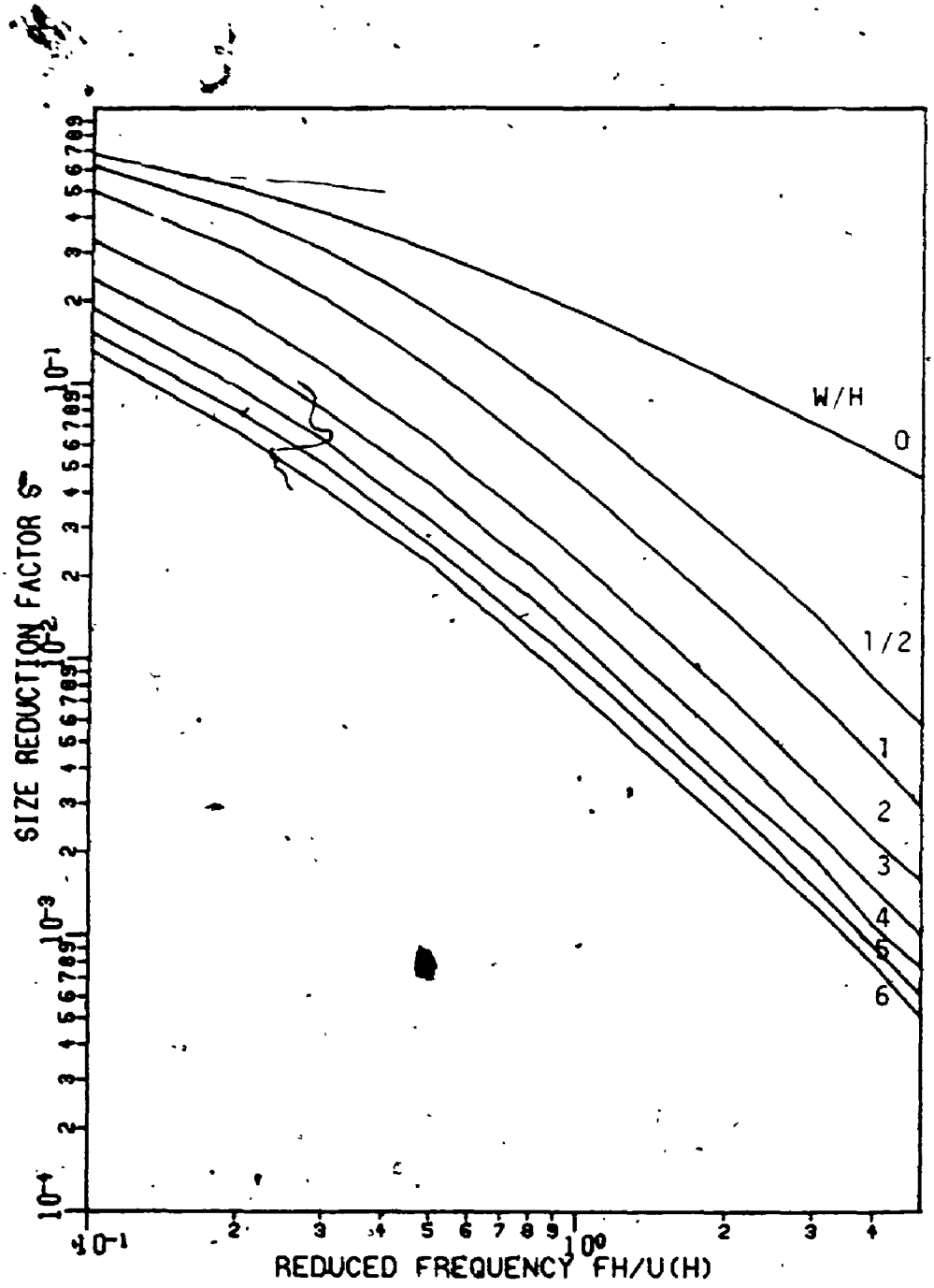

FIGURE 8.1 Size reduction factor - uniform mode

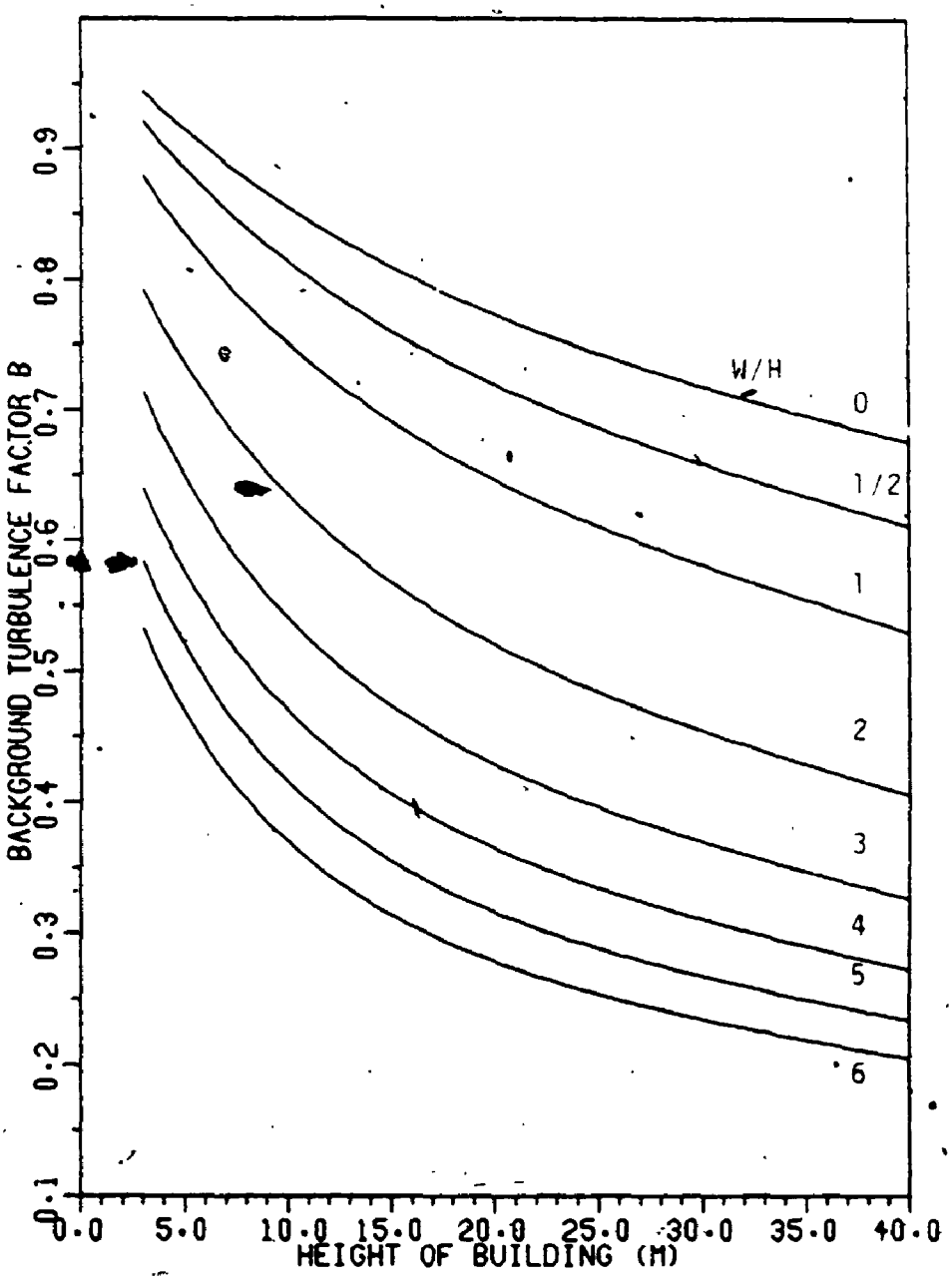

FIGURE 8.2 Background turbulence factor - uniform mode

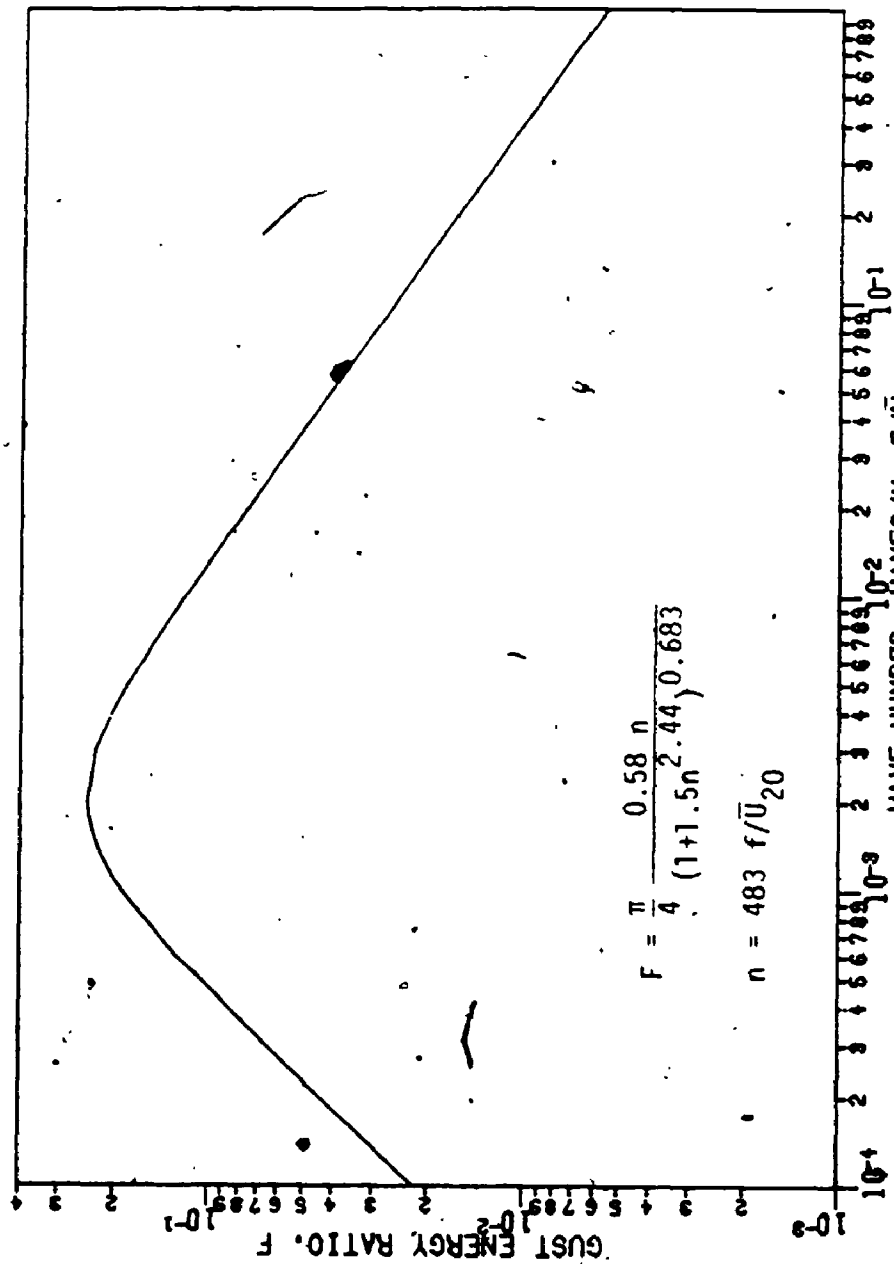

FIGURE 8.3 Gust energy ratio

TABLE-8.7 Gust Effect Factor Using Charts - Building B
(suburban exposure, $\bar{U}(H)$ = 20.6 m/s, I_u = 0.207)

	Fixed base	Base-Isolated
Roughness factor, r	$4I_u$ = 0.828	$2I_u$ = 0.414
Background turbulence factor, B, from Fig. 8.2 for H = 20 m and W/H = 3	0.108	0.43
Reduced frequency $n = f_1 H/\bar{U}_H$	2.02x20/20.6=1.96	0.98x20/20.6=0.95
Size reduction factor, s, from Fig. 8.1	0.0051/4 = 0.0013	0.012
Wave number, $WN = f/\bar{U}_H$	2.02/20.6 = 0.098	0.98/20.6 = 0.048
Gust energy ratio, F, from Fig. 8.3	.026	.043
Av. fluctuating rate, ν, from Eq. 8-49 (=.02)	.249	.233
Peak factor, g_p from Eq. 8-38 for T=3600 s	3.84	3.83
Gust effect factor, C_g from Eq. 8-44	2.05	2.07
Table 8.3, C_g	2.10	2.06

TABLE 8.8 Gust Factors for Four Buildings (aspect ratio W:H; Building D 10 m x 10 m with vibration properties of Building C; triangular mode for fixed base, uniform mode for base-isolated building)

	open		suburban		urban	
	fixed	isolated	fixed	isolated	fixed	isolated
Building A (120 m wide) (Aspect ratio 6:1)	1.59	1.57	1.88	1.84	2.48	2.42
Building C (84.6 m wide) (Aspect ratio 8.25:1)	1.61	1.61	1.92	1.90	2.58	2.55
Building B (60 m wide) (Aspect ratio 3:1)	1.73	1.72	2.10	2.06	2.80	2.75
Building D (10 m wide) (Aspect ratio 1:1)	2.03	2.15	2.51	2.60	3.39	3.55
Recommended values for preliminary analysis	2.0		2.5		3.0	

for a preliminary analysis (Table 8.8). These recommended values depend on the exposure and are conservative.

8.5.1 Correction for Non-Uniform Modes

The charts presented are for a uniform mode shape. The charts can still be used for other modes such as triangular or trapezoidal if an appropriate correction is made. The area bounded by the trapezoidal mode shape expressed in terms of dimensionless height and the modal coordinate equal to unity at the building top is

$$A_m = \int_0^1 \phi(z)dZ = (1+\varepsilon)/2 \qquad (8\text{-}58)$$

where ε is the value of the modal coordinate at the level of the base isolators. For constant wind profile ($\alpha_2 = 0$) Equation (8-57) becomes

$$r = \frac{2I_u}{\int_0^1 \phi(z)dZ} = \frac{2I_u}{A_m} \qquad (8\text{-}59)$$

The size reduction and background turbulence factors from the uniform mode charts are multipled by a mode shape correction factor as derived by Holmes (1987). If the dynamic forces are assumed to be fully correlated over the height of the structure (high correlation limit) then the mode shape correction, A_1, is given by

$$A_1 = [\int_0^1 \phi(z)dZ]^2 = (\frac{1+\varepsilon}{2})^2 = A_m^2 \qquad (8\text{-}60)$$

If the correlation is assumed to fall off rapidly, i.e. the correlation length is small compared to the height of the structure, the mode shape

correction for this low correlation limit is approximated by

$$A_2 = \int_0^1 \phi^2(z)dZ = \frac{1}{3}(1+\epsilon+\epsilon^2) \qquad (8\text{-}61)$$

which gives slightly more conservative values than A_1.

8.6 GENERAL RELATIONSHIP BETWEEN THE RESPONSE OF FIXED BASE AND BASE-ISOLATED BUILDINGS.

A general ratio of the peak displacement of a base-isolated building to that of a fixed base building can be established approximately. Based on the data in Tables 8.2-8.4, it may be assumed that the gust factor, and hence the peak wind pressure, is the same for both base conditions. Assuming the mode shape for the fixed base building is triangular and that of the base-isolated building is uniform, then the relationship of the generalized forces, F, is

$$F_i = 2F_f \qquad (8\text{-}62)$$

and for the generalized masses, M,

$$M_i = 3M_f \qquad (8\text{-}63)$$

where the subscript i refers to the base-isolated building and f to the fixed base building. The peak displacement is

$$\hat{x} = \frac{F}{\omega^2 M} \qquad (8\text{-}64)$$

Writing the ratio of the angular frequencies as

$$\omega_f = a\,\omega_i \text{ or } \omega_i = \frac{\omega_f}{a} \qquad (8\text{-}65)$$

the ratio of the peak displacements becomes

$$\hat{x}_i = \frac{2}{3} a^2 \hat{x}_f \qquad (8\text{-}66)$$

Thus the building response to gusting wind increases with the square of the frequency ratio; the factor 2/3 results from the difference in the vibration mode shapes. For Buildings A and B, the coefficient a = 2.06 and therefore $\hat{x}_i = 2.83\ \hat{x}_f$ while for Building C, a = 3.16, and $\hat{x}_i = 6.66\ \hat{x}_f$. These ratios are in good agreement with the ratios in Tables 8.2, 8.3 and 8.4.

8.7 TORSIONAL RESPONSE DUE TO ALONGWIND PRESSURES

Turbulent wind can produce torsional response even in perfectly symmetric buildings (Foutch and Safak, 1981, Novak, 1983, Isyumov, 1983 and Greig, 1980). The torsional moments generating such response arise from the lack of spatial correlation of the wind pressures across the face of the building and, usually to a lesser degree, from vortex shedding. For perfectly symmetric buildings the fundamental sway and torsional modes are uncoupled and for base-isolated buildings the fundamental sway and torsional frequencies may be close or equal. For small amplitude motions, the response in these two modes can be superimposed.

8.7.1 Torsional Response of a Building As a Rigid Body

Consider the effect of pressure fluctuations (Equation (8-4)) generating response in a torsional vibration mode represented by twisting of the rigid building on the isolators. For the horizontal coordinate, y, measured from the vertical edge of the building (Figure 8.4), the fluctuating torque about the geometric centre of the building is

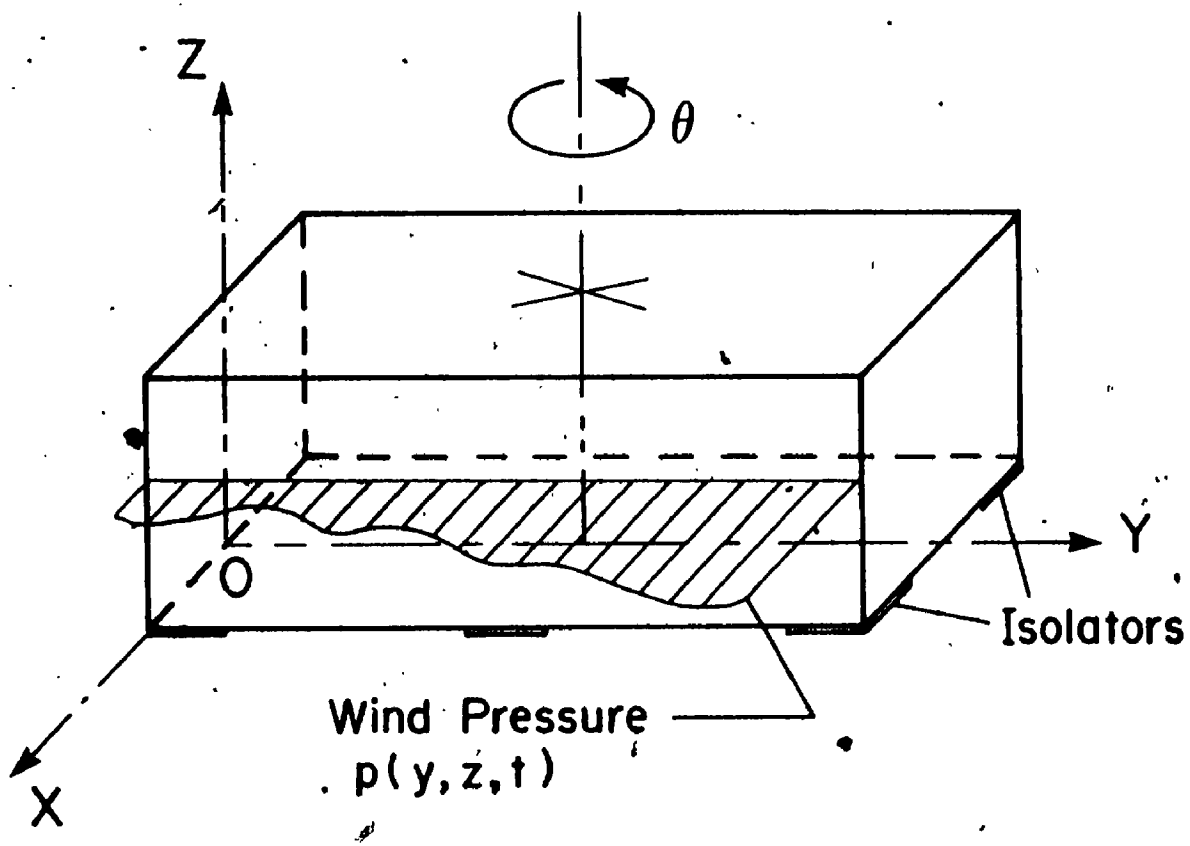

FIGURE 8.4 Schematic of building for torsion

$$T_\theta(t) = \int_A \rho\, C_p(y,z)\bar{U}(z)u(y,z,t)(y - \frac{W}{2})dA \qquad (8\text{-}67)$$

By modal analysis the angle of twist, $\theta(t)$, is given by

$$\theta(t) = \eta(t)\phi \qquad (8\text{-}68)$$

in which ϕ is the torsional modal coordinate and the generalized coordinate, η, is obtained from the equation

$$I\ddot{\eta} + 2\zeta_\theta\omega_\theta I\dot{\eta} + K_\theta\eta = T(t) \qquad (8\text{-}69)$$

in which I is the mass moment of inertia of the building about the vertical axis through its geometric centre, ω_θ is the angular frequency in twist, ζ_θ is the damping ratio in twist, $K_\theta = I\omega_\theta^2$ is the torsional stiffness and T(t) is the generalized torque. With the torsional modal coordinate equal to unit twist about the centre of rotation, i.e. $\phi = 1.0$, and being constant throughout the height of the building, the generalized fluctuating torque is

$$T(t) = \rho\, C_D\, \bar{U}_H\, W^2\, H \iint_0^1 Z^\alpha(Y - \frac{1}{2})u(y,z,t)dYdZ \qquad (8\text{-}70)$$

in which normalized coordinates are introduced. Following a procedure analogous to that outlined in Section 8.2, the spectrum of the generalized fluctuating torque becomes, similar to Equation (8-26),

$$S_T(f) = \rho^2\, C_D^2\, \bar{U}_H^4\, W^4H^2I_u^2\, \frac{S_u(f)}{\sigma_u^2(z)}\, J^2(f,W,H,\bar{U}_H) \qquad (8\text{-}71)$$

in which the joint acceptance function in torsion is

$$J^2(f,W,H,\bar{U}_H) = \iiiint_0^1 Z_1^{2\alpha}Z_2^{2\alpha}(Y_1 - \tfrac{1}{2})(Y_2 - \tfrac{1}{2})R(Y_1,Y_2,Z_1,Z_2,f)\, dY_1dY_2dZ_1dZ_2 \qquad (8\text{-}72)$$

and the normalized wind spectrum and root coherence function are the same as defined earlier.

The variance of the generalized torque is the integral of the torque spectrum, which is

$$\sigma_T^2 = \rho^2 C_D^2 \bar{U}_H^4 W^4 H^2 I_u^2 \int_o^\infty \frac{S_u(f)}{\sigma_u^2(z)} J^2(f,W,H,\bar{U}_H)df \qquad (8\text{-}73)$$

The variance of the twist is

$$\sigma_\theta^2 = \int_o^\infty S_\theta(f)df = \frac{1}{K_\theta^2} \int_o^\infty S_T(f) \, |H_\theta(f)|^2 \, df \qquad (8\text{-}74)$$

where $|H_\theta(f)|^2$ is the mechanical admittance function in torsion. In terms of the background and resonant twist, the variance is

$$\sigma_\theta^2 = \frac{1}{K_\theta^2} \int_o^{f_\theta} S_T(f)df + \frac{1}{K_\theta^2} \frac{\pi f_\theta}{4\zeta_\theta} S_T(f_\theta) \qquad (8\text{-}75)$$

in which f_θ is the frequency of twist. The peak twist, $\hat{\theta} = g_p \sigma_\theta$, with g_p being the peak factor for twist. The r.m.s. twist, σ_θ, can be computed from its background and resonant components as

$$\sigma_\theta = \frac{1}{K_\theta} \rho C_D W^2 H I_u \bar{U}_H^2 \left(B + \frac{sF}{\zeta_\theta}\right)^{1/2} \qquad (8\text{-}76)$$

where the background turbulence factor for torsion is,

$$B = \int_o^{f_\theta} \frac{S_u(f)}{\sigma_u^2(z)} J^2(f,W,H,\bar{U}_H)df \qquad (8\text{-}77)$$

With the wind spectrum given by Equation (7-29), the background turbulence factor for torsion was evaluated numerically and is plotted for different aspect ratios, W/H, in Figure 8.5. The decay parameters c_o and c_m are the same as those used for the charts in the alongwind response

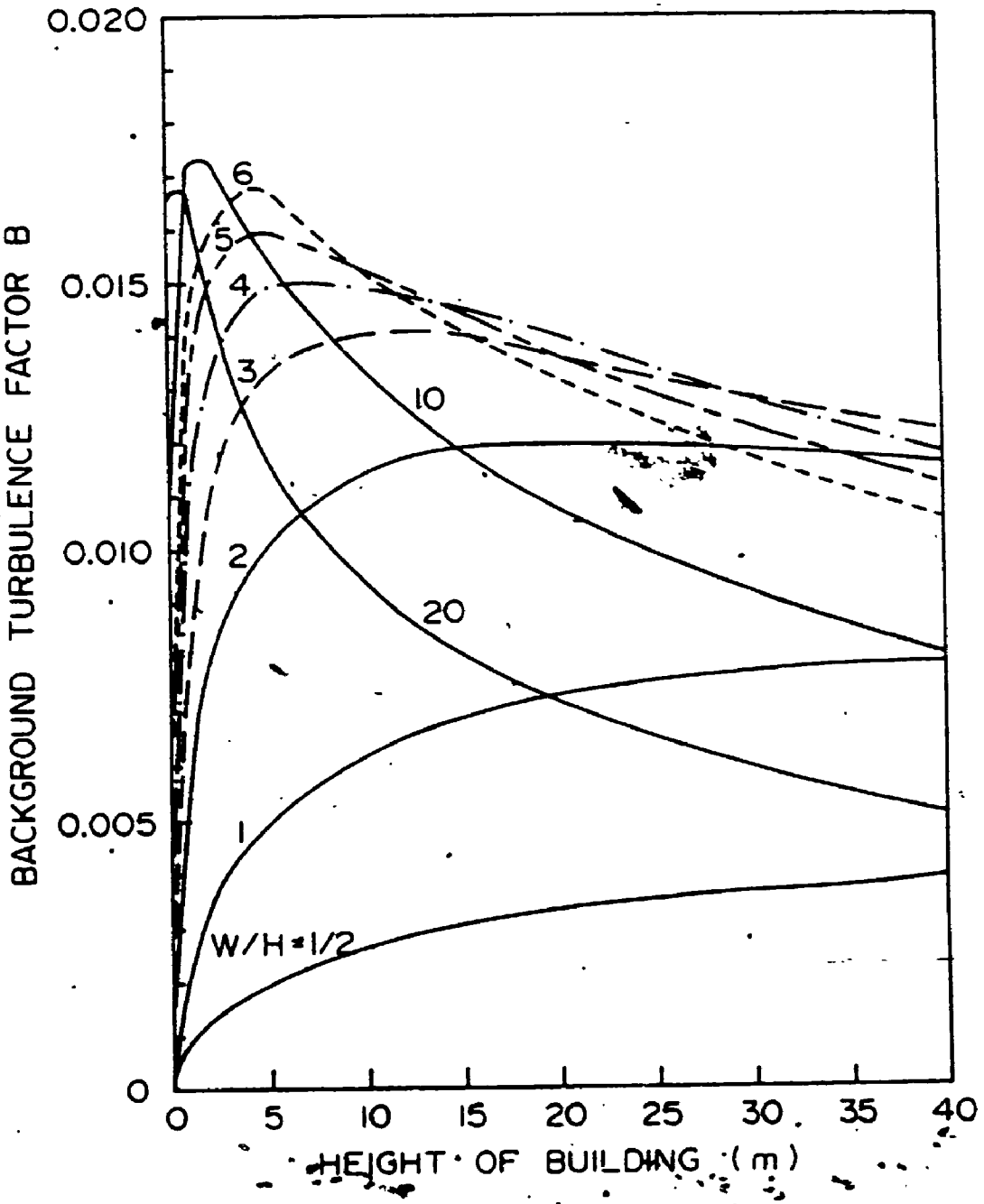

FIGURE 8.5 Background turbulence factor - torsional mode.

i.e., the coherences are dependent on both separation and elevation. The size reduction factor for torsion is

$$s = J^2(f_\theta, W, H, \bar{U}_H) \tag{8-78}$$

This factor is plotted for different aspect ratios and reduced frequencies in Figure 8.6. The gust energy ratio for torsion, F, is given by

$$F = \frac{\pi}{4} f_\theta \frac{S_u(f)}{\sigma_u^2(z)} \tag{8-79}$$

and is the same as in the case of the alongwind response and hence can be read from Figure 8.3 with the torsional frequency, f_θ, in lieu of the bending frequency. The average fluctuating rate is analogous to the alongwind case, i.e.

$$\nu = f_\theta \sqrt{\frac{sF}{sF+\zeta_\theta B}} \tag{8-80}$$

The curves in Figures 8.5 and 8.6 are applicable to any of the three exposures. The decay coefficients are taken as mentioned and the mean wind profile is taken to be constant over the height of the building. Using the charts, the torsional response to wind can readily be evaluated for any base-isolated building.

8.7.2 Torsional Response of a Flexible Building

If the superstructure is flexible, then the torsional modal coordinate varies in the x, y and z directions and the translation is given by

$$\mu(x,y,z,t) = \eta(t)\, \phi(x,y,z) \tag{8-81}$$

in which the generalized coordinate, $\eta(t)$, is obtained from the equation

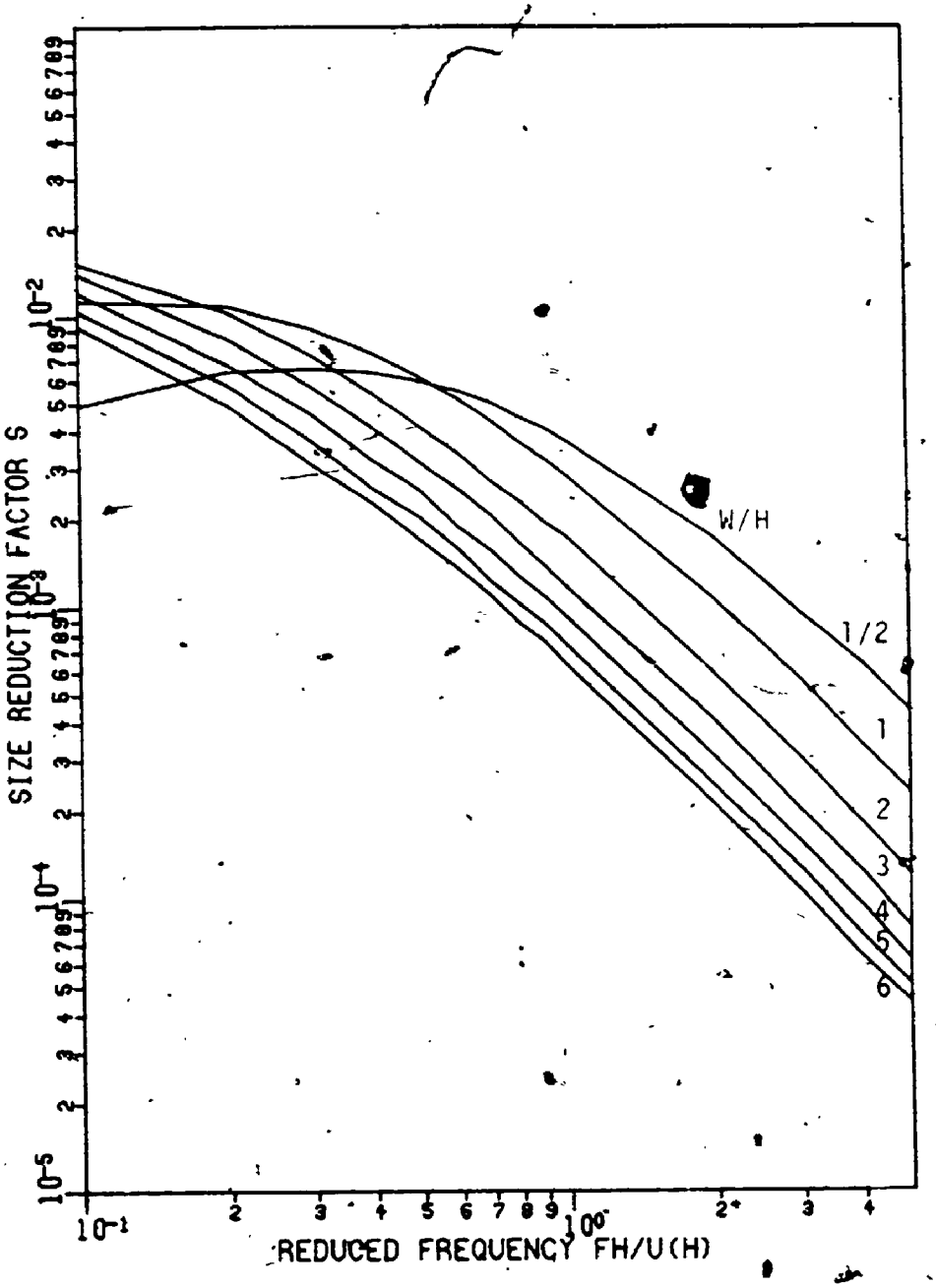

FIGURE 8.6 SIZE REDUCTION FACTOR - TORSIONAL MODE

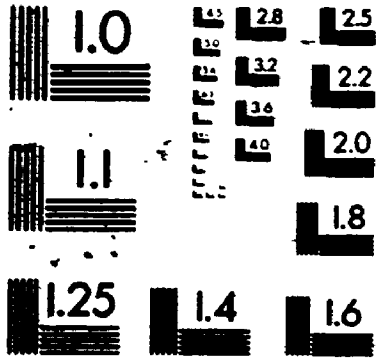

$$M_T\ddot{\eta} + 2\zeta_\theta\omega_\theta M_T\dot{\eta} + K_T\eta = F_T(t) \qquad (8\text{-}82)$$

in which M_T, K_T and $F_T(t)$ is the generalized mass, stiffness and force respectively. For a rigid building on isolators allowing sliding but no rocking, the modal coordinate is constant throughout the height and varies in the x and y directions (Figure 8.4) i.e. $\phi(x,y)$. Measuring y from the vertical edge of the building and choosing a normalized mode such that $\phi(0,0) = -1$ and $\phi(0,W) = 1$, the torsional modal coordinate is expressed as

$$\phi(x,y) = \frac{2}{W}\sqrt{x^2+(y-\frac{W}{2})^2} \qquad (8\text{-}83)$$

in which 2/W is the angle of rotation about the geometric centre and the horizontal coordinate, x, is measured from the centreline of the building. If m is the mass density of the building, the generalized mass, M_T, is

$$M_T = H\iint m\,\phi^2(x,y)dx\,dy$$

$$= \frac{4}{W^2}mH\int_0^W\int_{-\frac{D}{2}}^{\frac{D}{2}} x^2 + (y-\frac{W}{2})^2\,dx\,dy$$

$$= \frac{4}{W^2}I \qquad (8\text{-}84)$$

where I is the mass moment of inertia about the centroidal vertical axis. The generalized stiffness is $K_T = M_T\omega_\theta^2 = \frac{4}{W^2}I\,\omega_\theta^2$.

The fluctuating pressure on the face of the building, given by Equation (8-4), acts in the x-direction for which the modal coordinate is

$$\phi(y) = \frac{2y}{W} - 1 = 2Y-1 \qquad (8\text{-}85)$$

Therefore, the generalized force is expressed as

$$F_T(t) = \rho\, C_D\, \bar{U}_H\, W\, H \iint_0^1 Z^{\alpha}(2Y-1)\,dY\,dZ \tag{8-86}$$

The spectrum of the generalized force becomes

$$S_T(f) = \rho^2\, C_D^2\, \bar{U}_H^4\, W^2 H^2\, I_u^2\, \frac{S_u(f)}{\sigma_u^2(z)}\, J_T^2(f,W,H,\bar{U}_H) \tag{8-87}$$

in which the joint acceptance function is given by

$$J_T^2(f,W,H,\bar{U}_H) = \iiint\!\!\iint_0^1 Z_1^{2\alpha} Z_2^{2\alpha} (2Y_1-1)(2Y_2-1) R(Y_1,Y_2,Z_1,Z_2,f)\, dY_1\,dY_2\,dZ_1\,dZ_2 \tag{8-88}$$

and the normalized wind spectrum as well as the root coherence function are as defined earlier. Equation (8-88) can be rewritten as

$$J_T^2(f,W,H,\bar{U}_H) = 4 \iiint\!\!\iint_0^1 Z_1^{2\alpha} Z_2^{2\alpha} (Y_1 - \tfrac{1}{2})(Y_2 - \tfrac{1}{2}) R(Y_1,Y_2,Z_1,Z_2,f)\, dY_1\,dY_2\,dZ_1\,dZ_2$$

$$= 4J^2(f,W,H,\bar{U}_H) \tag{8-89}$$

in which J^2 is given by Equation (8-72). The difference between J_T^2 and J^2 is due only to the way in which the mode was normalized. If the modal coordinates are chosen so that the angle of rotation is equal to unity, then the mode $\phi(y) = y - W/2$ which is the same as the eccentricity used in the first approach and $J_T^2 = J^2$. The integral in Equation (8-88) is directly related to the one in Equation (8-72), by a factor of four, and therefore, the joint acceptance function need not be evaluated anew.

The variance of the edge displacement is

$$\sigma_{x_T}^2 = \frac{1}{K_T^2}\int_0^{f_\theta} S_T(f)df + \frac{1}{K_T^2}\frac{\pi f_\theta}{4\zeta_\theta} S_T(f_\theta) \qquad (8\text{-}90)$$

in which the spectrum of the generalized force is given by Equation (8-87) and Equation (8-88). Both procedures give identical results.

8.7.3 Examples of Evaluation of Torsional Response to Wind

The r.m.s. torque on Building B was computed for open terrain by Equation (8-73), using the wind parameters pertaining specifically to the open exposure (α_2, c_o, c_m). The computed r.m.s. torque is 1148 KN-m ($\bar{U}_e$ = 29.3 m/s) which is 81% of the torque measured on the model in the wind tunnel using the force balance, i.e. 1461 KN-m ($\bar{U}_g$ = 51.3 m/s). For Buildings A and C the calculated torque is 90 and 111 per cent of the torque measured, respectively. This suggests that the torsional vibration arises primarily from the lack of spatial correlation of the alongwind velocity with only a small contribution from vortex shedding.

Table 8.9 shows the computation of the edge displacement due to torsion for Building B using the charts. This peak displacement of 2.1 mm is superimposed on the alongwind peak response of 6.65 mm resulting in a total peak translation of 8.75 mm.

8.8 RESPONSE TO EXTREME WIND LOADS

Hurricanes (cyclones) can have very high surface wind velocities in excess of 250 km/hr (69 m/s). A gust velocity of 80 m/s was recorded in Northwest Australia. Base-isolated buildings constructed in such regions, e.g. in Japan, may experience extreme winds. The response

TABLE 8.9 Edge Displacement Due to Torsion - Building B, Open Exposure

Background turbulence factor B from Fig. 8.5 for H = 20 m, W/H = 3	.0136
Reduced frequency $n = f_\theta H/\bar{U}_H$	1.11x20/29.3 = 0.758
Size reduction factor, s, from Fig. 8.6	.0018
Wave number, $WN = f_\theta/\bar{U}_H$	1.11/29.3 =.037
Gust energy ratio, F, from Fig. 8.3	.05
Av. fluctuating rate, ν (for f_θ=1.11 Hz and ζ_θ=0.02) from Eq. 8-80	0.553
Peak factor, g_p, from Eq. 8-38 for T = 3600 s	4.04
Turbulence intensity from Table 8.3, I_u	0.134
ρ = 1.3 kg/m^3, C_D = 1.3, W = 60 m, H = 20 m, $\bar{U}_H$ = 29.3 m/s, K_θ = 1.0856x10^{11} N-m/rad	
rms twist, σ_θ (rad) from Eq. 8-76	1.735x10^{-5}
Peak twist, $\hat{\theta} = g_p\sigma_\theta$ (rad)	7.008x10^{-5}
Peak edge displacement, $\hat{\theta} \times \frac{W}{2}$ (mm)	2.1

computed in the previous sections is less than the yield displacement and the isolators remain in the elastic range. For very high winds, the isolators enter the non-linear range and the response is considerably greater. The response of Building B is computed assuming a mean wind velocity of 50 m/s at 20 m elevation in open exposure. The peak wind load is estimated by applying a building gust factor of 2.0 to the mean wind load as recommended in Table 8.8. The mean wind load is computed by Equation (8-9) with the power law exponent $\alpha = 0$. For base isolators with properties as described in Chapters 3 and 5, the peak displacement is estimated to be 47 mm. Using this displacement, an equivalent linear stiffness, k_e, and damping, β, is computed by the secant modulus linearization ($u_o = 47$ mm). The natural frequency of the building in the elastic range, 0.98 hz, is adjusted by the square root of the ratio of the equivalent stiffness to the elastic stiffness of the isolators, i.e. $(k_e/k_1)^{1/2}$. With this adjusted frequency and the equivalent viscous damping, the peak displacement of the building is recomputed. Iterating thrice, the peak displacement is 53 mm which is less than the 74 mm displacement due to earthquakes. The fundamental frequency for the final equivalent stiffness is 0.58 Hz. Therefore, the charts presented earlier are applicable even when the isolator displaces into the non-linear range.

CHAPTER 9

CONCLUSIONS

AND

RECOMMENDATIONS FOR FUTURE RESEARCH

9.1 CONCLUSIONS

The conclusions for the three parts of the study are given separately.

9.1.1 Conclusions - Free Vibration Analysis

The theoretical study of the modal properties of base-isolated buildings suggests the following conclusions:

. Rocking in the isolators more effectively reduces the fixed base frequencies and provides a significant increase in the second mode damping. This should assist in reducing the resonant response especially in the second mode where the frequency is brought closer to the high energy portion of the earthquake spectrum.

. The effect of soil-structure interaction on the modal properties of the base-isolated buildings examined is negligible.

. A simplified analysis, idealizing the building as a rigid body on springs, approximately establishes the fundamental mode properties but may result in significant errors in the second mode properties.

9.1.2 Conclusions - Seismic Analysis

From the seismic analysis, the following are concluded:

. Base isolation reduces the peak acceleration and seismic forces induced in the building.

. Idealizing the building as a rigid body sliding on the isolators approximately predicts the peak displacement and acceleration of the base-isolated building.

. Equivalent linearization is an adequate technique to account for the non-linear behaviour of the isolators.

9.1.3 Conclusions - Wind Characteristics and Wind Response Analysis

The conclusions for the experimental investigation of wind properties and wind forces relevant to low-rise base-isolated buildings are as follows:

. The mean wind velocity may be taken as constant and equal to the value at roof level.

. The turbulence intensity may be taken as constant and equal to the value at 10 m.

. The dimensionless spectrum of wind velocity fluctuations expressed as a function of reduced frequency does not vary much with height or exposure. Thus, one theoretical model with overall mean parameters adequately describes the wind spectrum for all exposures and all heights.

. The vertical and horizontal coherences depend on frequency, separation and elevation. The decay parameters appropriate for computing coherences are presented.

. The peak drag coefficient of the models tested is on the average about 1.3, i.e. in line with the NBCC recommendation, but for some buildings and angles of attack it can be as high as 1.6.

. Overturning moments from roof suction can be comparable to the drag overturning moments and occur especially for lower buildings, i.e. about 10 m high. A significant increase in the axial loads may occur.

The conclusions from the theoretical analysis of the response to gusting wind are:

. The forces measured on the model using the force balance agree well with the calculated forces for both drag and torsion.

. The peak displacements, resulting from a wind velocity corresponding to a 1 in 30 year return period, are less than the 10 mm yield displacement usually prescribed for the isolators.

. Despite the differences in the local wind spectrum and the coherences, the NBCC and the ANSI code predict the response of the base-isolated buildings adequately (except by the ANSI code for urban terrain).

. The difference in the background displacements by the NBCC and the direct analysis translates into a difference in the r.m.s. displacement which when multiplied by the peak factor approximately accounts for the difference in the peak displacements.

. The gust factors computed using the charts agree well with the gust factors from the direct analysis.

. The charts presented herein can be used to predict the response even when the wind loads are large enough to cause non-linear displacements in the isolators.

9.2 RECOMMENDATIONS FOR FUTURE RESEARCH

The effect of introducing rocking should be investigated to determine whether the increased damping to be derived from it would result in a smaller response than the sliding system.

Dynamic models of the base-isolated buildings analyzed should be tested in the wind tunnel as an additional check of the displacement calculated herein.

Extensive seismic analyses are required with a view to developing a code for specifying the magnitude and distribution of seismic forces on base-isolated buildings.

APPENDIX I

FORCE COEFFICIENTS FROM THE BASE BALANCE

The force coefficients relate the balance results to the full-scale forces. The experimental mean and r.m.s. force coefficients are defined as

C_{M_x} = bending moment due to forces in the x-dir$(M_x)/q_g DH^2$

C_{M_y} = bending moment due to forces in the y-dir$(M_y)/q_g WH^2$

C_{M_t} = torque $(M_t)/q_g WDH$

C_{S_x} = shear due to forces in the x-dir$(S_x)/q_g DH$

C_{S_y} = shear due to forces in the y-dir$(S_y)/q_g WH$

in which $q_g = \frac{1}{2}\rho U_g^2$ is the dynamic pressure at the gradient height and H, W and D are the height, breadth and depth of the model respectively. The orientation of the axes with respect to the plan of the models is shown in Figure I.1. The plots of the force coefficients versus azimuth angle are shown in Figures I.2 through I.10. The values are listed in Tables I.1 through I.3. Generally, the maximum values occur when the angle of incidence is slightly off the normal to the face (20°-30°). This is attributed to the separation points (the dimension the wind 'sees') being slightly farther apart and to the wider wake.

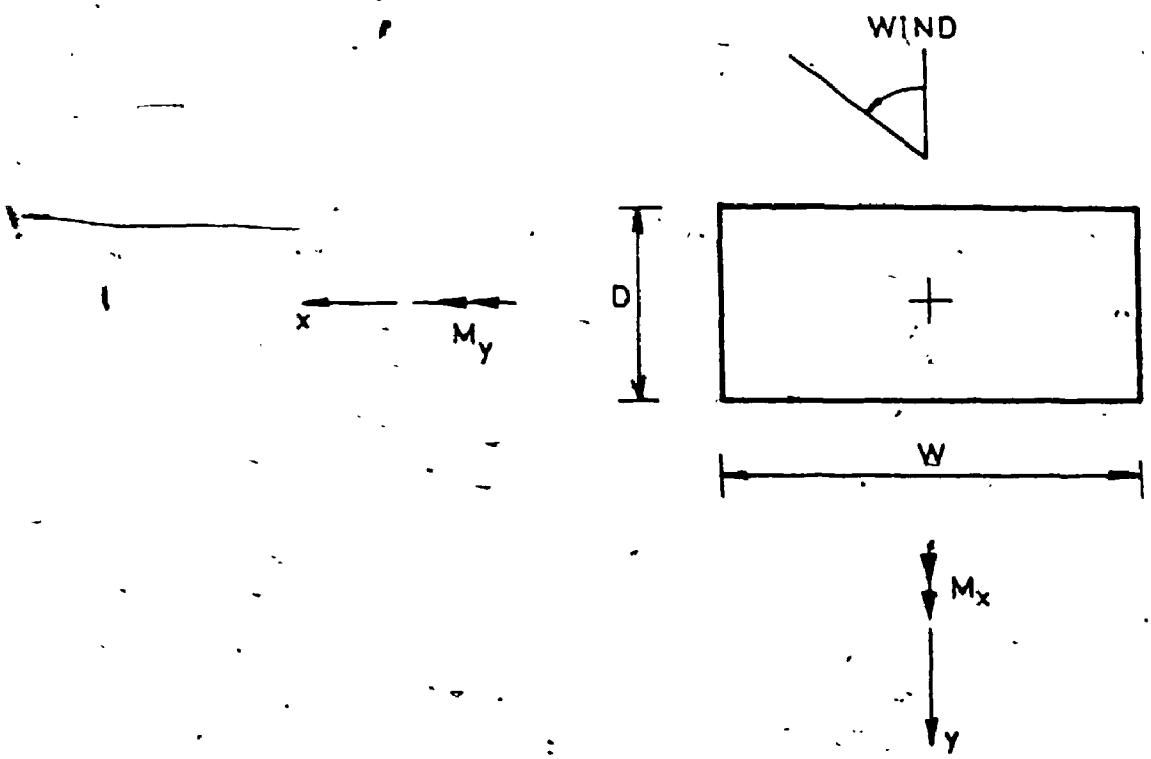

FIGURE I.1 Orientation of axes w.r.t. plan of models

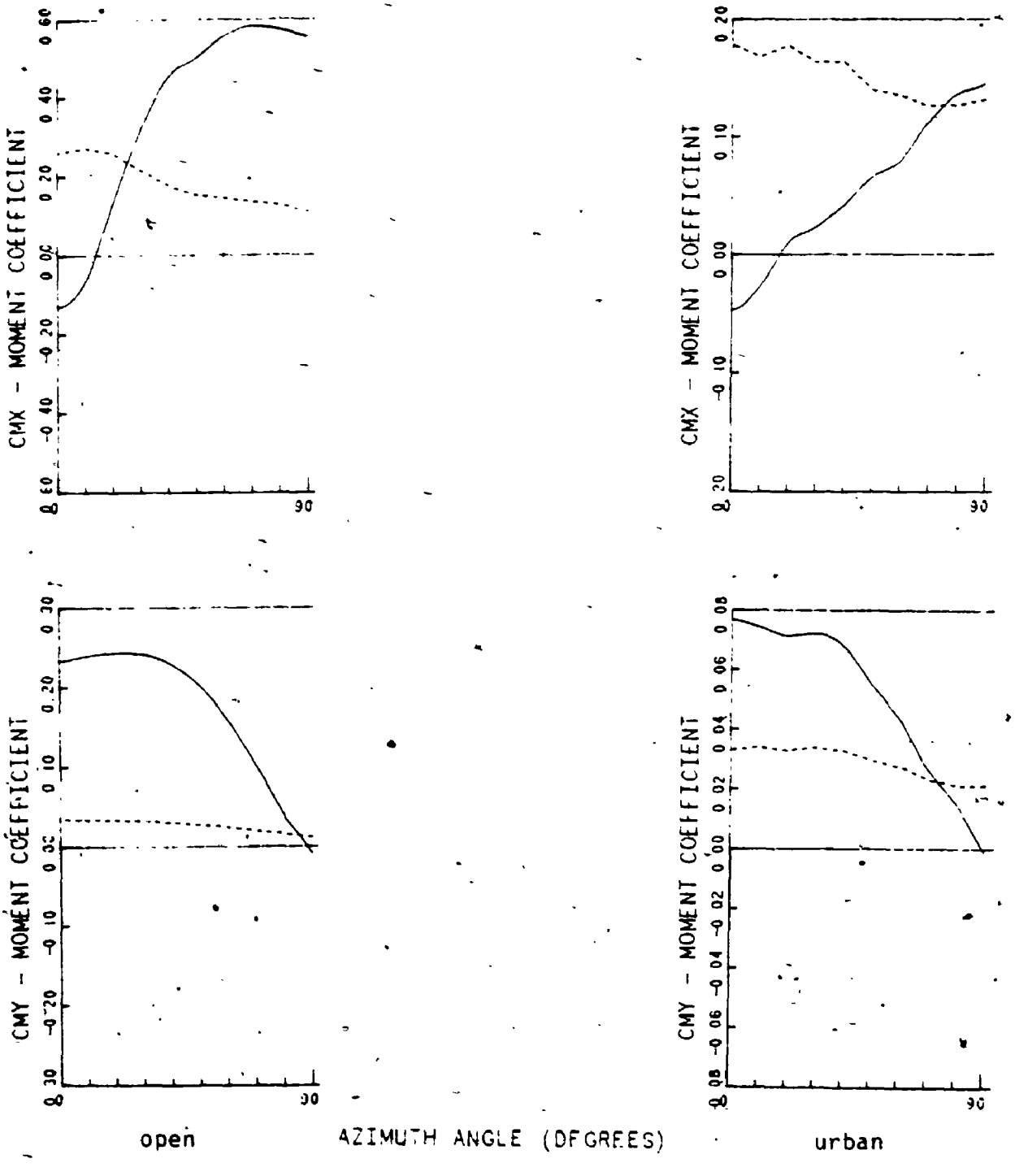

FIGURE I.2 Variation of moment coefficient with azimuth angle (Model A)

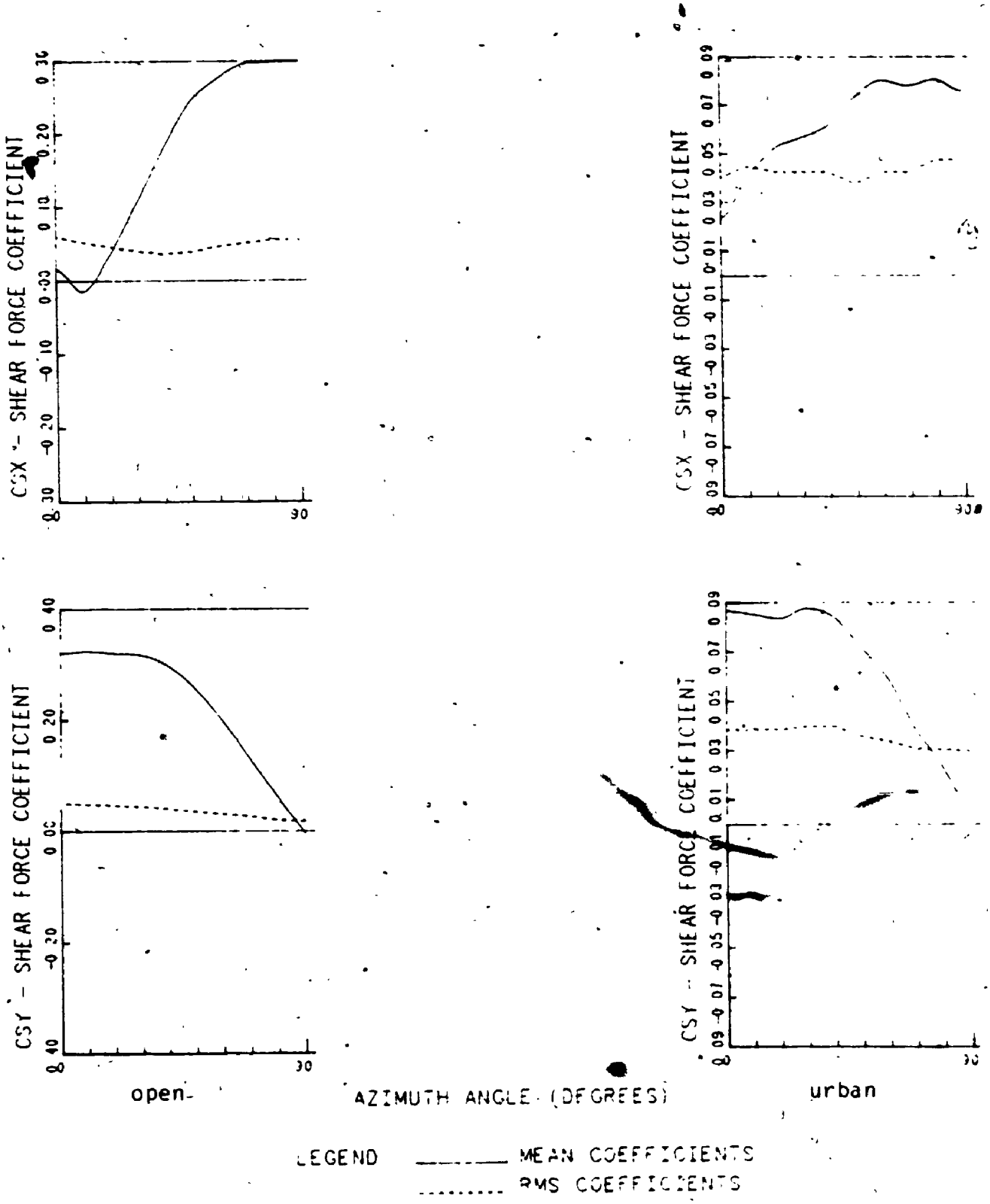

FIGURE I.3 Variation of shear coefficient with azimuth angle (Model A)

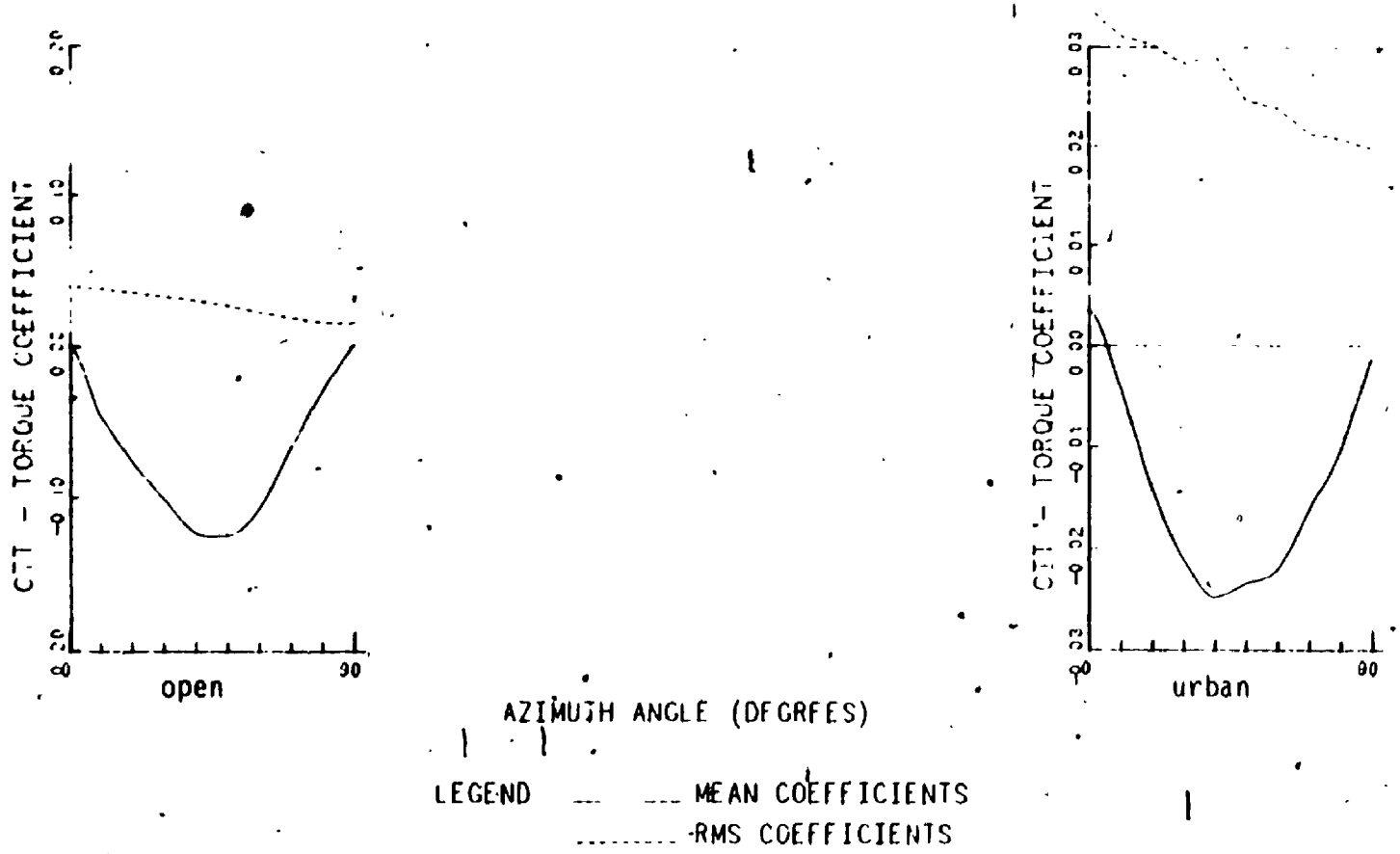

FIGURE I.4 Variation of torque coefficient with azimuth angle (Model A)

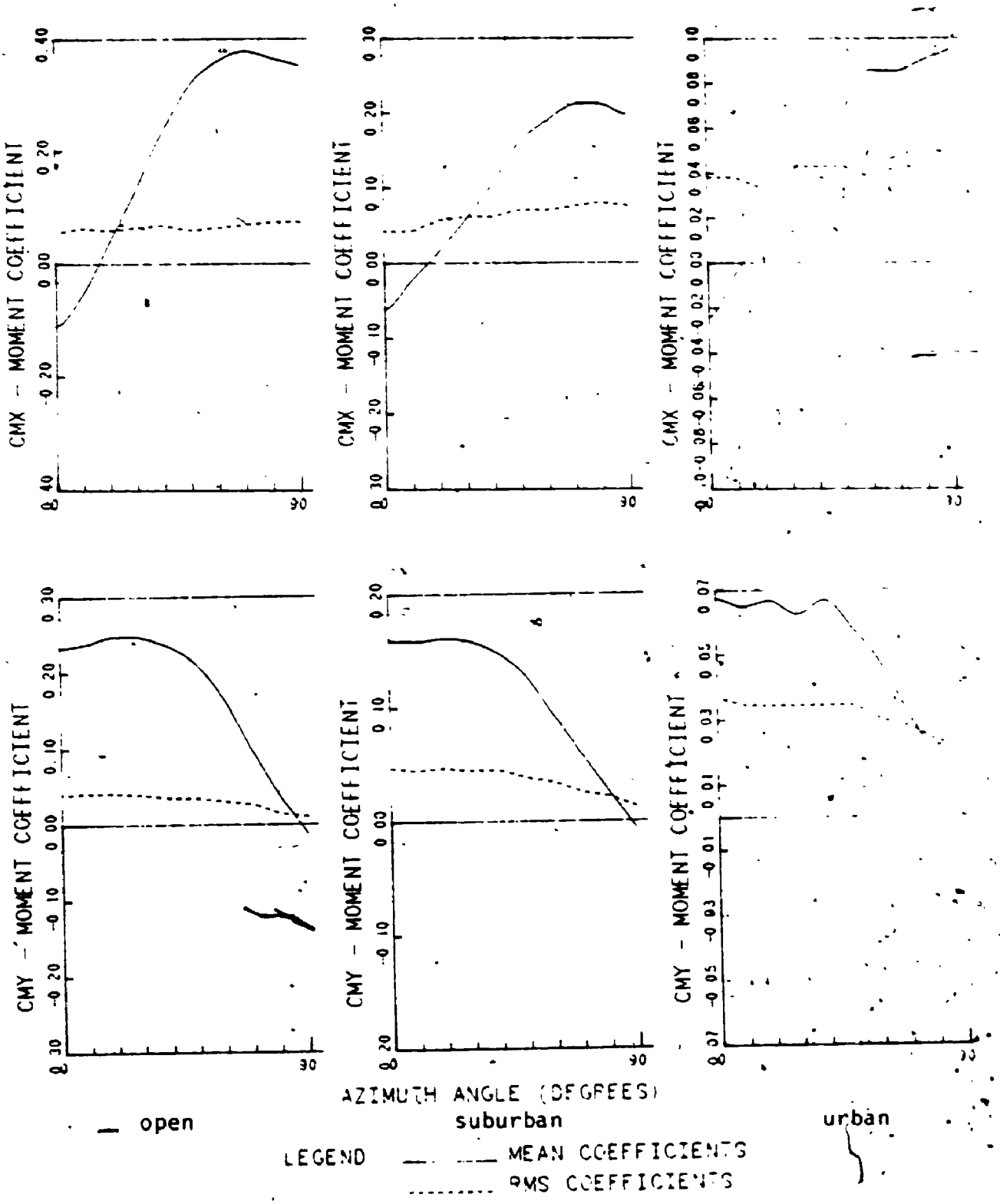

FIGURE I.5 Variation of moment coefficient with azimuth angle (Model B)

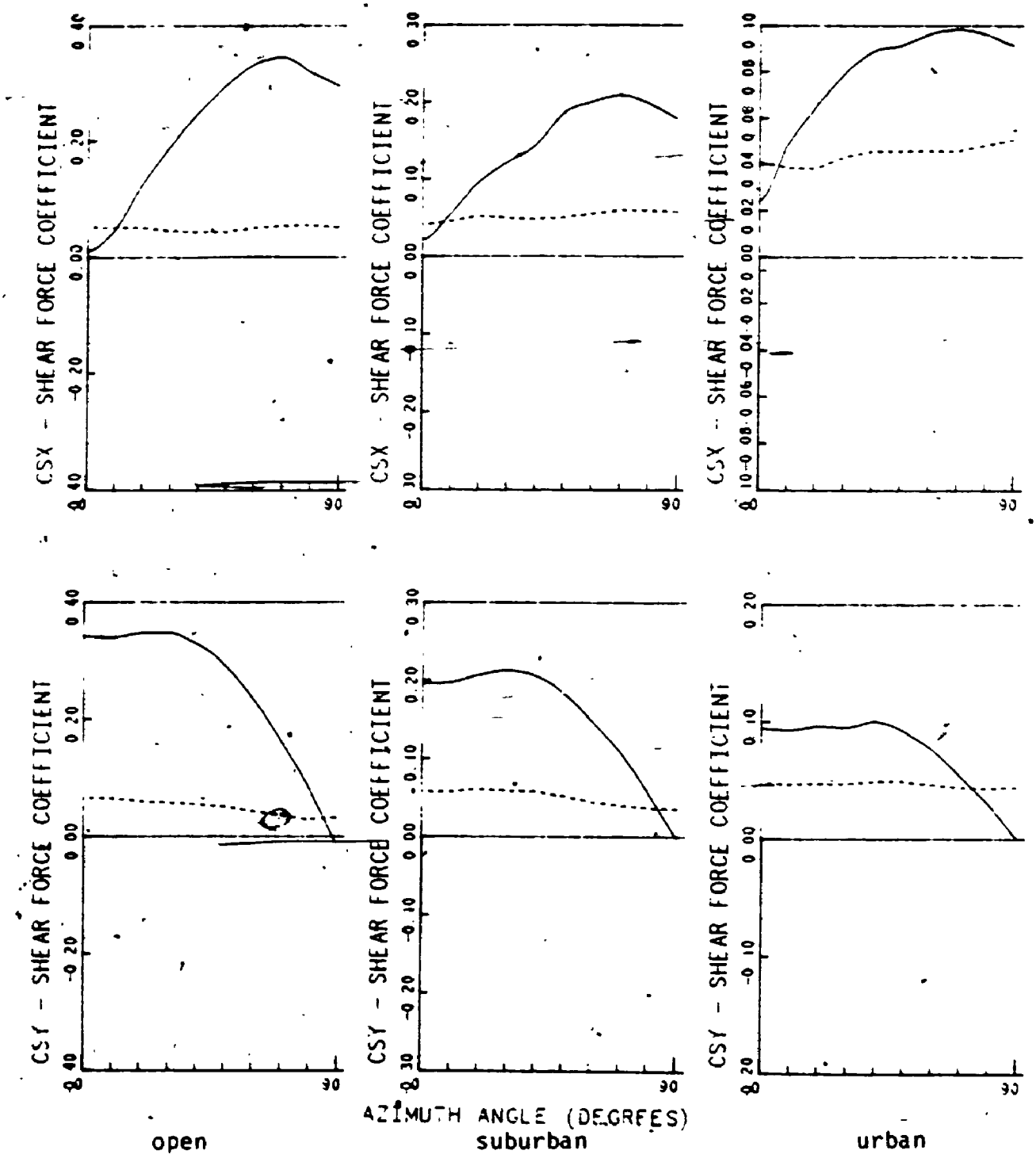

FIGURE I.6 Variation of shear coefficient with azimuth angle (Model B)

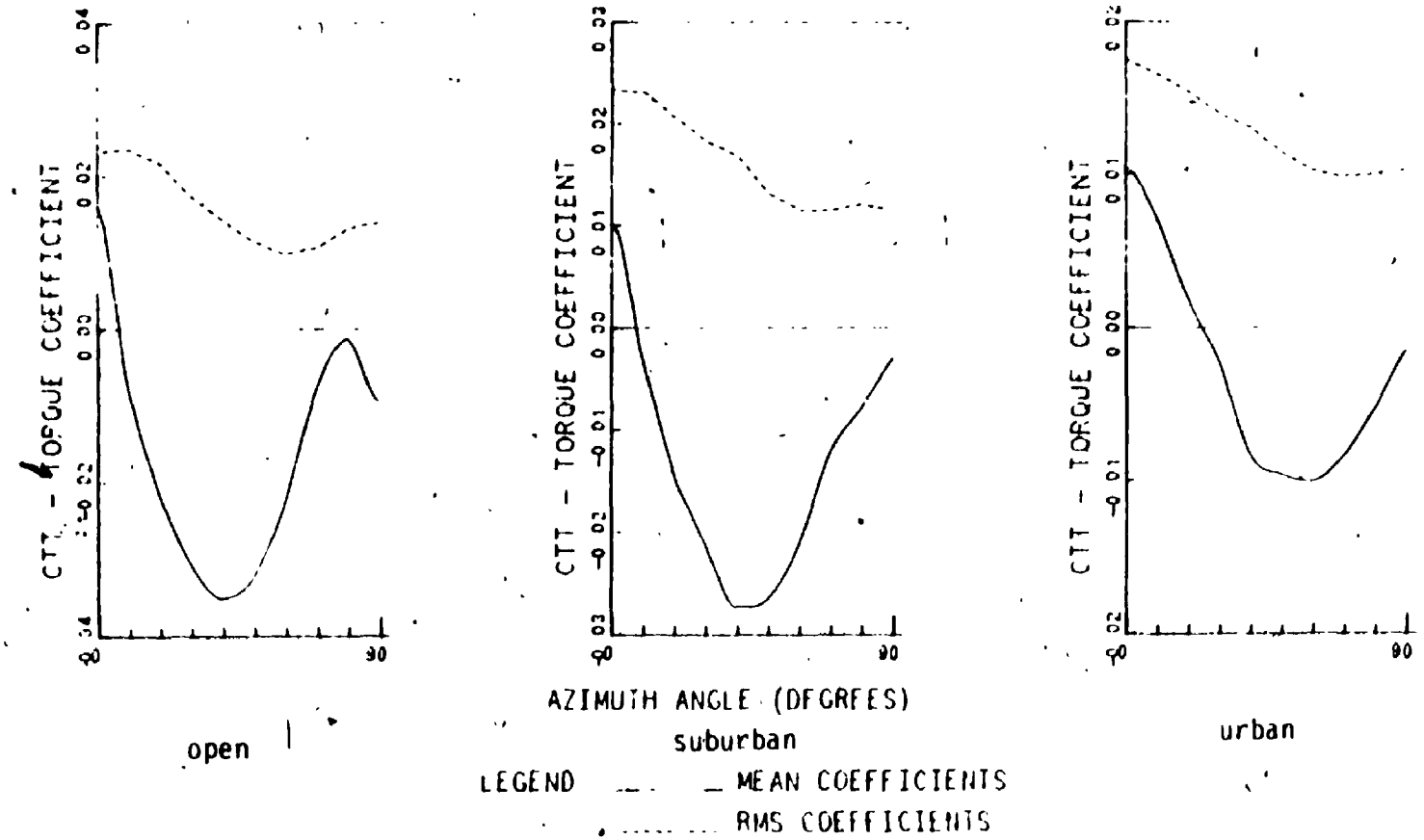

FIGURE I.7 Variation of torque coefficient with azimuth angle (Model B)

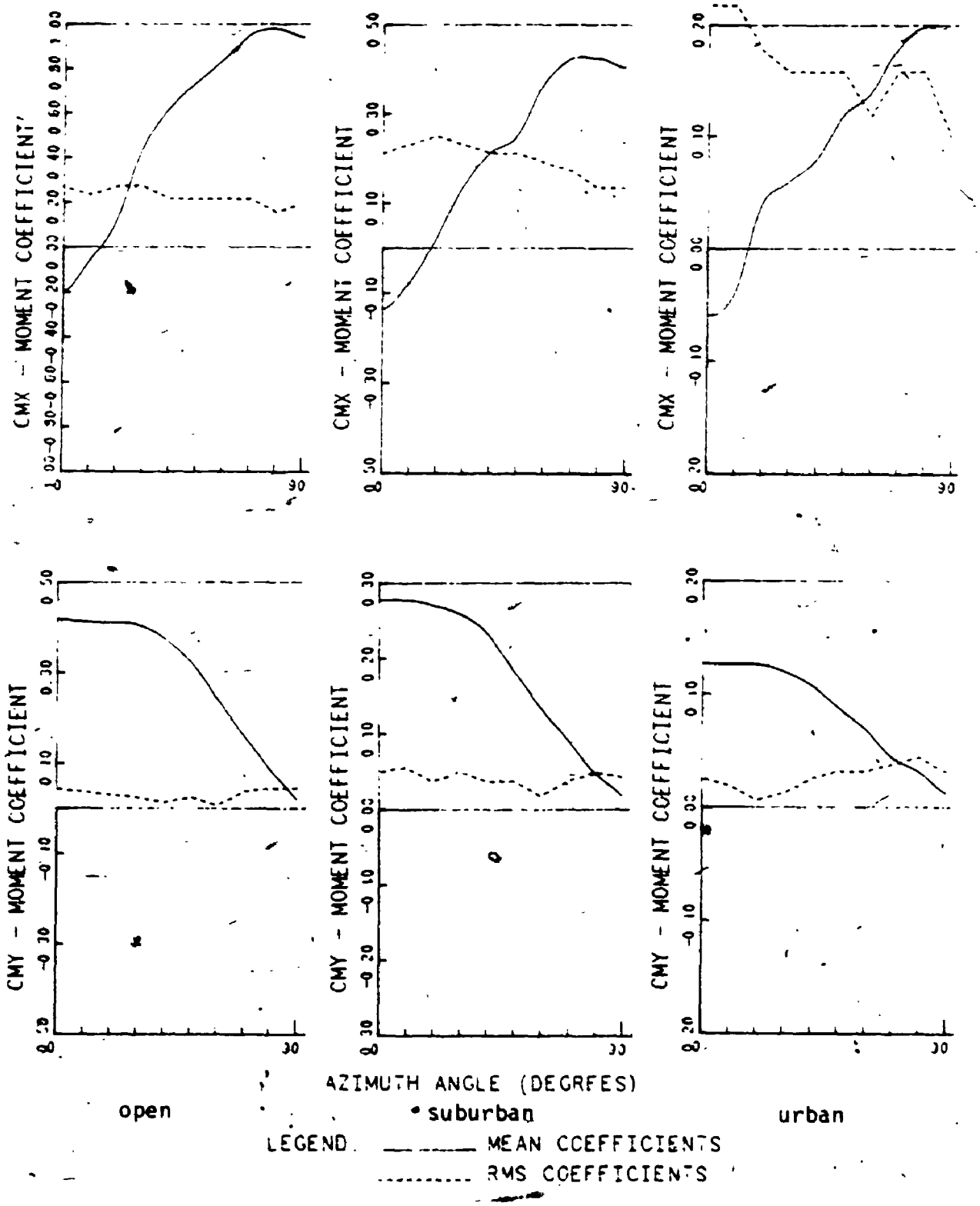

FIGURE I.8 Variation of moment coefficient with azimuth angle (Model C)

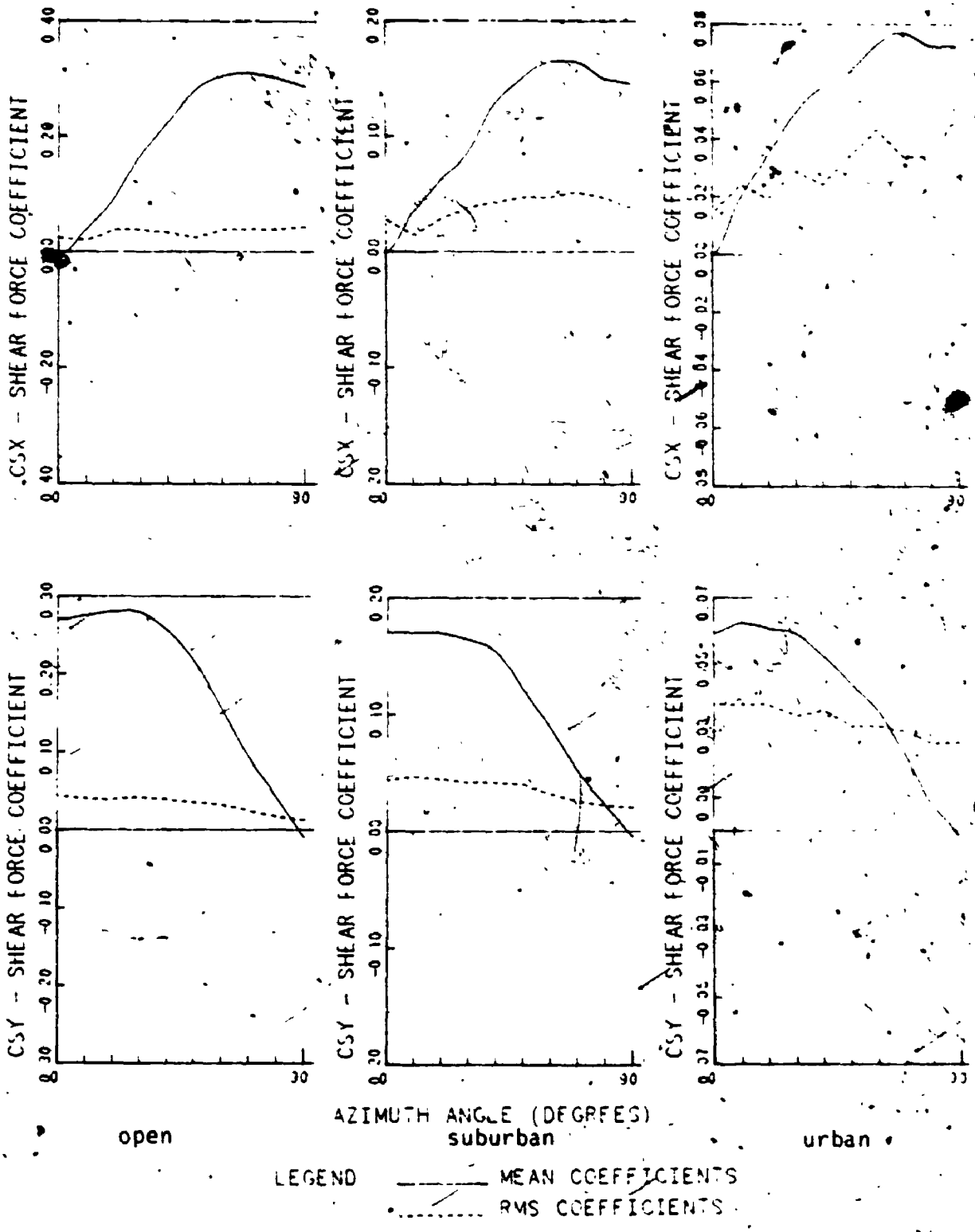

FIGURE I.9 Variation of shear coefficient with azimuth angle (Model C)

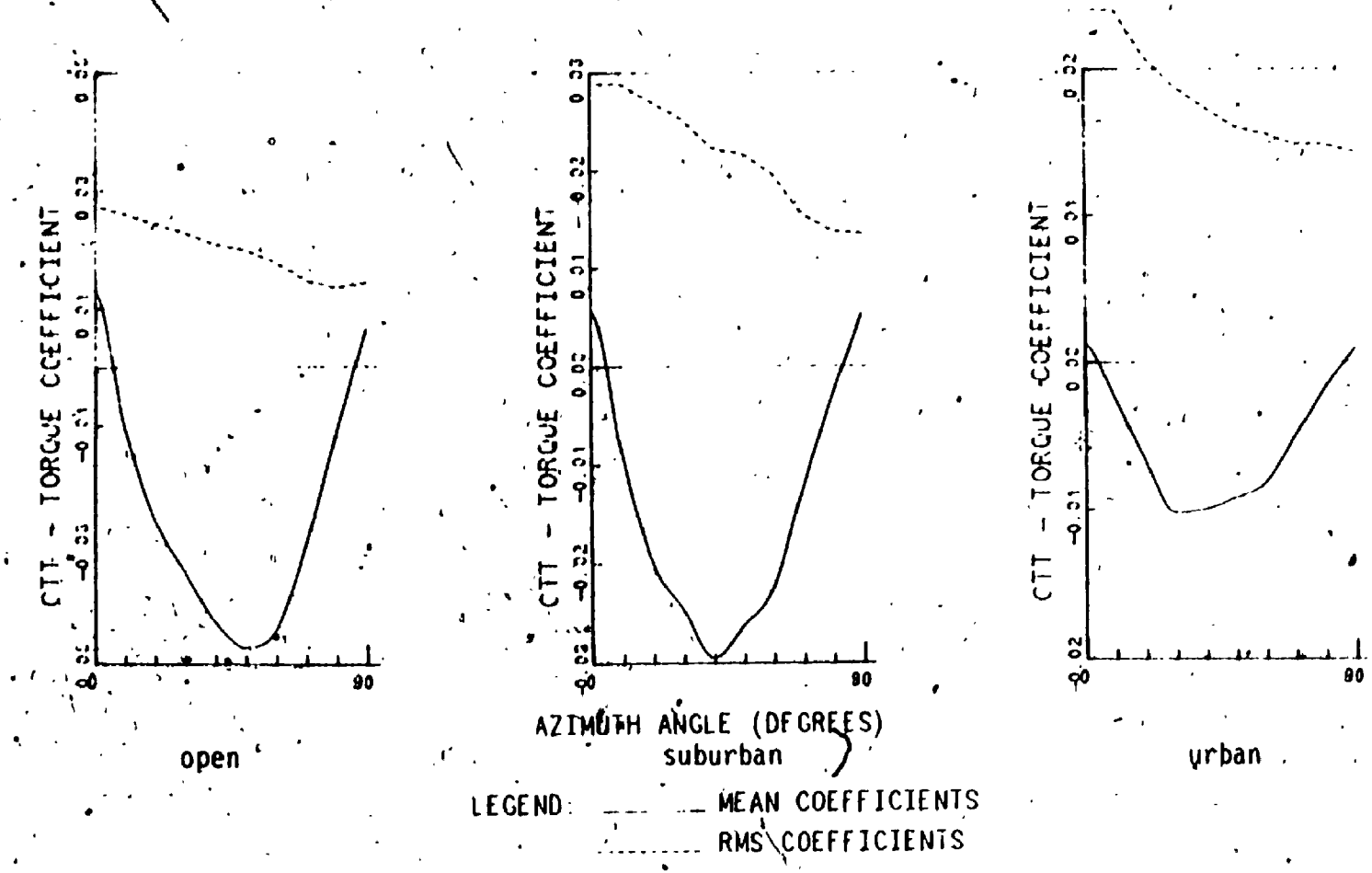

FIGURE I.10 Variation of torque coefficient with azimuth angle (Model C)

TABLE I.1 Force Coefficients for Model A

ANGLE	X MOMENT		Y MOMENT		X SHEAR		Y SHEAR		TORQUE		
	MEAN	RMS	MEAN	RMS	MEAN	RMS	MEAN	RMS	MEAN	RMS	
0.00	-0.128	0.261	0.234	0.035	0.016	0.060	0.320	0.051	0.001	0.041	
10.00	-0.068	0.273	0.240	0.034	-0.010	0.053	0.324	0.049	-0.045	0.039	
20.00	0.128	0.260	0.244	0.034	0.035	0.046	0.319	0.047	-0.075	0.036	
30.00	0.315	0.219	0.242	0.033	0.104	0.042	0.316	0.044	-0.100	0.034	
40.00	0.453	0.179	0.230	0.031	0.179	0.037	0.297	0.041	-0.122	0.031	
50.00	0.503	0.155	0.204	0.028	0.243	0.039	0.254	0.036	-0.124	0.028	open
60.00	0.557	0.146	0.161	0.025	0.275	0.046	0.196	0.031	-0.107	0.023	
70.00	0.585	0.137	0.104	0.021	0.296	0.051	0.128	0.027	-0.067	0.020	
80.00	0.576	0.128	0.040	0.017	0.299	0.056	0.060	0.020	-0.029	0.017	
90.00	0.555	0.109	-0.008	0.011	0.300	0.055	-0.003	0.018	0.002	0.016	

ANGLE	X MOMENT		Y MOMENT		X SHEAR		Y SHEAR		TORQUE		
	MEAN	RMS	MEAN	RMS	MEAN	RMS	MEAN	RMS	MEAN	RMS	
0.00	-0.047	0.178	0.077	0.033	0.024	0.040	0.087	0.039	0.004	0.034	
10.00	-0.028	0.168	0.074	0.034	0.040	0.045	0.085	0.038	-0.004	0.031	
20.00	0.009	0.178	0.071	0.033	0.052	0.043	0.084	0.038	-0.014	0.030	
30.00	0.023	0.163	0.072	0.034	0.057	0.043	0.088	0.040	-0.021	0.028	
40.00	0.042	0.164	0.068	0.033	0.062	0.043	0.084	0.040	-0.025	0.029	urban
50.00	0.065	0.140	0.055	0.030	0.073	0.038	0.072	0.036	-0.023	0.025	
60.00	0.079	0.135	0.043	0.028	0.080	0.043	0.059	0.034	-0.022	0.024	
70.00	0.112	0.126	0.027	0.023	0.078	0.043	0.039	0.031	-0.016	0.021	
80.00	0.136	0.127	0.015	0.021	0.081	0.048	0.023	0.030	-0.010	0.021	
90.00	0.145	0.131	-0.001	0.021	0.076	0.047	0.003	0.030	-0.001	0.020	

TABLE I.2 Force Coefficients for Model B

ANGLE	X MOMENT		Y MOMENT		X SHEAR		Y SHEAR		TORQUE		
	MEAN	RMS	MEAN	RMS	MEAN	RMS	MEAN	RMS	MEAN	RMS	
0.00	-0.110	0.055	0.233	0.040	0.012	0.053	0.341	0.068	0.016	0.025	
10.00	-0.055	0.064	0.239	0.041	0.049	0.051	0.339	0.068	-0.008	0.024	
20.00	0.037	0.060	0.248	0.042	0.128	0.051	0.346	0.060	-0.021	0.022	
30.00	0.132	0.064	0.246	0.039	0.194	0.046	0.348	0.052	-0.031	0.017	
40.00	0.237	0.068	0.234	0.035	0.252	0.044	0.330	0.045	-0.035	0.014	open
50.00	0.319	0.059	0.211	0.035	0.300	0.044	0.295	0.05	-0.032	0.011	
60.00	0.360	0.064	0.164	0.031	0.335	0.051	0.240	0.043	-0.023	0.010	
70.00	0.378	0.068	0.097	0.027	0.347	0.053	0.167	0.037	-0.008	0.011	
80.00	0.365	0.073	0.037	0.015	0.319	0.056	0.088	0.030	-0.001	0.013	
90.00	0.352	0.073	-0.012	0.010	0.297	0.051	0.011	0.033	-0.009	0.014	

ANGLE	X MOMENT		Y MOMENT		X SHEAR		Y SHEAR		TORQUE		
	MEAN	RMS	MEAN	RMS	MEAN	RMS	MEAN	RMS	MEAN	RMS	
0.00	-0.061	0.043	0.159	0.047	0.022	0.041	0.196	0.058	0.010	0.023	
10.00	-0.024	0.042	0.158	0.045	0.055	0.045	0.198	0.057	-0.003	0.023	
20.00	0.014	0.057	0.161	0.047	0.096	0.053	0.207	0.061	-0.014	0.021	
30.00	0.056	0.061	0.158	0.045	0.122	0.050	0.213	0.059	-0.021	0.018	
40.00	0.104	0.061	0.148	0.045	0.144	0.048	0.206	0.058	-0.027	0.017	suburban
50.00	0.160	0.071	0.128	0.038	0.186	0.050	0.184	0.052	-0.027	0.013	
60.00	0.188	0.071	0.094	0.034	0.201	0.055	0.149	0.045	-0.021	0.012	
70.00	0.211	0.075	0.060	0.026	0.209	0.059	0.108	0.041	-0.012	0.012	
80.00	0.212	0.080	0.026	0.021	0.198	0.060	0.057	0.038	-0.006	0.012	
90.00	0.198	0.075	-0.006	0.013	0.179	0.057	-0.002	0.036	-0.003	0.012	

ANGLE	X MOMENT		Y MOMENT		X SHEAR		Y SHEAR		TORQUE		
	MEAN	RMS	MEAN	RMS	MEAN	RMS	MEAN	RMS	MEAN	RMS	
0.00	-0.024	0.038	0.067	0.037	0.024	0.041	0.094	0.048	0.011	0.018	
10.00	-0.005	0.038	0.065	0.035	0.048	0.039	0.093	0.046	0.007	0.017	
20.00	0.014	0.033	0.067	0.034	0.065	0.038	0.096	0.047	0.002	0.015	
30.00	0.038	0.043	0.062	0.034	0.079	0.043	0.095	0.047	-0.002	0.014	
40.00	0.052	0.043	0.067	0.034	0.089	0.046	0.100	0.049	-0.008	0.013	
50.00	0.067	0.043	0.058	0.035	0.091	0.046	0.092	0.049	-0.010	0.011	urban
60.00	0.086	0.038	0.048	0.030	0.096	0.046	0.077	0.046	-0.010	0.010	
70.00	0.085	0.043	0.032	0.028	0.099	0.046	0.054	0.044	-0.008	0.010	
80.00	0.090	0.043	0.017	0.024	0.096	0.048	0.030	0.043	-0.005	0.010	
90.00	0.095	0.052	0.000	0.022	0.091	0.051	0.001	0.044	-0.001	0.010	

TABLE I.3 Force Coefficients for Model C

ANGLE	X MOMENT		Y MOMENT		X SHEAR		Y SHEAR		TORQUE		
	MEAN	RMS	MEAN	RMS	MEAN	RMS	MEAN	RMS	MEAN	RMS	
0.00	-0.195	0.274	0.419	0.044	-0.005	0.024	0.270	0.044	0.013	0.028	
10.00	-0.059	0.234	0.412	0.037	0.038	0.019	0.274	0.041	-0.010	0.026	
20.00	0.117	0.272	0.411	0.031	0.090	0.038	0.280	0.039	-0.026	0.024	
30.00	0.449	0.273	0.406	0.025	0.167	0.038	0.279	0.042	-0.035	0.023	
40.00	0.626	0.215	0.376	0.013	0.224	0.033	0.255	0.039	-0.043	0.021	
50.00	0.742	0.215	0.325	0.025	0.281	0.024	0.216	0.036	-0.047	0.020	open
60.00	0.842	0.215	0.244	0.006	0.305	0.038	0.155	0.033	-0.045	0.018	
70.00	0.956	0.215	0.162	0.037	0.309	0.038	0.092	0.024	-0.030	0.015	
80.00	0.979	0.157	0.088	0.044	0.301	0.038	0.041	0.016	-0.011	0.014	
90.00	0.939	0.196	0.019	0.044	0.286	0.043	-0.010	0.013	0.006	0.014	

ANGLE	X MOMENT		Y MOMENT		X SHEAR		Y SHEAR		TORQUE		
	MEAN	RMS	MEAN	RMS	MEAN	RMS	MEAN	RMS	MEAN	RMS	
0.00	-0.135	0.212	0.278	0.049	0.000	0.028	0.170	0.043	0.006	0.029	
10.00	-0.077	0.232	0.278	0.056	0.033	0.014	0.170	0.047	-0.009	0.029	
20.00	0.019	0.250	0.271	0.037	0.061	0.028	0.169	0.045	-0.020	0.027	
30.00	0.135	0.232	0.260	0.049	0.085	0.038	0.164	0.042	-0.025	0.025	
40.00	0.212	0.212	0.234	0.037	0.127	0.042	0.154	0.042	-0.030	0.022	
50.00	0.250	0.211	0.184	0.037	0.150	0.047	0.121	0.040	-0.026	0.022	suburban
60.00	0.366	0.193	0.136	0.018	0.164	0.047	0.088	0.032	-0.023	0.020	
70.00	0.424	0.173	0.093	0.037	0.164	0.052	0.051	0.026	-0.012	0.016	
80.00	0.425	0.135	0.049	0.049	0.151	0.047	0.022	0.022	-0.003	0.014	
90.00	0.404	0.135	0.018	0.043	0.146	0.038	-0.005	0.021	0.005	0.014	

ANGLE	X MOMENT		Y MOMENT		X SHEAR		Y SHEAR		TORQUE		
	MEAN	RMS	MEAN	RMS	MEAN	RMS	MEAN	RMS	MEAN	RMS	
0.00	-0.059	0.218	0.127	0.025	0.000	0.014	0.059	0.038	0.001	0.024	
10.00	-0.039	0.217	0.126	0.019	0.019	0.024	0.062	0.038	-0.002	0.024	
20.00	0.040	0.178	0.126	0.006	0.034	0.019	0.061	0.038	-0.007	0.021	
30.00	0.059	0.158	0.120	0.013	0.048	0.029	0.059	0.034	-0.010	0.019	
40.00	0.079	0.158	0.108	0.025	0.058	0.024	0.053	0.036	-0.010	0.017	urban
50.00	0.118	0.158	0.088	0.032	0.063	0.034	0.044	0.031	-0.009	0.016	
60.00	0.138	0.119	0.070	0.032	0.072	0.043	0.036	0.031	-0.008	0.016	
70.00	0.178	0.158	0.044	0.038	0.077	0.034	0.023	0.030	-0.005	0.015	
80.00	0.198	0.158	0.032	0.044	0.072	0.034	0.008	0.026	-0.002	0.015	
90.00	0.197	0.099	0.013	0.032	0.072	0.048	-0.002	0.026	0.001	0.014	

APPENDIX II

COMPUTER PROGRAMS USED IN THE STUDY

The main computer programs developed in the course of the study are:

FREVIB	Performs the free vibration analysis of plane frames including soil-structure interaction.
MULTC	Performs the time history analysis of a multi-degree of freedom system with localized non-linearity and isolators yielding in simple shear.
GUST	Computes the response of a building to gusting wind.

REFERENCES

1. American National Standard Institute. 1982. Minimum Design Loads for Buildings and Other Structures. National Bureau of Standards.

2. Berman, S. 1965. Estimating the Longitudinal Wind Spectrum Near the Ground. Quarterly Journal of the Royal Meteorological Society, Vol. 91, 302-317.

3. Blakeley, R.W.G., A.W. Charleson, H.C. Hitchcock, L.M. Megget, M.J.N. Priestley, R.D. Sharpe and R.I. Skinner. 1979. Recommendations for the Design and Construction of Base Isolated Structures. Bull. New Zealand National Soc. for Earthq. Eng., 12(2): 136-157.

4. Boardman, P.R., B.J. Wood and A.J. Carr. 1983. Union House - A Cross Braced Structure With Energy Dissipators. Bull. New Zealand Natl. Soc. Earthquake Engrg., 16(2): 83-97.

5. Caspe, M.S. 1970. Earthquake Isolation of Multi-Storey Concrete Structures. Journal of the American Concrete Institute, 11, 923-933.

6. Caspe, M.S. 1984. Base Isolation From Earthquake Hazards, An Idea Whose Time Has Come! Proc. 8th World Conference on Earthquake Eng., San Francisco, 5, 1031-1038.

7. Caughey, T.K. and M.E.J. O'Kelly. 1965. Classical Normal Modes in Damped Linear Dynamic Systems. J. Applied Mechanics, ASME, 32, 583-588.

8. Celebi, M. and J.M. Kelly. 1985. The Implementation of Seismic Hazard Reduction by Base Isolation. Proc. 2nd Int. Conf. on Soil Dyn. and Earthquake Eng., 1-59: 1-68.

9. Chopra, A.K., D.P. Clough and R.W. Clough. 1973. Earthquake Resistance of Buildings With a 'Soft First Storey'. International Journal of Earthquake Engineering and Structural Dynamics, 1, 347-355.

10. Clough, R. and J. Penzien. 1975. Dynamics of Structures. McGraw-Hill, New York.

11. Cook, N.J. 1985. The Designer's Guide to Wind Loading of Building Structures. Part 1, Butterworths, London.

12. Davenport, A.G. 1961. The Spectrum of Horizontal Gustiness Near the Ground in High Winds. Journal of the Royal Meteorological Society, Vol. 87, 194-211.

13. Davenport, A.G. 1965. The Relationship of Wind Structure to Wind Loading. Proc. of Conference on Wind Effects on Buildings and Structures, National Physical Laboratory, H.M.S.O., 54-102.

14. Davenport, A.G. 1967. Gust Loading Factors. J. Struct. Div., ASCE, Vol. 93, No. ST3, 11-34.

15. Davenport, A.G. and N. Isyumov. 1967. The Application of the Boundary Layer Wind Tunnel to the Prediction of Wind Loading. Proceedings, International Seminar on Wind Effects on Buildings and Structures, Ottawa, Vol. 1, 201-230.

16. Davenport, A.G. and D.J. Surry. 1974. The Pressures on Low Rise Structures in Turbulent Wind. Canadian Structural Engineering Conference, Toronto, 1-39.

17. Davenport, A.G. 1977. The Prediction of the Response of Structures to Gusty Wind. Safety of Structures Under Dynamic Loading TAPIR, Vol. 1, 257-283.

18. Davenport, A.G. 1964. Note on the Distribution of the Largest Value of a Random Function With Application to Gust Loading. Proceedings of the Institution of Civil Engineers, Paper No. 6739, Vol. 28, 187-196.

19. Delfosse, G.C. 1980. Full Earthquake Protection Through Base Isolation System. Proc. 7th World Conference on Earthquake Engineering, Istanbul, Turkey, 8, 61-68.

20. Elsesser, E. and M. Walters. 1987. Seismic Isolation of the Existing City and County Building in Salt Lake City - A Case Study. Proc. Conf. on Soil-Structure Interaction, Princeton, 283-296.

21. ESDU. 1986. Characteristics of Atmospheric Turbulence Near the Ground. Part II: Single Point Data for Strong Winds (Neutral Atmosphere). Item No. 85020, ESDU International Ltd., London.

22. Fichtl, G.H. and G.E. McVehil. 1970. Longitudinal and Lateral Spectra of Turbulence in the Atmospheric Boundary Layer at the Kennedy Space Center. J. App. Met., Vol. 9, 51-63.

23. Fintel, M. and R.F. Khan. 1969. Shock Absorbing Soft Story Concept for Multistory Earthquake Structures. Journal of the American Concrete Institute, 66-29, 318-390.

24. Flaga, A. and B. Wrana. 1987. Analysis of Empiric Formulae of Power Spectral Densities of Three Wind Velocity Vector Components. Proc., 7th Int. Conf. on Wind Engineering, Aachen, Vol. 1, 11-20.

25. Foss, K.A. 1958. Co-ordinates Which Uncouple the Equations of Motion of Damped Linear Dynamic Systems. J. of Applied Mech., ASME, 25: 361-364.

26. Foutch, D.A. and E. Safak. 1981. Torsional Vibration of Alongwind Excited Structures. Journal of the Eng. Mech. Div., ASCE, Vol. 107, No. EM2, 323-337.

27. Frazer, R.A., W.J. Duncan and A.R. Collar. 1946. Elementary Matrices. Cambridge University Press, London.

28. Gaul, L. 1977. Dynamic Interaction of a Foundation With Visco-elastic Halfspace. Proc. Dynamical Methods in Soil and Rock Mechanics, Karlsruhe, Germany, Vol. 1, 167-183.

29. Ghali, A. and A.M. Neville. 1978. Structural Analysis. Chapman and Hall, London.

30. Guyan, R.J. 1965. Reduction of Stiffness and Mass Matrices. American Inst. of Aeronautics and Astronautics Journal, 3(2): 380.

31. Hadjian, A.H. 1982. A Re-Evaluation of Equivalent Linear Models for Simple Yielding Systems. J. Earthquake Eng. and Struct. Dyn., Vol. 10, 759-767.

32. Harris, R.I. 1971. The Nature of the Wind. Proc. of Seminar on the Modern Design of Wind-Sensitive Structures, Construction Industry Research and Information Association, London.

33. Holmes, J.D. 1987. Mode Shape Corrections for Dynamic Response to Wind. Short Communication Eng. Struct., Vol. 9, 210-212.

34. Housner, G.W. and P.C. Jennings. 1964. Generation of Artificial Earthquakes. J. of Eng. Mech., ASCE, Vol. 90, EM1, 113-150.

35. Hüffmann, G. 1984. Shaking Table Tests of a 5-Storey Steel Frame. Res. Report, GERB, Essen, Germany.

36. Irons, B. 1965. Structural Eigenvalue Problems: Elimination of Unwanted Variables. AIAA Journal, Vol. 3, No. 5, 961-962.

37. Iwan, W.D. 1980. Estimating Inelastic Response Spectra From Elastic Spectra. Earthquake Eng. Struct. Dyn., 8, 375-388.

38. Jennings, P.C. 1968. Equivalent Viscous Damping for Yielding Structures. J. Eng. Mech., ASCE, Vol. 94, No. EM1, 103-116.

39. Joubert, P.N. et al. 1967. The Drag of Bluff Bodies Immersed in a Turbulent Boundary Layer. Proc., International Research Seminar - Wind Effects on Buildings and Structures, Ottawa, Vol. 1, 297-335.

40. Kaimal, J.C. et al. 1972. Spectral Characteristics of Surface-Layer Turbulence. Quarterly Journal of the Royal Meteorological Society, Vol. 98, 563-589.

41. Kelly, J.M. and T. Pan. 1984. Seismic Response of Base-Isolated Structures With Vertical-Rocking Coupling. Earthquake Engineering and Structural Dynamics, Vol. 12, 681-702.

42. Kelly, J.M. 1985. Aseismic Base Isolation. The Shock and Vibration Digest, Vol. 17, No. 7, 3-14.

43. Kelly, J.M. 1986. Aseismic Base Isolation: Review and Bibliography. Soil Dyn. and Earthq. Eng. 5(3): 202-216.

44. Li, Li. 1987. Advances in Base Isolation in China. Proc. Conf. on Soil-Structure Interaction, Princeton, 297-309.

45. Lythe, G. and D. Surry. 1983. Wind Loading of Flat Roofs With and Without Parapets. Journal of Wind Engineering and Industrial Aerodynamics, 11, 75-94.

46. Luco, J.E. and R.A. Westmann. 1971. Dynamic Response of Circular Footings. Journal of Engineering Mechanics, ASCE, Vol. 97, No. EM5, 1381-1395.

47. Mahin, S.A. et al. 1987. The FPS Earthquake Resisting System. NEWS, National Information Service for Earthquake Engineering, Vol. 10, No. 3.

48. Martel, R.R. 1929. The Effects of Earthquake on Buildings With a Flexible First Storey. Bull. of the Seismological Society of America, 19, 3, 167-178.

49. Megget, L.M. 1978. Analysis and Design of a Base-Isolated Reinforced Concrete Frame Building. Bulletin of the New Zealand National Society for Earthquake Engineering, 11, 4, 245-254.

50. National Building Code of Canada. 1985. Commentary B to Part 4, Design, National Research Council of Canada.

51. Newmark, N.M. 1959. A Method of Computation for Structural Dynamics. Proc., ASCE, J. of Eng. Mech. Div., 85, 67-94.

52. Novak, M. and L. El Hifnawy. 1983. Effect of Soil-Structure Interaction on Damping of Structures. J. Earthq. Eng. and Struct. Dyn., Vol. 11, 595-621.

53. Novak, M. et al. 1983. DYNA - A Computer Program for Calculation of Response of Rigid Foundations to Dynamic Loads. The University of Western Ontario. SACDA, London, Ontario, Canada.

54. Novak, M. 1983. Random Vibration of Structures. Proc. Fourth Int. Conf. on Applications of Statistics and Probability in Soil and Structural Engineering, Italy, 539-549.

55. Ng, J.Y. 1986. The Structure of the Turbulent Flow at the Test Section of BLWT II. B.E.Sc. Report, The University of Western Ontario.

56. Olesen, H.R., S.E. Larsen and J. Højstrup. 1984. Modelling Velocity Spectra in the Lower Part of the Planetary Boundary Layer. Boundary Layer Meteorology, Vol. 29, 285-312.

57. Pais, A. and E. Kausel. 1985. Stochastic Response of Foundations. Research Report R85-6, M.I.T., Cambridge, Mass.

58. Panofsky, H. and J. Dutton. 1984. Atmospheric Turbulence. Wiley, New York.

59. Pasquill, F. 1962. Atmospheric Diffusion. Van Nostrand, London.

60. Penzien, J. and S. Liu. 1969. Nondeterministic Analysis of Nonlinear Structures Subjected to Earthquake Excitations. Proc. of the 4th World Conf. on Earthq. Eng., Santiago, Chile, Vol. I, A-1, 114-129.

61. Pipes, L.A. and S.A. Hovanessian. 1969. Matrix-Computer Methods in Engineering. Wiley, New York.

62. Plichon, C. and F. Jolivet. 1978. Aseismic Foundation Systems for Nuclear Power Stations. Proc. of SMIRT Conf., Paper No. C190/78, 193-205.

63. Popov, E.P. 1987. Observations on the Mexico Earthquake of 19 September 1985. Engineering Structures, Vol. 9, 74-83.

64. Rice, S.O. 1945. Mathematical Analysis of Random Noise, Pt. III. Bell Syst. Tech. J., Vol. 24, 46-156.

65. Robinson, W.H. and A.G. Tucker. 1977. A Lead-Rubber Shear Damper. Bulletin of the New Zealand National Society for Earthquake Engineering, 10, 3, 151-153.

66. Rosenbleuth, E. and I. Herrera. 1964. On a Kind of Hysteretic Damping. J. Eng. Mech. Div., ASCE, 90, No. EM4, 37-48.

67. Simiu, E. and D.W. Lozier. 1975. The Buffeting of Tall Structures by Strong Winds. Building Science Series 74, National Bureau of Standards, Washington, D.C.

68. Simiu, E. and R.H. Scanlan. 1985. Wind Effects on Structures. 2nd Ed. John Wiley, New York.

69. Solari, G. 1982. Alongwind Response Estimation: Closed Form Solution. J. Structural Div., ASCE, 108(1), 225-244.

70. Stiemer, S.F. and B.B. Barwig. 1985. Seismic Base Isolation for Steel Structures. Canadian Journal of Civil Engineering, 12, 73-81.

71. Suen, E. 1987. Seismic Response of Dams. M.E.Sc. Thesis, University of Western Ontario, Canada.

72. Tajimi, H. 1960. A Statistical Method of Determining the Maximum Response of a Building Structure During an Earthquake. Proc. 2 WCEE, Vol. 2, 781-797, Science Council of Japan, Japan.

73. Tarics, A.G. and D. Way. 1984. Rubber Pads Protect Buildings From Seismic Shock. ASCE Magazine, Vol. 54, No. 8, 12.

74. Tarics, A.G. 1987. The Acceptance of Base Isolation for Earthquake Protection of Buildings. Proc. Conf. on Soil-Structure Interaction, Princeton, 311-338.

75. Tezean, S., A. Civi and G. Hüffmann. 1978. Spring-Dashpot Vibration Isolators Against Earthquakes. Proc. 7th WCEE, Istanbul, Turkey, 8, 53-57.

76. Tschanz, T. 1982. Measurement of Total Dynamic Loads Using Elastic Models With High Natural Frequencies. Proc. of Int. Workshop on Wind Modeling Criteria and Techniques, National Bureau of Standards, Maryland. III. 4-1: 4-17.

77. Tschanz, T. 1983. The Base Balance Measurement Technique and Applications to Dynamic Wind Loading of Structures. Ph.D. Thesis, The University of Western Ontario, Faculty of Engineering Science, London, Ontario.

78. Tyler, R.G. 1977. Dynamic Tests on Laminated Rubber Bearings. Bull. N.Z. National Society for Earthquake Engineering, Vol. 10, No. 3, 143-150.

79. Vanmarke, E.H., C.A. Cornell, D.A. Gasparini and S.N. Hou. 1969. SIMQKE, A Program for Artificial Motion Generation, Dept. of Civil Eng., M.I.T. (revised 1976).

80. Veletsos, A.S. and C.E. Ventura. 1986. Modal Analysis of Non-Classically Damped Linear Systems. Earthquake Engineering and Structural Dynamics, Vol. 14, 217-243.

81. Vellozzi, J. and E. Cohen. 1968. Gust Response Factors. J. Structural Div., ASCE, Vol. 94 (6), 1295-1313.

82. Vickery, B.J. 1971. On the Reliability of Gust Loading Factors. Civil Engineering Transactions, 1-9.

83. Waller, R.A. 1969. Buildings on Springs. Pergamon Press, Oxford.

84. Watanabe, H. and H. Tochigi. 1985. A Consideration of the Equivalent Linearization of Restoring Force Characteristics of Structures. Proc. Japan Society of Civil Engineers Structural Engineering/ Earthquake Engineering, 2(1): 195-205.

85. Weaver, W. and J.M. Gere. 1980. Matrix Analysis of Framed Structures. Van Nostrand, New York, 235-242.

86. Whitbread, R.E. 1965. Model Simulation of Wind Effects on Structures. Symposium on Wind Effects on Buildings and Structures, National Physical Laboratory, HMSO, 238-306.

87. Wilson, E. 1974. The Static Condensation Algorithm. International Journal for Numerical Methods in Engineering, Vol. 8, 198-203.

88. Wolf, J.P. et al. 1983. Response of a Nuclear-Power Plant on Aseismic Bearings to Horizontally Propagating Waves. Earthquake Engineering and Structural Dynamics, 11, 483-499.

89. Wong, H.L. and J.E. Luco. 1976. Dynamic Response of Rigid Foundations of Arbitrary Shape. International Journal of Earthquake Engineering and Structural Dynamics, Vol. 4, 579-587.

90. Wong, H.L. and J.E. Luco. 1978. Tables of Impedance Functions and Input Motions for Rectangular Foundations. Report No. CE78-15, University of Southern California.

91. Yang, J.H. and Y.K. Lin: 1981. Along-Wind Motion of Multy-Storey Building. J. Eng. Mechanics Div., ASCE, 295-307.

92. Isyumov, N. 1983. Wind Induced Torque on Square and Rectangular Building Shapes. Journal of Wind Engineering and Industrial Aerodynamics, 13, 183-196.

93. Isyumov, N. 1987. Torsional Response. Wind Loading and Wind-Induced Structural Response A State-of-the-Art Report, ASCE, New York.

94. Greig, G.L. 1980. Towards an Estimate of Wind-Induced Dynamic Torque on Tall Buildings. M.Eng. Thesis, University of Western Ontario.